AD-A093 652 GTE LABS INC WALTHAM MA F/G 20/5
NONLINEAR INTERACTIONS BETWEEN LASER RADIATION AND SPIN-ALIGNED--ETC(U)
NOV 80 E J JOHNSON, R W DAVIES, A LEMPICKI F49620-78-C-0082
UNCLASSIFIED AFOSR-TR-80-1324 NL

1 of 2
AD A 093652

(12

NONLINEAR INTERACTIONS BETWEEN LASER RADIATION AND SPIN-ALIGNED CARRIERS IN SEMICONDUCTORS

by

E. J. Johnson
R. W. Davies
A. Lempicki

AIR FORCE OFFICE OF SCIENTIFIC RESEARCH
Electronic & Solid State Sciences Programs
Bolling Air Force Base, D. C. 20332

Contract No. F49620-78-C-0082

November 25, 1980

GTE LABORATORIES INCORPORATED
40 Sylvan Road
Waltham, Massachusetts 02154

UNCLASSIFIED

SECURITY CLASSIFICATION OF THIS PAGE (When Data Entered)

REPORT DOCUMENTATION PAGE	READ INSTRUCTIONS BEFORE COMPLETING FORM
1. REPORT NUMBER: AFOSR-TR-80-1324	2. GOVT ACCESSION NO.: AD-A093 652
3. RECIPIENT'S CATALOG NUMBER	
4. TITLE (and Subtitle): NONLINEAR INTERACTIONS BETWEEN LASER RADIATION AND SPIN-ALIGNED CARRIERS IN SEMICONDUCTORS	5. TYPE OF REPORT & PERIOD COVERED: Final
	6. PERFORMING ORG. REPORT NUMBER
7. AUTHOR(s): E.J. Johnson, R. Davies, A. Lempicki	8. CONTRACT OR GRANT NUMBER(s): F49620-78-C-0082
9. PERFORMING ORGANIZATION NAME AND ADDRESS: GTE Laboratories Incorporated, 40 Sylvan Road, Waltham, Massachusetts 02254	10. PROGRAM ELEMENT, PROJECT, TASK AREA & WORK UNIT NUMBERS: 2306/C2, 61102F
11. CONTROLLING OFFICE NAME AND ADDRESS: Air Force Office of Scientific Research (NE), Electronic & Solid State Sciences Programs, Bolling Air Force Base, D.C. 20332	12. REPORT DATE: Nov 1980
	13. NUMBER OF PAGES: 98
14. MONITORING AGENCY NAME & ADDRESS (if different from Controlling Office)	15. SECURITY CLASS. (of this report): Unclassified
	15a. DECLASSIFICATION/DOWNGRADING SCHEDULE

16. DISTRIBUTION STATEMENT (of this Report)

Approved for public release; distribution unlimited.

17. DISTRIBUTION STATEMENT (of the abstract entered in Block 20, if different from Report)

18. SUPPLEMENTARY NOTES

19. KEY WORDS (Continue on reverse side if necessary and identify by block number)

Spin alignment, optical orientation, semiconductors, GaAs, spin-lattice relaxation, luminescence, polarization of luminescence

20. ABSTRACT (Continue on reverse side if necessary and identify by block number)

The central theme of this work is the effect of radiation upon the vector orientation of characteristic properties of photo-excited carriers in semiconductors. The orientation is referred to the direction of propagation and the polarization state of the exciting light. Initially the emphasis was on the optical properties of spin-aligned electrons, particularly their behavior in stimulated emission. The scope was extended to include ordering of orbital angular moments, and electron wave vectors as well. The material of choice

DD FORM 1 JAN 73 1473

UNCLASSIFIED

SECURITY CLASSIFICATION OF THIS PAGE (When Data Entered)

was GaAs, now rapidly emerging as most important for a variety of optical, electronic and optoelectronic applications. The work performed falls into three categories: (a) development of novel experimental techniques (b) development of new theoretical approaches and (c) development of improved material. In the short duration of this contract the work remains, incomplete; however, we have made progress of considerable consequence in the areas where we had anticipated difficulty, thus providing a longer term challenge. Sophisticated instrumentation has been developed to observe simultaneously photoluminescence and subtle effects in the polarization of photoluminescence of semiconductors over a wide range of excitation and luminescence photon energies and many orders of magnitude in luminescence intensity. Applications of the full capability of this set up to studies of optical orientation effects and dynamics of photoexcited carriers have just begun. Already we have observed structure in the circular polarization that cannot be explained on the basis of current theory. This situation indicates that a detailed interpretation of radiative and nonradiative processes in III-V compounds is far from complete. The potential for studies using ultrapure insulating GaAs has been demonstrated. We have advanced considerably in theoretically relating the optical orientations to the selection rules. Mechanisms for orientation of orbital angular momentum and electron wave vectors have been demonstrated. Let E_g denote the energy gap and let Δ denote the spin-orbit splitting parameter. As valence band energies approach $-2/3\ \Delta$, the wave functions approach those for pure spin states which should severly reduce spin alignment for excitation energies approaching $E_g + \Delta$. This provides an alternative explanation to experimental observations to that advanced by others. A phenomenological rate equation approach to the dynamics of spin polarization which replaces matrix elements by energy and spin dependent generation rates has been developed. A general solution is formidable and conclusions are possible only for very specific cases such as quasi-thermalized nondegenerate carriers. An important underlying theoretical question is whether it is valid to treat the absorption and emission problems as essentially separate processes. We have applied this approach, but we also advance a more sophisticated light scattering approach which treats the two processes as coupled. The choice of using orientational effects as a tool for studying a variety of interactions in GaAs has proved to be extremely rewarding and is likely to play an increasing role in the future. The termination of the contract leaves the work at a point where (a) the experimental facility is fully operational, (b) a large body of data has been collected and a good grasp of the theory is at hand, (c) a promise of very significant new work is evident from the cursory observations made on new, ultra pure material, and (d) detailed comparisons of experiment and theory remain to be done.

TABLE OF CONTENTS

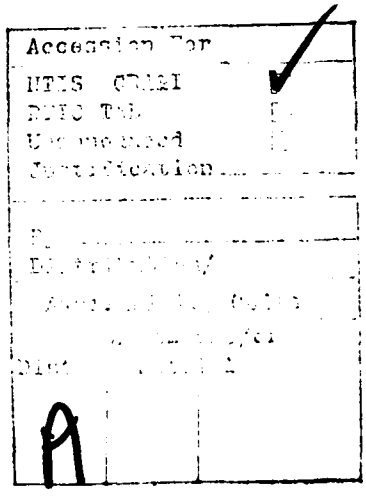

ILLUSTRATIONS

1. INTRODUCTION

The central theme of the work described in this Report is the effect of radiation upon the vector orientation of some characteristic properties of photo-excited carriers in semiconductors. The orientation is referred to the direction of propagation and is influenced by the polarization state of the exciting light in the medium.

Initially the object of this work was to study the optical properties of spin-aligned electrons. The interest was on how they could be produced optically, how they relax their spin polarization, and how they interact with other optical fields particularly those present in stimulated emission.

This work was encouraged by the extensive investigations performed by the group headed by Lampel[1.1] at Ecole Polytechnique and by the Russian workers at A.F. Ioffe Physicotechnical Institute on optical spin alignment. Additional stimulation was provided by prospects of using optical orientation phenomena for performing tasks utilizing optical-matter interactions for tasks now confined to the field of electronics which utilize interactions between electrical currents and matter. The optical matter interactions show promise of being faster and would be more practical in data transmission where the carrier is already optical, eliminating the need for repetitive cycles of conversion from optical to electrical and back again as a signal moves through the communication system. Conceptually a completely optical AND gate was demonstrated by us[1.2] in 1975 using dye lasers. Since that time various types of optical bistability and optical transistor action have been demonstrated.[1.3]

The material of choice for the study of these effects was GaAs, now rapidly emerging as one of the most important materials for a variety of optical and electronic applications. GaAs and its various alloys provide now the source for optical (fiber) communication and in the foreseeable future will become the basis of a new electronic technology likely to surpass the performance of silicon integrated circuits. In addition, for optoelectronic phenomena GaAs has the potential for miniaturation and incorporation in integrated circuits which would be virtually impossible using dye lasers as in our earlier work.

The implementation of GaAs technology requires a degree of basic understanding, probably unmatched in the history of Solid State Physics. The work which we are reporting has been helpful in delineating some of the properties, problems and promises of this fascinating material.

The choice of using orientational effects as a tool for studying a variety of interactions in GaAs has proved to be extremely rewarding and is likely to play an increasing role in the future.

The orientational characteristics of light, namely, its direction of propagation and state of polarization interact with the orientational characteristics of the carrier which fall under the following headings:

- spin angular momentum
- orbital angular momentum
- wave vector (direction of propagation)

Of these only the first is reasonably well documented in the literature. A full experimental and theoretical description of orienting and disorienting processes is a formidable task which we do not claim to have accomplished. As initially proposed we envisioned a three to five year program since we were all too aware of some of the difficult tasks required in the areas of developing a sufficiently sensitive and flexible experimental setup and in developing the concepts and detailed theory to understand the phenomena involved. As a result of several exigencies the program was shortened to a two-year program.

As the work progressed, various influences resulted in changes in emphasis. From our theoretical work and from experimental work by Russian workers,[1.4,1.5] it became obvious that spin alignment is only a special case of more generalized alignments involving orbital angular momenta and electron wave vectors. We have come to apply the term optical orientation to these general optical ordering phenomena. If one is to understand optical spin alignment one cannot ignore these more generalized effects.

The work is incomplete, but we have made progress of considerable consequence in the areas where we had anticipated difficulty. In fact, herein lies some of the longer term challenge and value. Bringing this line of work to full fruition and value both for the understanding of GaAs and as a possible source of new phenomena and uses requires:

a. development of novel experimental techniques

b. development of new theoretical approaches

c. development of improved material.

In the past two years (duration of this contract) item (a) has essentially been solved although it proved even more demanding than originally thought. Good progress has been made in item (b) but, as will be seen, this work remains unfinished. We believe however that the right questions have been posed and outlines of the theoretical structure formulated. Item (c) requires special comment and consideration. During the duration of this contract, fundamental strides in the preparation of bulk, pure, semi-insulating GaAs have taken place. Up to now we have only partially benefited from these most relevant developments and primarily through the courtesy of others.* We expect to take full advantage of these developments in the future.

The magnitude of the task and the particular dynamics of the thrusts (a), (b), and (c) leaves us in a situation where full benefits of these developments have not yet been realized. Expressing it in another way, the termination of the contract leaves the work at a point where:

- Experimental facility is fully operational
- A large body of data has been collected
- A good grasp of the theory is at hand

*J. Kafalas of MIT Lincoln Laboratories, presently at GTE Laboratories.

- A promise of very significant new work is evident from the cursory observations made on new, ultrapure material

- Detailed comparisons of experiment and theory remain to be done.

The synthesis of these developments fall, however, outside of the time frame of this particular contract. In the body of this report we shall describe fully the accomplishments without undue regard for the obvious lack of completeness and synthesis. We hope however to leave the reader with a clear and documented message that solid foundations have been laid for a very powerful new methodology and technique which will play a major role for the development of GaAs technology in the next few years.

2.0 EXPERIMENTAL SETUP

The basic experiment used in this study was to analyze the circular polarization of photoluminescence of GaAs type samples. The classical procedure for analyzing the polarization state of light involves a set of intensity measurements performed while one manipulates a linear polarizer and a $\lambda/4$ plate inserted into the beam. This procedure is simple but is lacking in several respects for our purposes. It does not lend itself very well to experiments where measurements over a range of excitation and emission wavelengths are required. Rotating optics are notorious for producing artifacts and are useless for detecting subtle effects in the polarization. Further, when close to resonance conditions between excitation and emission wavelengths are required, special precautions are required. A necessary additional requirement for the experimental setup is to be able to perform measurements of photoluminescence over several orders of magnitude to correlate with the polarization measurements.

A considerable amount of effort was expended during this contract period in developing a sensitive setup for routinely obtaining highly accurate polarization data over a wide range of photon energy and luminescent intensity. We describe in the following the experimental setup as it has evolved during the course of this work. As a result of the developments that have occurred, we are able to observe very subtle effects in the polarization of photoluminescence. We describe the results we have obtained in Section 3. Some of the difficulties we had to overcome to accomplish these measurements are described in the latter part of the section.

A block diagram of the experimental setup is shown in Figure 2.0.1. An infrared dye laser provides pulsed and tunable excitation light which can be polarized in any one of four states. This light excites a sample in a dewar and the photoluminescence is collected and either sent directly to the spectrometer or the intensity of alternate pulses rendered proportional to the two polarization components by the analyzer before entering the spectrometer. The output of the spectrometer is sensed by appropriate detectors and processed by either a two-channel photon counter or two-channel box car integrator depending upon wavelength and detector used. A crystal clock integral with the analyzer activates digital electronics which synchronizes the pulsing of the dye laser and the data processing of the photon counter or box car integrator. A microprocessor communicates with the dye laser, sample dewar, spectrometer and photon counter (box car) monitoring and orchestrating their performance and receiving and reducing data. The digital data can then be printed; converted to analog data, and read out on an x-y recorder or sent to the main computer for more extensive data reduction. The latter two functions are just now being implemented.

2.1 Excitation Source

The excitation source is shown in Figure 2.1.1. It consists of a Spectra Physics Model 375 dye laser pumped with a Spectra Physics Model 171 Krypton ion dye laser with accessories for cavity dumping and mode locking. This is a very flexible setup. Depending upon the particular configuration of components various combinations of output intensity and pulse widths are available. Examples of these are cw dye laser output of 0.5 W and 20 picosecond pulses of 1.5 kW at frequencies up to 2 megahertz. Narrower pulses can be obtained at a sacrifice of power and higher output intensity pulses can be obtained directly from the ion laser at the sacrifice of tunability. With suitable dyes the tuning range varies from the green to beyond 1.0 micron, with shorter wavelength lines available from the ion laser.

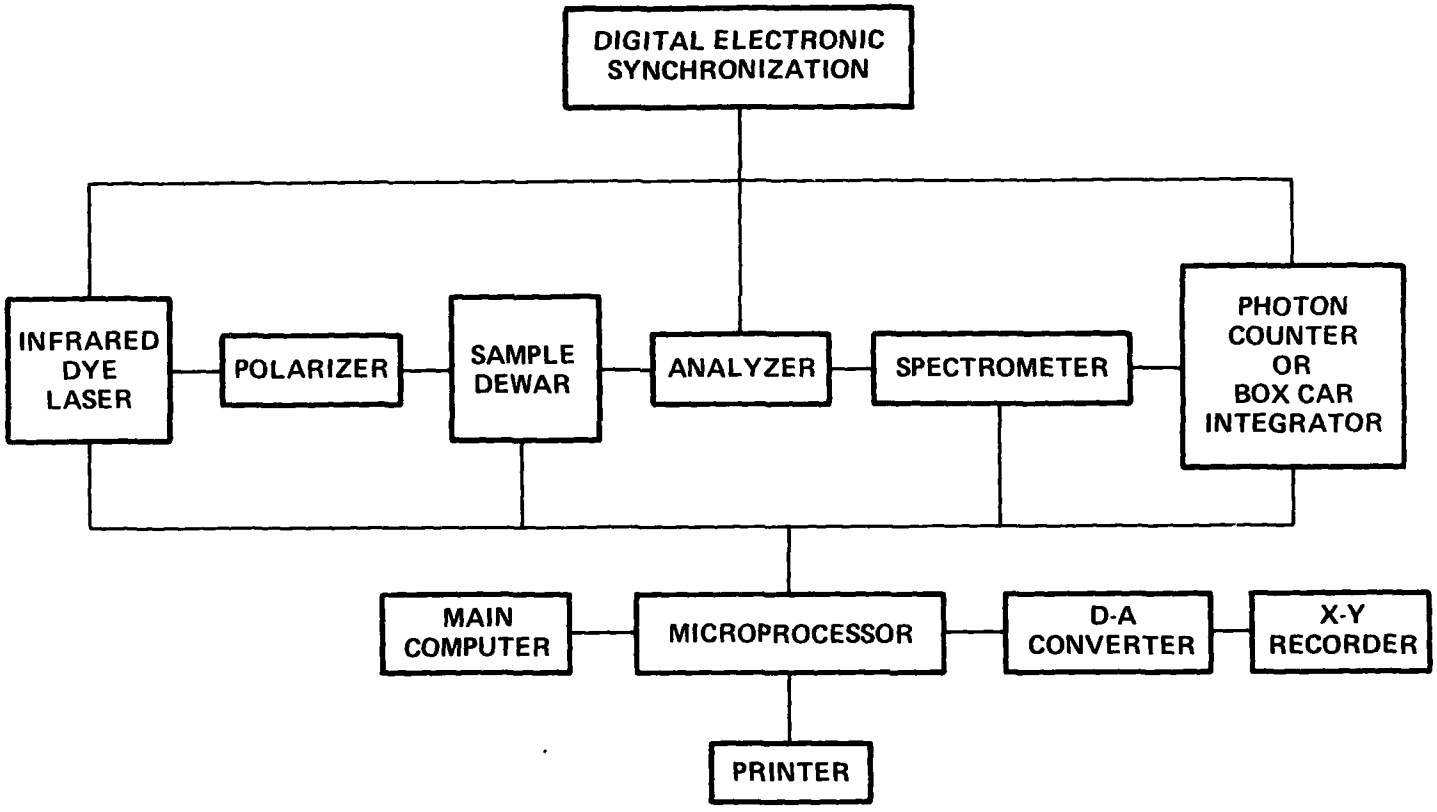

Figure 2.0.1. Experimental Setup

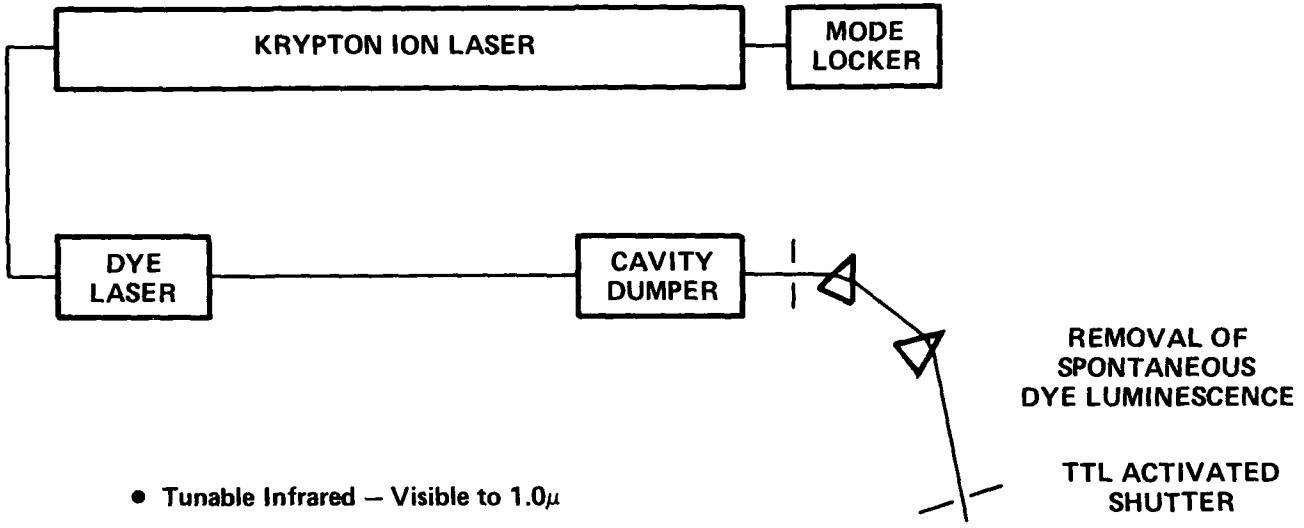

Figure 2.1.1. Excitation Source

The output from any dye laser is contaminated by a tail of spontaneous emission that extends surprisingly far to the long wavelengths. When observing weak sample luminescence, it is important to remove this spontaneous dye emission from the exciting beam - this is accomplished using a pair of apertures and two small prisms. The second aperture is incorporated in a TTL activated shutter obtained from UniBlitz which is operated by the microprocessor and serves the additional function of providing a means of periodically observing the dark counts on the photomultiplier during a measurement. Our present arrangement for removing the spontaneous emission results in a 50% insertion loss. We expect to reduce the insertion loss using Brewster angle prisms or spatial filtering.

2.2 Sample Arrangement

The sample arrangement is shown schematically in Figure 2.2.1. The sample is contained in one of two types of dewars - one an Air Products continuous flow cryostat which permits sample temperatures from about 10°K to 300°K and a glass dewar [2.1] that permits immersion in liquid helium and sample temperatures near 1.7°K.

The light from the source is rendered approximately circularly polarized using a $\lambda/4$ retardation plate. This is followed by a Glan-Thompson polarizer and a Fresnel Rhomb. By rotating the polarizer between positions $\pi/4$ apart any one of the four states of polarization can be obtained with approximately the same intensity. The light is focused on the sample by the edge of a lens of focal length 4.5 cm and aperature f/3. The photoluminescence is collected and collimated by the same lens with the normal to the sample lying along the optical axis of the lens. The specular reflection from the sample is removed by stopping the lens down to f/8. The angle between the incident beam and the principal ray of the luminescence is on the order of 9° to minimize distortion of the circular polarization.

The heart of the polarization analyzer is a piezoelectrically driven time varying retardation plate (Morview Model PEM3) with retardation varying from + $\lambda/4$ to - $\lambda/4$ at 50 kHz, for analyzing circular polarized light. Additional retardations are available for analyzing for linear polarization. In an alternative arrangement, the Fresnel Rhomb and the time varying retardation plate can be interchanged. A simple analysis shows that these two arrangements result in essentially the same operation, with the difference that in the second arrangement the sample is excited in each pulse by light oppositely polarized to that in the previous pulse. This arrangement is important in isolating effects due to nuclear spin alignment which has exceedingly slow relaxation times.

The piezoelectrically driven retardation plate also acts as a crystal clock and provides a timing pulse to synchronize the firing of the pulse laser only at retardations of + $\lambda/4$ and - $\lambda/4$ and to synchronize the data processing of the photon counter and the box car integrator. Associated electronics were developed for this purpose.

The time varying retardation plate converts the alternately circularly polarized components into linearly polarized components which pass the polarizer on alternate pulses. These pairs of pulses are spectrally analyzed by the Spex Model 1404 Double Monochrometer, the spectrometer with a stray light rejection of 10^{14} permits near resonance photoluminescence experiments.

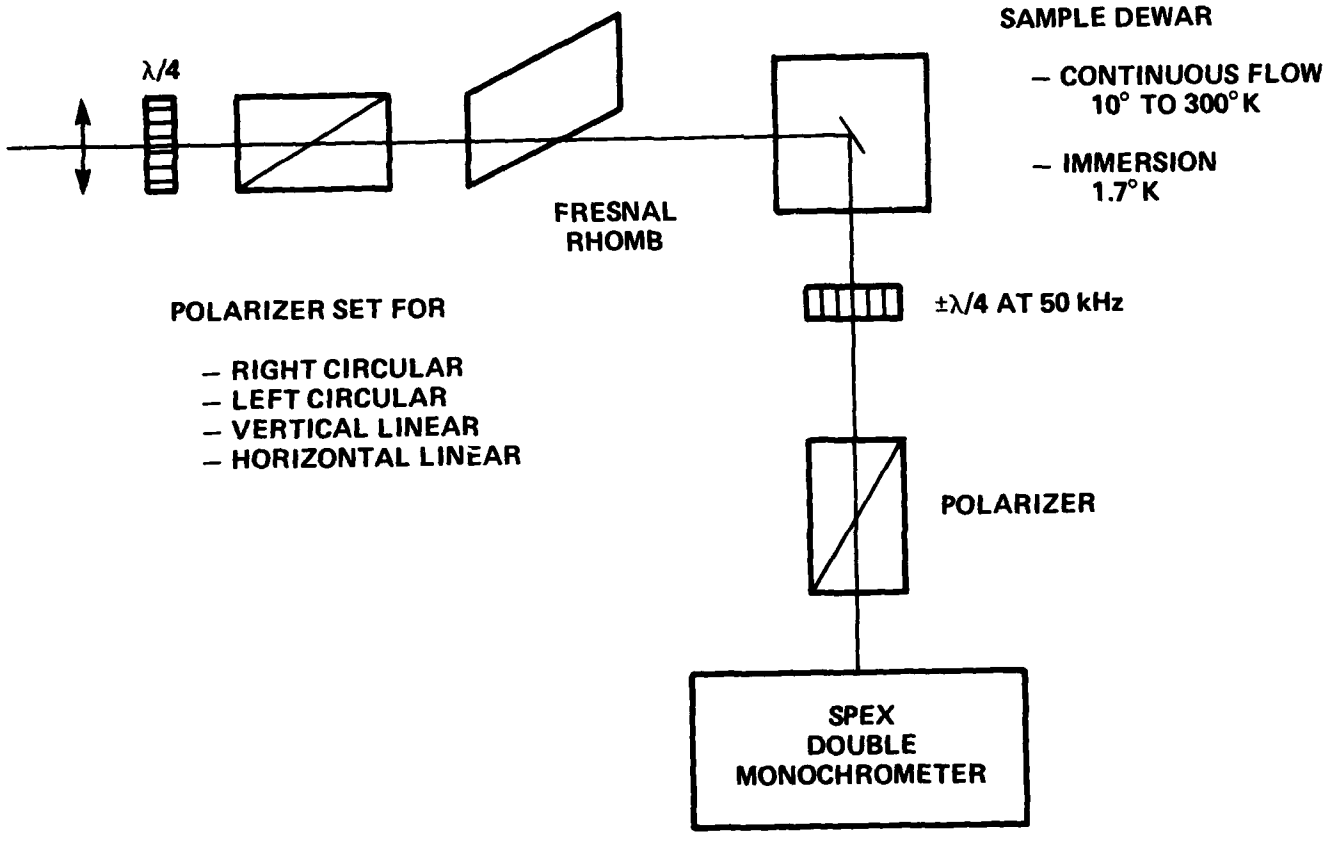

Figure 2.2.1. Sample Arrangement

2.3 Detection System

Different detectors and data processing electronics (shown in Figure 2.3.1) are used depending upon the wavelength region and the sensitivity required. For the visible to about 0.95 microns, a cooled GaAs photomultiplier (RCA Model C31034A) and a PAR Model 1112 two-channel photon counter with a Model 1121 amplifier-discriminator is used.

For the range 0.95 to 1.8 microns, we are in the process of incorporating a cooled germanium detector into the experimental setup. For use with the piezoelectric driven retardation plate and a PAR Model 162 Box Car integrator, we will use a cooled germanium detector (North Coast Model EO-817P) capable of a 300 nanosecond response and an NEP approaching 2×10^{-14}W. For greater sensitivity a slower germanium detector (North Coast Model EO-817L) will be used with an NEP of 10^{-15}W. For polarization measurements a stepwise (90° steps) rotating quarter waveplate assembly has been constructed, since this detector cannot follow the peizoelectric driven retardation plate. This slower mechanically driven time varying retardation plate has some of the usual disadvantages of rotating optics but can be used with highly sensitive but slow infrared detectors and can be used with a duty cycle as large as 90%.

2.4 Computer Analysis and Orchestration of Experiments

The output of the photomultipler or infrared detector consists of twin pulses corresponding to the intensities of the two polarization components. These two signals are demultiplexed by appropriate gating derived from digital electronics activated by the clock pulses from the piezoelectrically driven retardation plate. The box car integrater provides dual analog signals. Appropriate analog circuitry using op amps have been built to operate upon these signals to produce dc outputs proportional to the polarization and to the luminescence intensity which are plotted on a chart recorder. However, analog data processing is notoriously unstable and using the box car in a linear averaging mode with weak signals produces severe problems with dc zero line drift. We are in the process of setting up a new arrangement using analog to digital conversion, exponential averaging and a microprocessor which should minimize most of these problems.

We have incorporated microprocessor techniques into our experiments when we utilize the cooled GaAs photomultiplier and photon counting. Much of this work was performed in our laboratory by a summer student, Lauren Martens, from Harvey Mudd College the summer of 1980 under a NSF Industrial Undergraduate Research Participation Grant to the University of Nevada, Reno. A copy of his report is enclosed in the Appendix.

The work consisted in interfacing all of the appropriate instruments to an AIM 65 microprocessor so that each of these instruments could be interrogated for data and controlled to orchestrate their performance in an experiment. A block diagram of the interfacing is given in Figure 2.4.1. The various interfacing tasks required extensive hardware expansion of the AIM 65 and additional software development.

In a typical experiment after the command to initiate an experiment, the AIM asks the operator for the initial wavelength, the stepping interval and number of points to be taken along with sample information. Upon receipt of this information the AIM drives the spectrometer to the initial wavelength and commands the photon counter to begin counting. When the count is completed the AIM collects the data, performs the desired calculations, and prints out the photon-energy, photoluminescence intensity and polarization. The spectrometer advances to the next point and repeats the cycle as needed. Additional functions of the microprocessor are to maintain

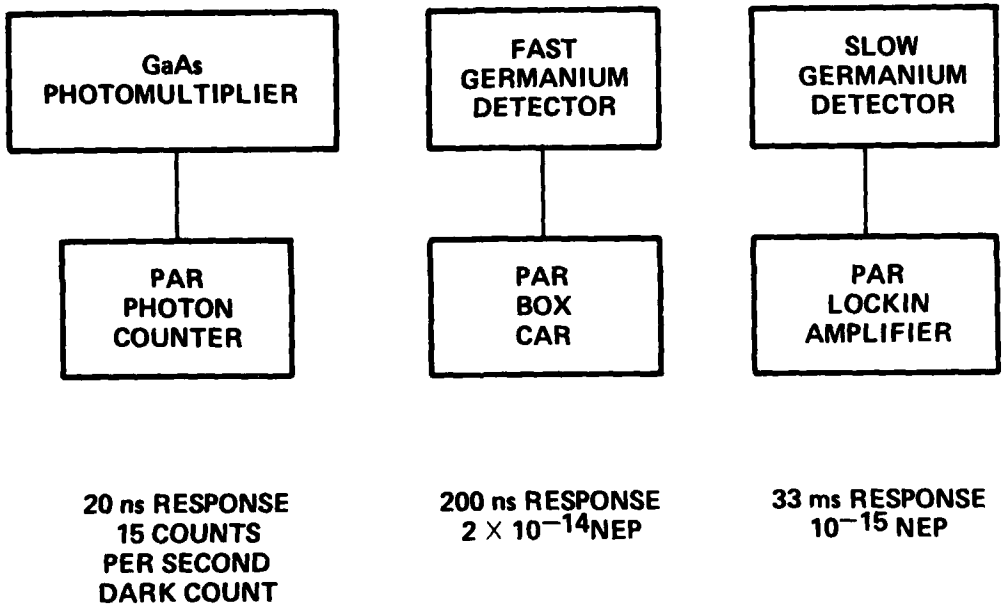

Figure 2.3.1. Detection System

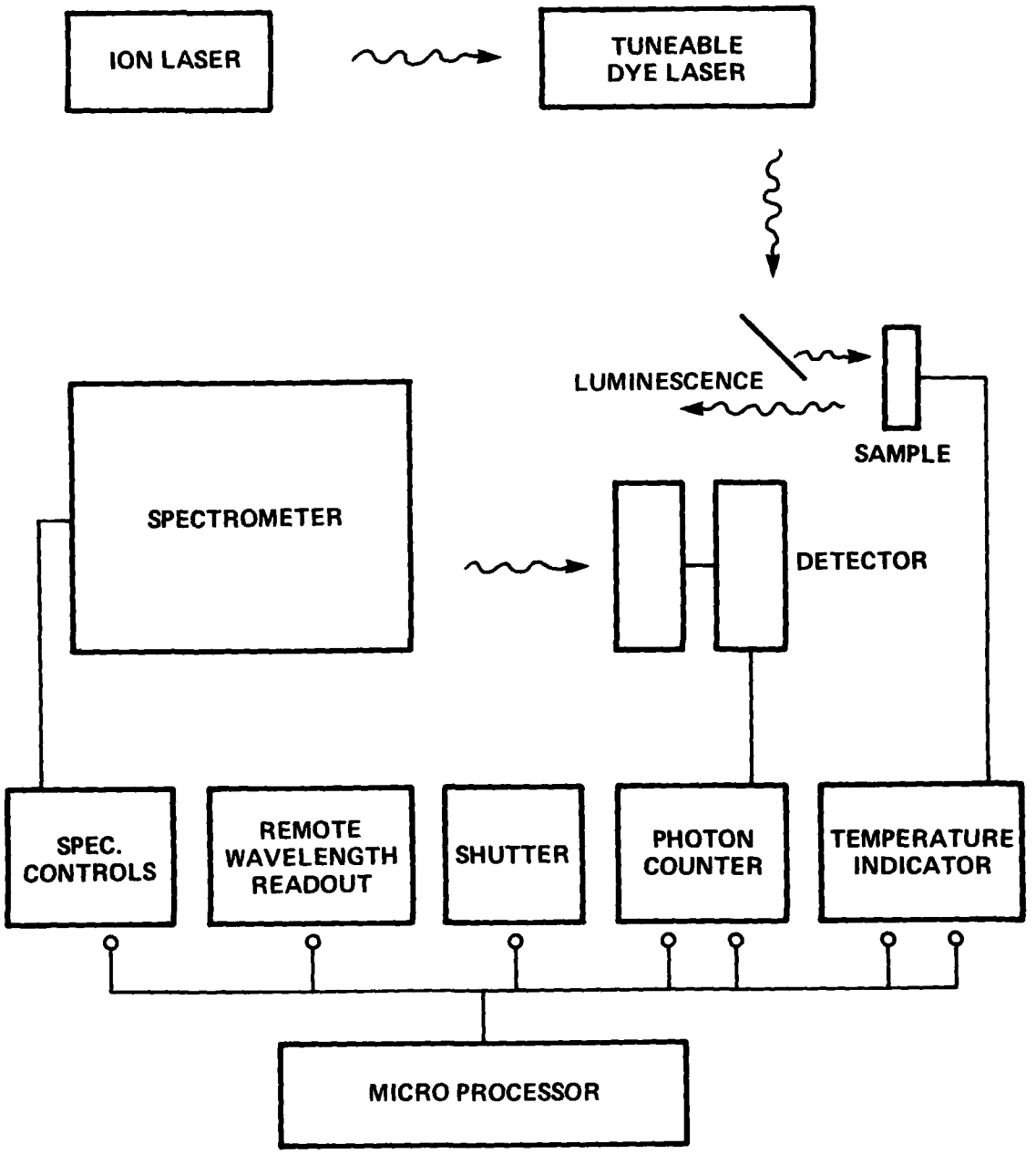

Figure 2.4.1. Interfacing with Microprocessor

a constant signal-to-noise ratio as the intensity of the luminescence varies, monitor and correct for dark counts via a TTL activated shutter, and monitor the sample temperature. Additional features planned are to monitor and correct for source fluctuations and locate peaks. With the main computer for more complicated data analysis, we will be able to account for such things as spectrometer and detector spectral response.

2.5 Developments of Tunable Pulsed Sources

This sensitive setup for observing luminescence and analyzing the polarization of the luminescence was not available except toward the end of the two years of the contract period. The concept for using a pulsed laser as excitation source synchronized to a piezoelectrically driven retardation plate was new and good tunable pulsed lasers for the near infrared are still in the state of development. Different modes of operation needed to be tested as well as techniques for performing the data processing electronically. Initially it was not appreciated how important it was to be able to observe polarization in the far wings of the photoluminescence. The obvious solutions to these problems were to purchase and incorporate photon counting electronics and a Spex double monochrometer into the experimental setup. All this lead to investing more time into the development of the experimental setup than was anticipated. Some of this work will be discussed in the next pages.

Developing a suitably intense pulsed laser source for exciting luminescence has provided some difficulties. We require a tunable laser with pulse widths less than 2 microseconds and repetition rates of 100 kHz. Initially, it appeared that an infrared dye laser pumped with a cavity-dumped Krypton ion laser was the easy way to go. However, cavity dumping techniques were new and we have had to investigate their subtleties and to modify our approach.

Experience and theoretical analysis of pumping lasers with short pulses has shown that, for efficient operation, one must operate the ion laser cw and cavity dump a long cavity dye laser. We are in the process of preparing a manuscript describing this analysis.* Below we give a brief summary of the results.

The conditions that must be satisfied if a dye is to lase under short pulse conditions are (1) threshold inversion must be attained sometime during the pumping pulse and (2) the inversion must remain above threshold long enough for the photon flux to build up by on the order of 12 orders of magnitude. Theoretical analysis shows that these two requirements can be satisfied if a certain energy threshold is exceeded independent of the pulse width over a wide range. For short pulses this may require pumping intensities orders of magnitude greater than the cw threshold intensity. The situation is made even worse by the insertion loss of the cavity dumper in the laser cavity which may be as much as 90%.

If the lifetime of the dye is much shorter than the pump pulse width, the energy threshold is given by:

$$E_t = (W_t)_{cw} \left[T + \frac{2\ell}{c} \quad \frac{\ln Q_o}{\ln \frac{1}{R}} \right] \tag{2.5.1}$$

where $(W_t)_{cw}$ is the cw intensity threshold T is the pulse width, $\frac{2\ell}{c}$ is the laser transit time, R is the reflectivity of the output mirror and Q_o is the number of modes in the gain band width, typically on the order of 10^{12}.

*This analysis was conducted in conjunction with work on short pulse pumping of Transition Metal Complexes under AFOSR Contract No. F4962-77-C-0015.

Once one has satisfied the energy threshold one must consider efficiencies. For short pulses, the maximum energy per pulse in the dye laser output is approximately that energy stored in a time equal to the dye lifetime. Therefore for constant energy pulses with widths greater than the dye lifetime, the output intensity per pulse is approximately inversely proportional to the pump pulse width, favoring short pulse widths. For longer, more intense pulses significant pumping occurs after the onset of lasing and one can get efficiencies approaching cw. The shortest pulses in a cavity-dumped Spectra Physics Model 166 ion laser is about 15 nanoseconds. With dye lifetimes on the order of nanoseconds this would give a maximum efficiency of about 7%. Calculation of the threshold intensity under 15 nanosecond pulsed operation indicates an increase by a factor of about 98 over cw threshold. Since cavity dumping increases intensities by only about 10 - 30 X cw intensities, achieving threshold is even more difficult with cavity dumping. This agrees with our experience. Dyes with cw thresholds just below the maximum output of the ion laser lase poorly cavity dumped. Dyes with somewhat lower cw thresholds lase much better cavity dumped.

In pumping dyes with short pulses, an additional effect occurs which we attribute to the inversions associated with the much higher pumping intensities required to obtain lasing during a short pulse. Experimentally we find that the high inversions shift the dye absorption edge to shorter wavelengths. As a result the dye lases initially at significantly shorter wavelengths than cw and chirps (sweeps) to longer wavelengths. Averaged over a pulse this has the same effect as a broadening of the laser output. These considerations lead to the conclusion that the preferable technique for obtaining high frequency dye lase pulses is to use an ion laser of greater output capacity and operate the ion laser cw and to cavity dump the dye laser. These measures we implemented during the duration of the contract.

2.6 Summary

During the course of this work, we have developed a sensitive setup for simultaneously observing the photoluminescence intensity, and the photoluminescence polarization over several orders of magnitude in intensity and a wide range of exciting and emission photon energies. This sytem is automated and prints out reduced data. Extensive work went into developing this setup based upon synchronizing the pulsing of a dye laser with the operation of a piezoelectrically driven retardation plate, particularly in regard to incorporating a suitable pulsed laser source. The work that has gone into the development of this experimental setup has proven to be very fruitful and has enhanced greatly the quality of the experimental data taken in the latter stages of the contract.

3.0 EXPERIMENTAL RESULTS

The principal objective of the experiments was to observe the variation of circular polarization of the photoluminescence with photon energy. However, one must first characterize the samples by measuring the photoluminescenic spectrum to show what transitions are occurring in the photoluminesce and to provide the basis for understanding structure observed in the variation of circular polarization with energy.

We have studied luminescence for five types of samples:

1. a p-type GaAs sample doped with germanium and zinc, $p = 2,3 \times 10^{18}$ cm^{-3}
2. a GaAlAs film on a GaAs substrate
3. a semiinsulating sample heavily doped with Cr ($\rho \approx 10^{8} \Omega$ cm)
4. an insulating sample with no intentional doping ($\rho \approx 10^{8} \Omega$ cm)
5. and a p-type InP sample (Zn, $p = 2 \times 10^{18}$ cm^{-3}).

Polarization measurements on most of these samples have been performed, although at this point these measurements have to be considered as preliminary survey measurements that point the way to extensive studies which have potential for unraveling some of the mysteries of the relaxation dynamics of photo excited carriers.

The most promising material for such studies is the pure insulating GaAs which was grown at Lincoln Laboratory by Jim Kafalas who is continuing the development of the growth of such material at GTE Laboratories. This material is further of extreme technological interest since a long standing problem in GaAs I.C. technology is the fabrication of suitable insulating substrate material. From the viewpoint of polarization studies this material is very interesting. As in the case of Cr-doped semi-insulating GaAs all the carriers that participate in the band edge photoluminescence are nonequilibrium carriers. This provides a situation where both the electrons and the holes can be optically oriented. Further, the transitions involving the various carrier-exciton-impurity complexes involved in the dynamics of recombination are well resolved.

3.1 Photoluminescence

In Figure 3.1.1 we show the luminescent spectrum observed over four orders of magnitude for a p-type sample of GaAs doped with Zn and germanium at 4.5K excited by pulsed dye laser light at 1.710 eV.

The spectra is dominated by conduction band to acceptor level transitions, which can be identified by reference to spectra reported in literature.[3.1, 3.2] There are peaks at 1.482 due to Ge and 1.491 due to Zn with a shoulder at lower energies probably due to an additional unidentified acceptor. At low intensity levels two shoulders occur apparently due to internal electron transitions involving complexes of vacancies with germanium and silicon respectively.

The luminescence drops sharply on the high energy side of the conduction band to Zn acceptor level peak and at higher energies shows a tail probably due to transitions involving electrons high in the conduction band. The initial portion of the tail is approximately linear on the semilog plot which would seem to indicate quasi thermalized electrons with an electron temperature obtained from the slope of about 95°K.

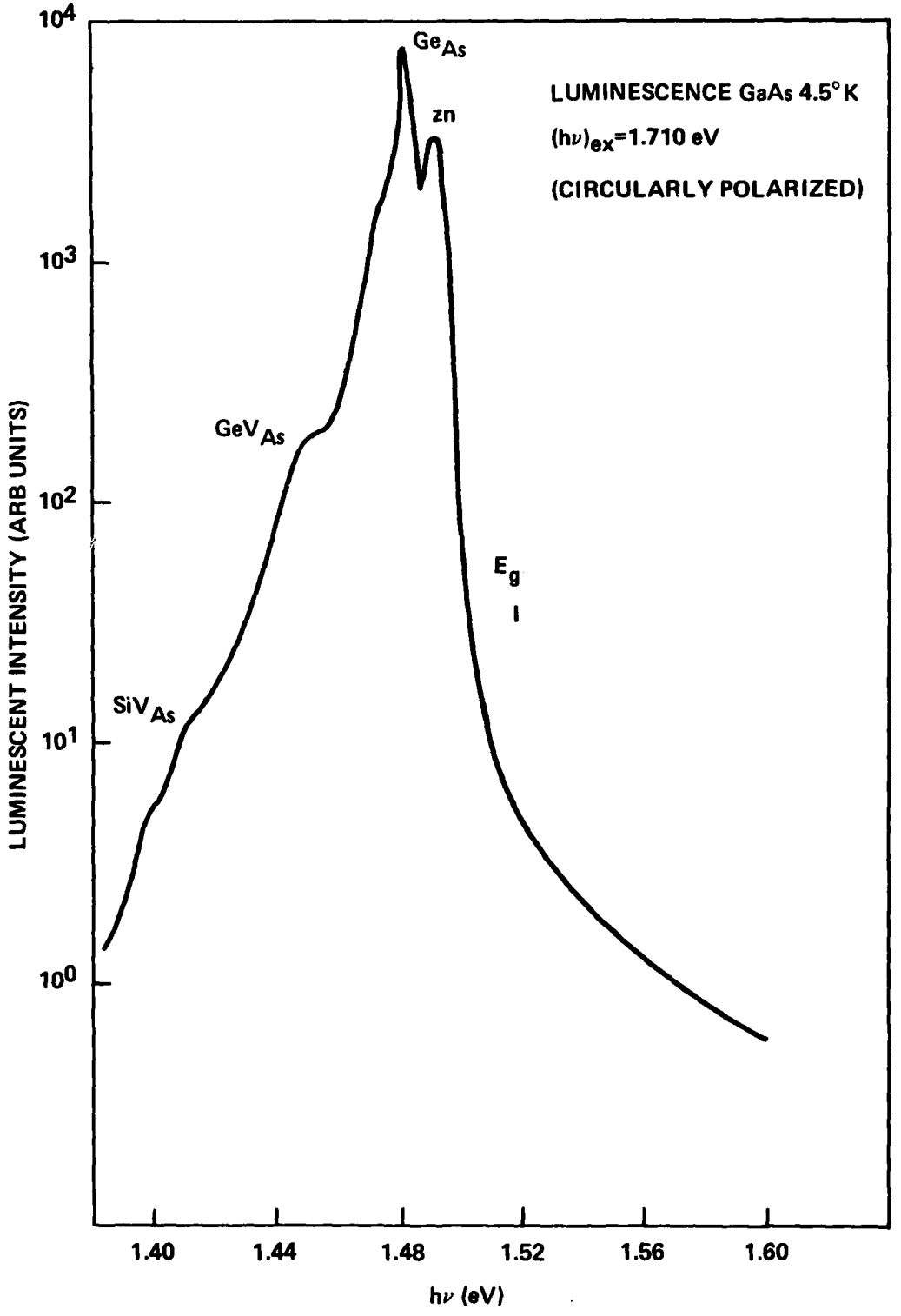

Figure 3.1.1. Luminescence GaAs 4.5°K $(h\nu)_{ex}$ = 1.710 eV (Circularly Polarized) (Sample 1)

Previous work 3.3 has shown that under illumination conditions appropriate to photoluminescence experiments electron temperatures considerably in excess of lattice temperatures can exist. At higher energies the slope decreases perhaps indicating a transition to nonthermalized electrons as the excitation energy is approached.

In Figure 3.1.2 we show the edge luminescence at 10°K for a chrominum doped semi-insulating sample. The excitation photon energy was 1.7669 eV. The luminescence posseses a double peak one corresponding transitions from the conduction band to a carbon acceptor and one occurring near energies corresponding to transitions involving an exciton, an exciton bound to a neutral donor and an excitor bound to an ionized donor. These transitions are not resolved and the high energy side appears to be dominated by broadening of these transitions. If quasi thermalized free carrier recombination is present on the high energy side the slope would indicate a maximum electron temperature of 58°K. The luminescence falls off slowly at low photon energies which, by comparison with Figure 3.1.3, would indicate a series of unresolved transitions.

In Figure 3.1.3 we show the photoluminescence under cw excitation at 1.650 eV for ultra pure insulating GaAs grown by J. Kafalas of Lincoln Laboratory. This material had no intentional doping and was grown with liquid encapsulation by the Czochralski method. The room termperature resistivity is 10^8 Ωcm comparable to the best chromium doped semi-insulating material.

Several sharp features are apparent in the spectrum indicating that the material is indeed quite pure. These are illustrated better in the succeeding figures.

The photoluminescence of this sample has shown some very strange behavior particularly when the material was freshly grown and freshly etched. Most of the measurements reported here were made after the sample had aged somewhat and earlier instabilities in the spectrum had settled down.

The original data taken at 10°K showed a single peak characteristic of exciton transitions but shifted to lower photon energies. On the low energy side there was no luminescence attributable to transitions involving impurities. The high energy side shows a linear portion characteristic of band to band transitions. As shown in Fig. 3.1.4 both the peak position and the apparent electron temperature vary with excitation energy. These are both approximately linear as shown in Fig. 3.1.5. There are two possible explanations to this strange behavior. Either one was observing an electron hole plasma and band gap renormalization under cw excitation or a trivial heating effect occurred in some way. The former might occur if the fresh sample had an exceedingly low surface recombination velocity which deteriorated with time. Indeed some of the spectral instability was traced to the presence of a film of vacuum pump oil on the surface of the sample. The temperature effect would appear to be ruled out since a chromel iron doped gold thermocouple attached to the sample indicated a temperature of 10°K compared to lattices temperatures on the order of 80° required to explain the behavior as a trivial heating effect. Further, subsequent measurements indicate electron temperatures comparable to the earlier measurements but the peak positions indicate lattice temperatures comparable to the 5-10°K indicated by the thermometer. However, time has not permitted detailed attempts to establish precisely the source of these instabilities. It is suspected that conditions at the surface are responsible and experiments using both excitation and further surface treatment are planned.

Also in Fig. 3.1.4 we show the photoluminescence after the surface conditions had stabilized. The principal peak shifted to a position close

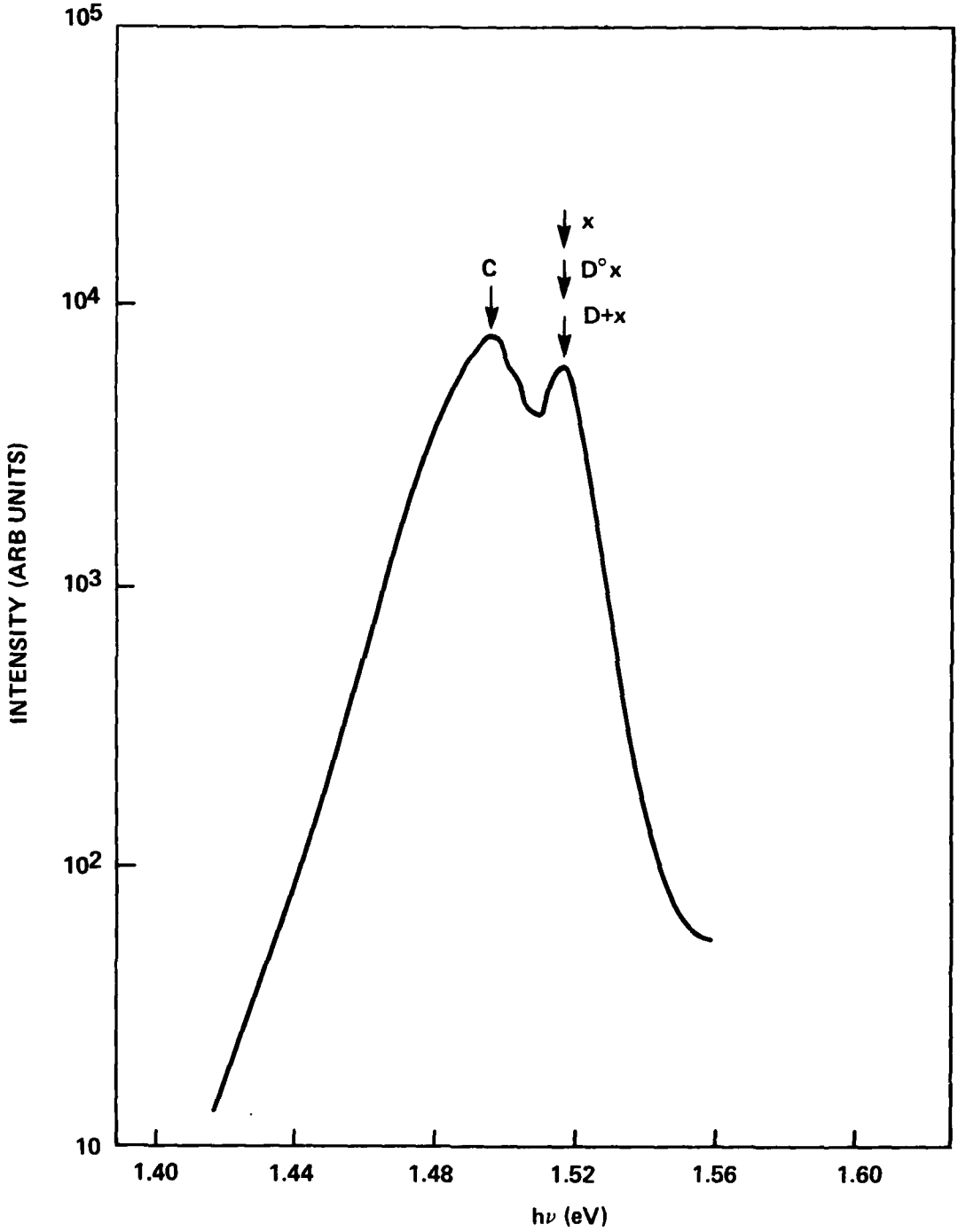

Figure 3.1.2. Photoluminescence of Chromium Doped GaAs (Sample 3)

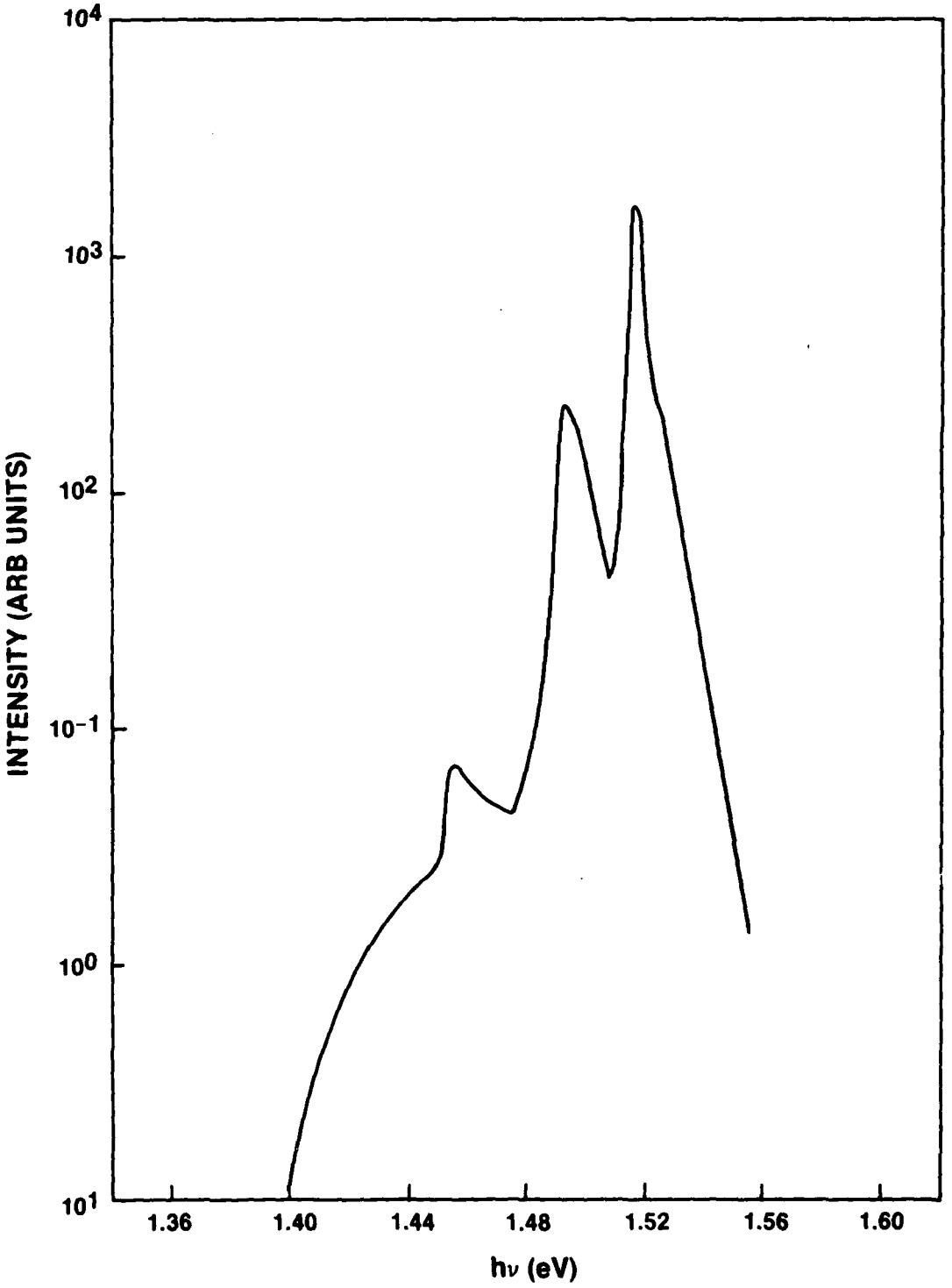

Figure 3.1.3. Photoluminescence of Ultra Pure Insulating GaAs (Sample 4)

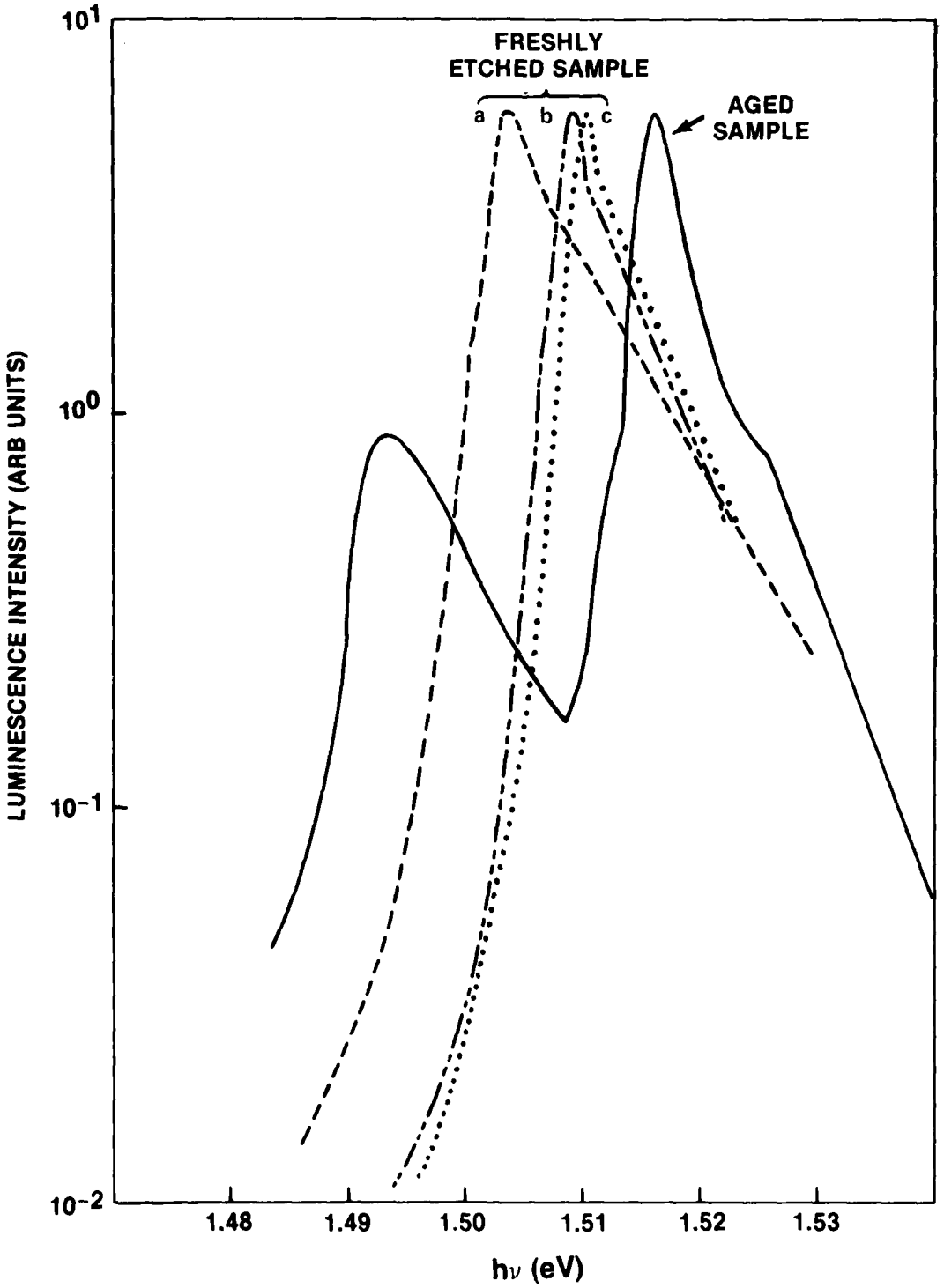

Figure 3.1.4. Photoluminescence of Ultra Pure GaAs Under Different Conditions: Excitation Intensities (a) 0.5 watts (b) 0.1 watts (c) 0.01 watts

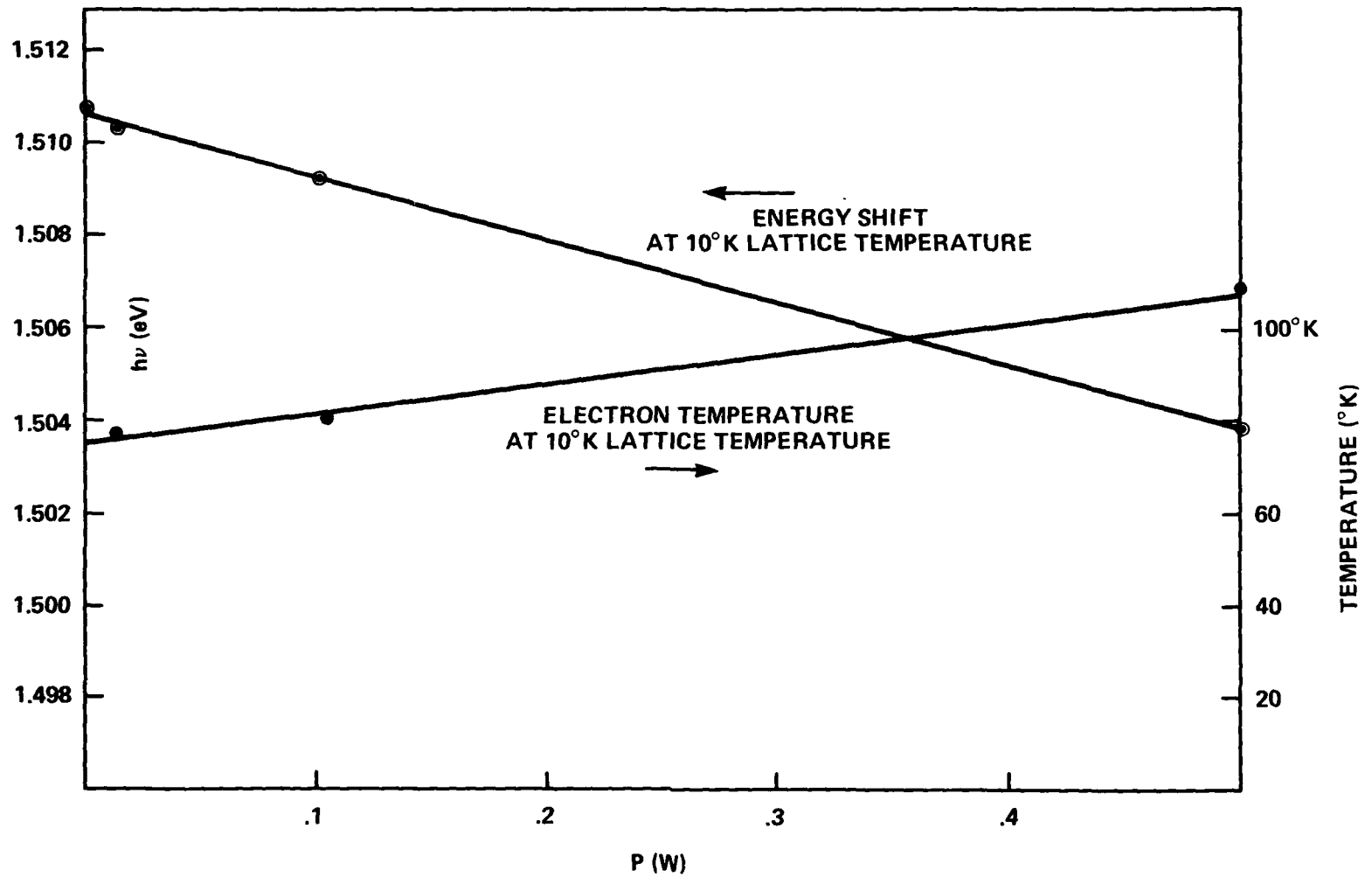

Figure 3.1.5. Shift of Photoluminescence Peak and Electron Temperature with Change in Excitation Intensity

to the free exciton position and luminesce involving acceptors show up at lower photon energies. Details of this spectra are shown in expanded scale in the subsequent figures.

In Fig. 3.1.6 we show details of the main peak which occurs at 1.516 eV and agrees well with published values for the free exciton energy.

On the high energy side a expedential region occurs indicating transitions by free electron hole pairs with an electron temperature of 67°K. On the lower energy side a shoulder occurs which may be remnant of an electron-hole plasma or a two hole transition[3.2] involving an exciton and a neutral carbon acceptor.

In Fig. 3.1.7 we compare the data of Fig. 3.1.6 with similar data taken at a low excitation level. The main peak broadens out and shows structure that can be attributed to transitions involving excitons, complexes of excitons with neutral and ionized donors and two hole transitions involving an exciton neutral acceptor complex. Subsequent measurements indicate that even better resolution of this structure is possible.

In Fig. 3.1.8 we show the luminescence associated with conduction band to ionized acceptor transitions. The principal peak appears at 1.4933 eV and is probably due to a carbon acceptor. Some small wiggles occur at intensity levels more than an order of magnitude lower. Comparison of the photon values with published data would indicate that these may be associated with silicon and germanium acceptors. However subsequent measurements have shown sharp line transitions in this region which may indicate a more complicated source for these transitions.

In Fig. 3.1.9 the photoluminescence at the lowest intensities is shown. There is a sharp peak superimposed upon a broad luminescence. The sharp peak appears at 1.454 eV which is removed by 39 meV from the main acceptor peak which suggests that it may be associated with a band to carbon acceptor transition involving the emission of an optical phonon.[3.4] The broad luminescence is probably associated with a germanium-arsenic vacancy complex. [3.5]

3.2 Polarization Measurements

In Figure 3.2.1 we show the polarization spectrum for the p-type sample doped with Zn and germanium at a series of sample temperatures ranging from 4.2K to 76K. A considerable amount of structure is observed some of which can be correlated with features in the luminescent spectrum and some cannot. For each temperature there is a peak in the polarization somewhere near 1.50 eV, which might be loosely associated with the two principal peaks in the luminescence spectrum. At lower energies the polarization decreases showing plateaus apparently associated with the different transitions seen in the luminescent spectrum. For energies greater than 1.5 eV the polarization is particularly temperature sensitive. At low temperature it decreases accentuating the 1.5 eV peak, whereas at higher temperatures it increases well beyond the peak.

The simplest model one could hope to apply to the polarization spectrum would assume that the luminescence is dominated by transitions from the conduction band to the Zn acceptor. One would assume that the electrons in the conduction band are in quasi-thermal equilibrium such that the population of electrons of each spin can be characterized by individual quasi-Fermi levels. Further, one would assume that only the spins of the electrons retain their optical alignment and the holes do not contribute to the polarization. In this case as discussed in the theoretical section the variation of the polarization with energy would be monotonic being

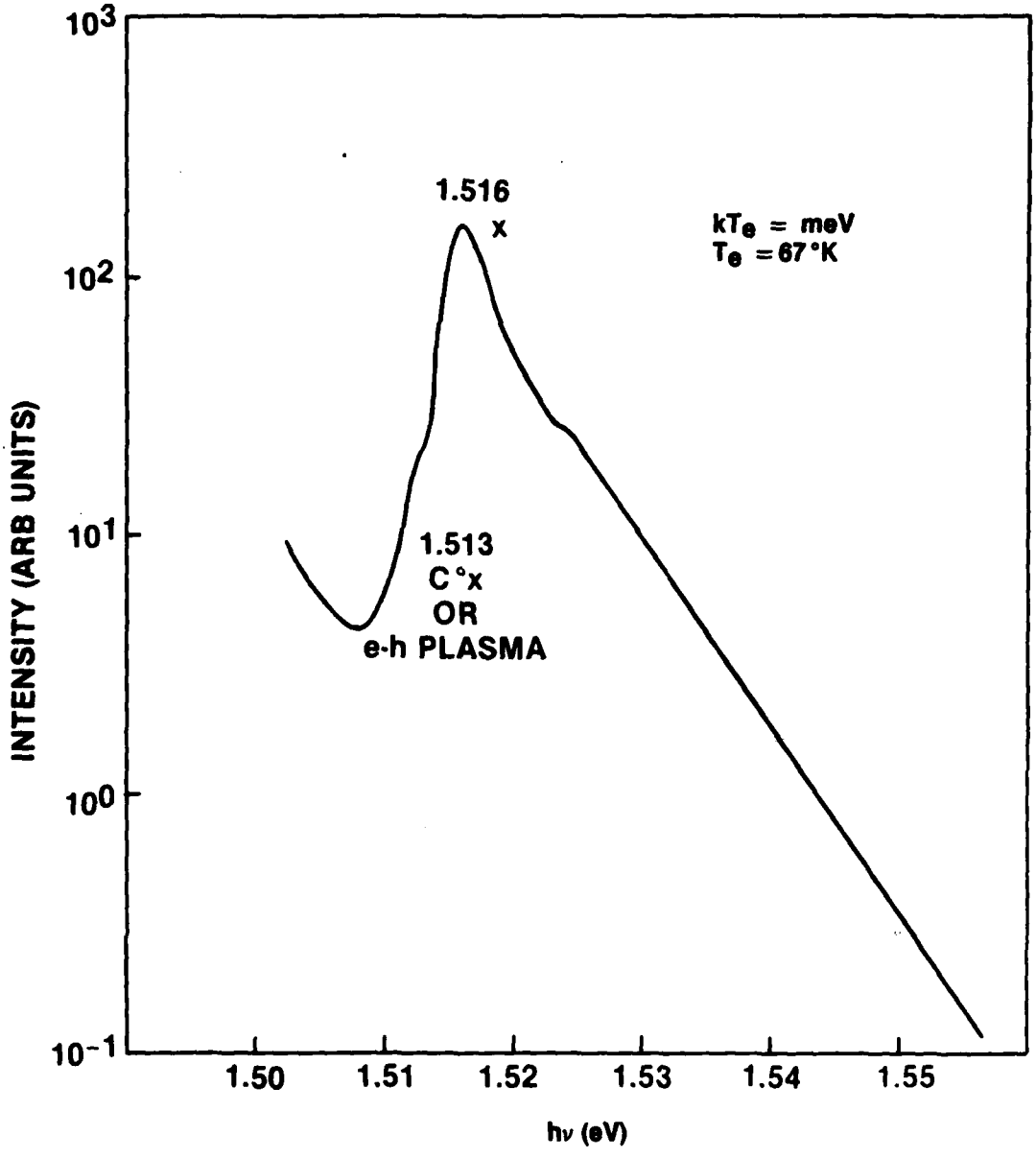

Figure 3.1.6. Photoluminescence in the Exciton Region for Ultra Pure GaAs

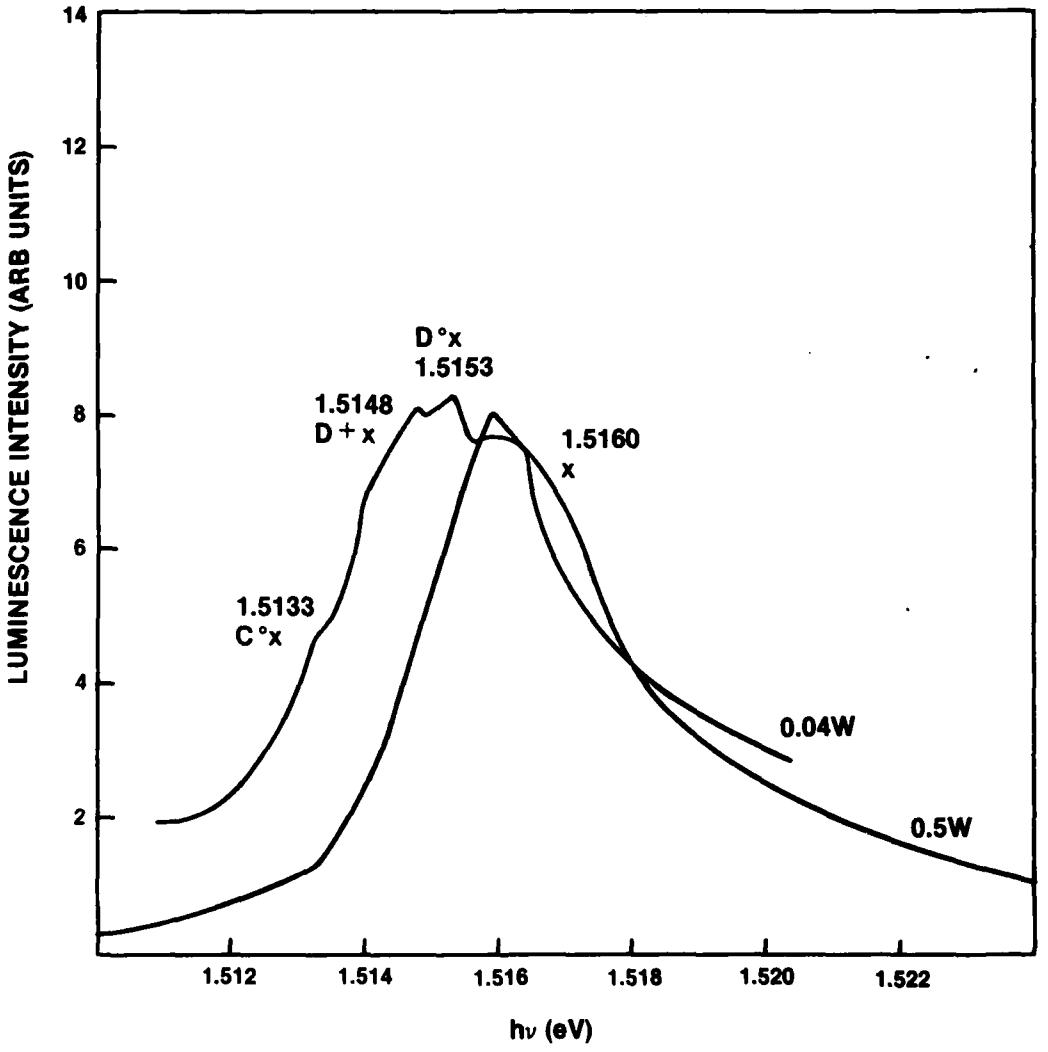

Figure 3.1.7. Structure Observed at Low Excitation Intensities Near the Exciton Peak for Ultra Pure GaAs

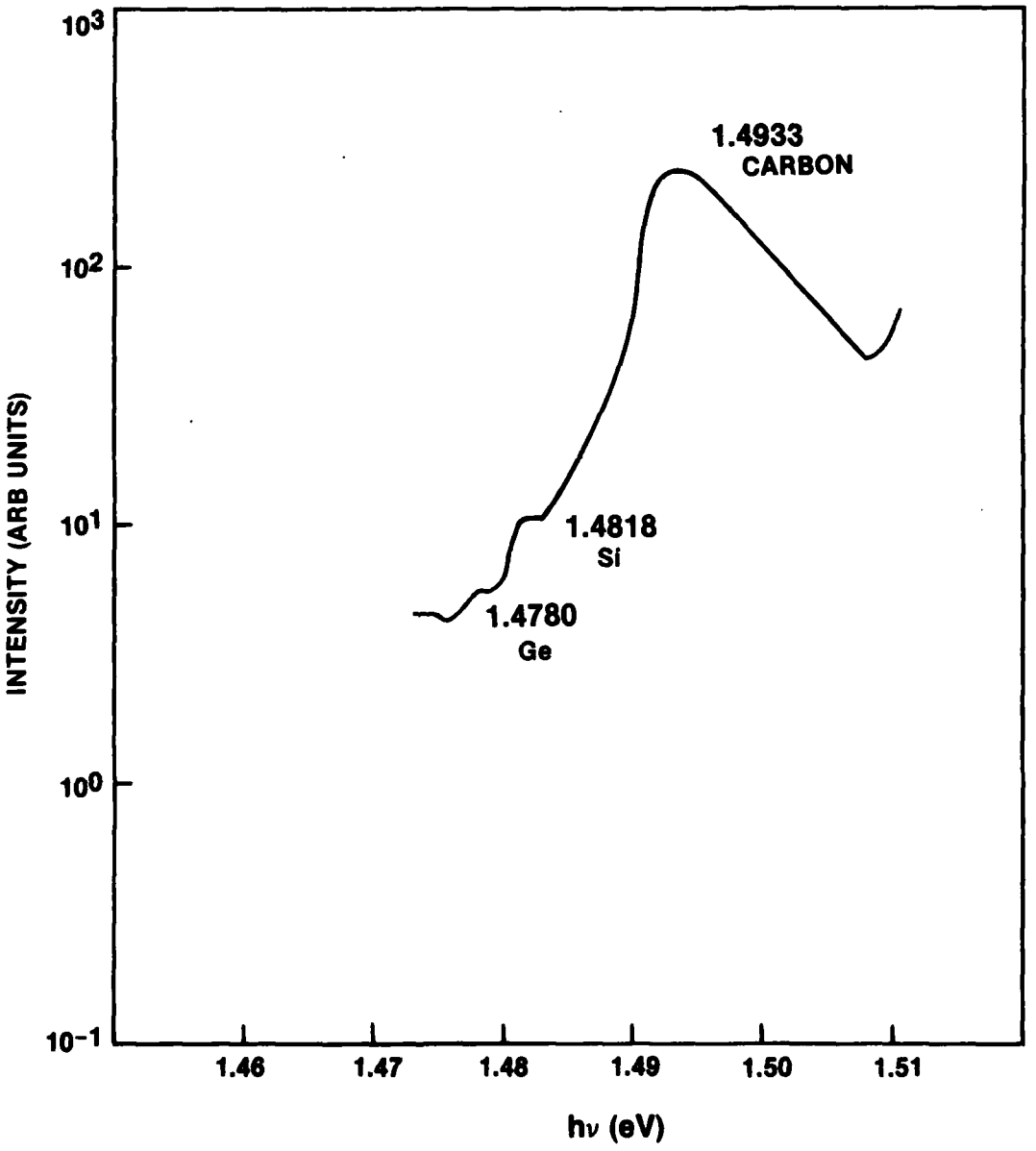

Figure 3.1.8. Acceptor Related Photoluminescence for Ultra Pure GaAs

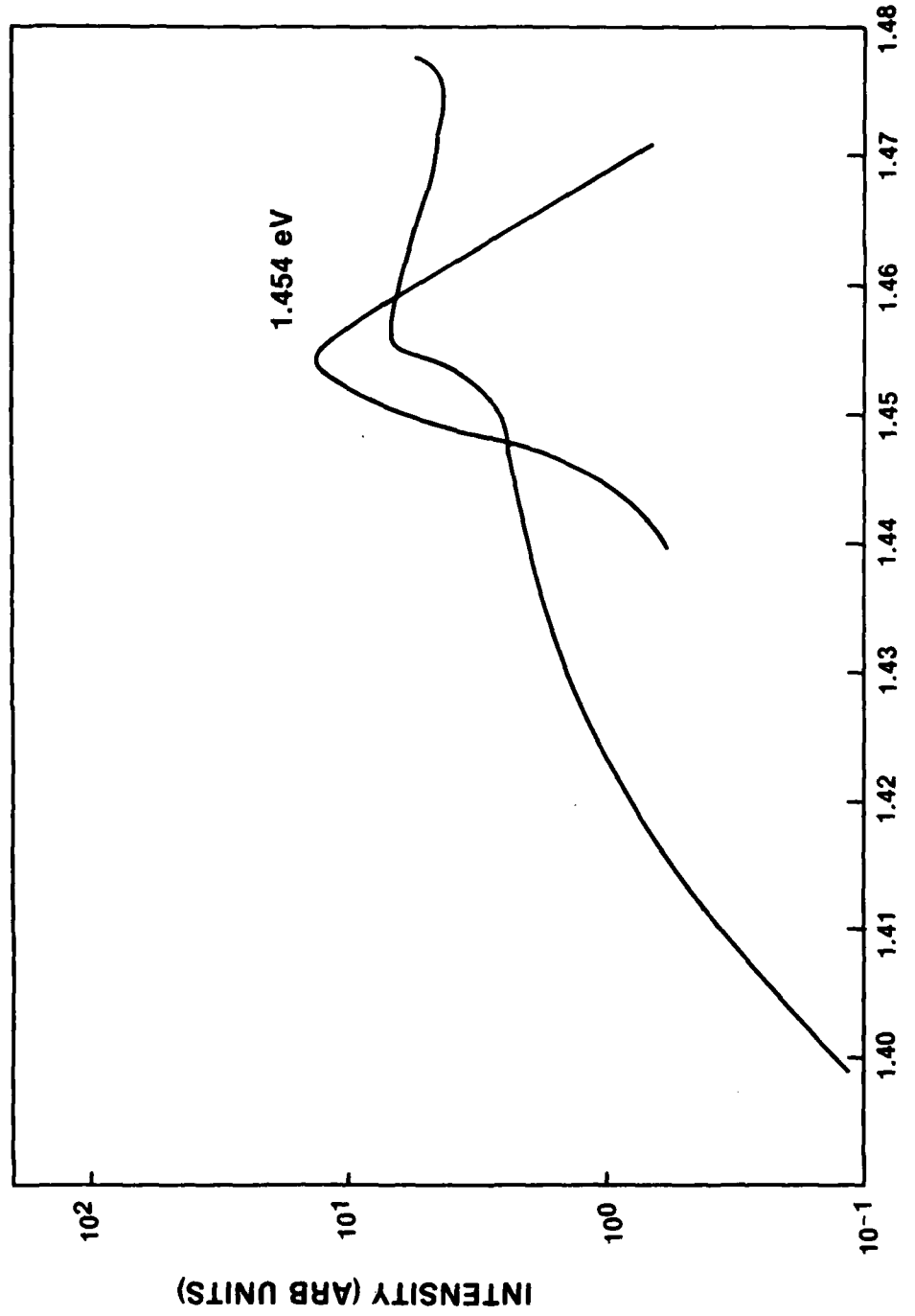

Figure 3.1.9. Photoluminescence at Low Intensity Levels for Ultra Pure GaAs

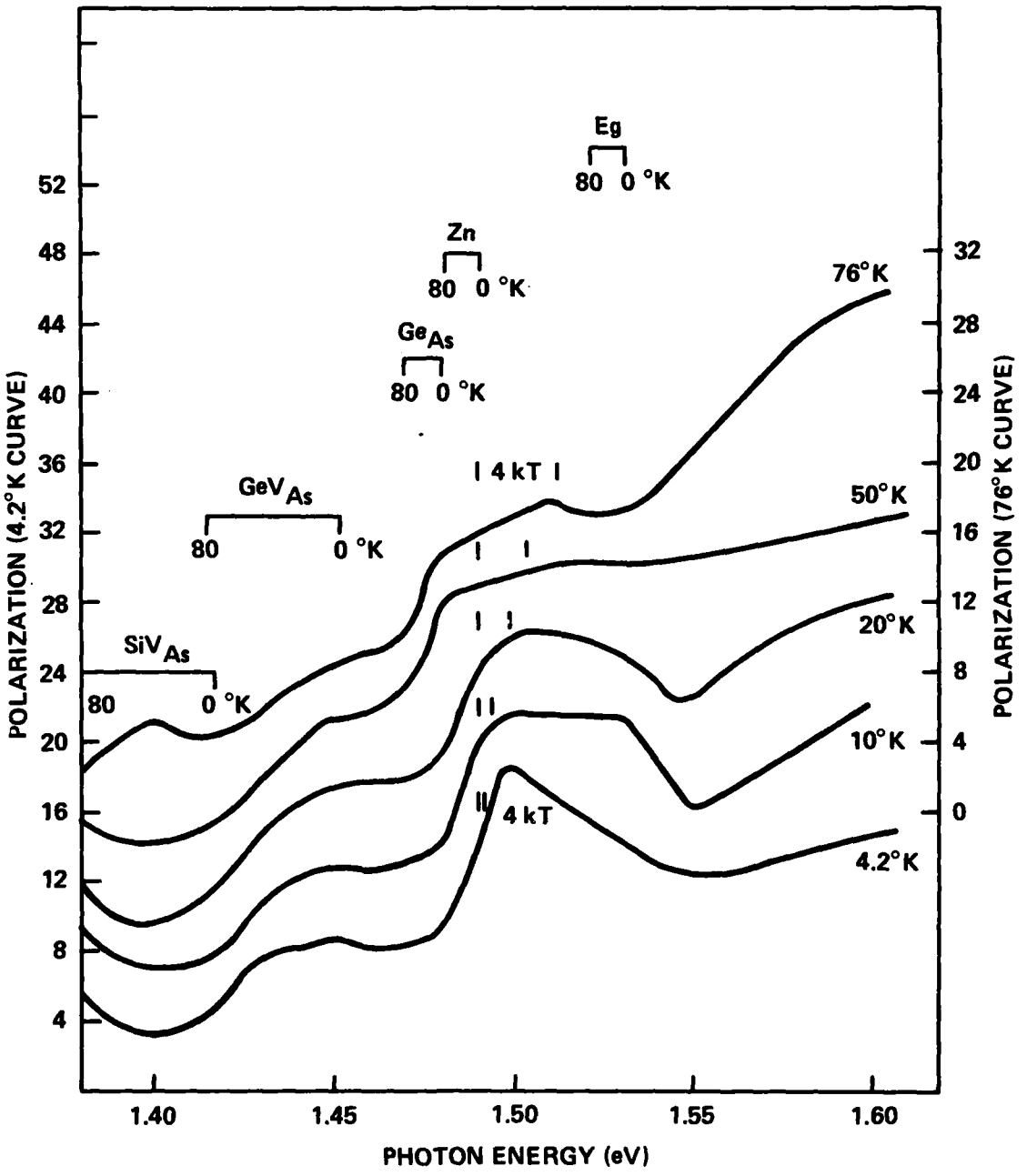

Figure 3.2.1. Circular Polarization Spectra for GaAs $(h\nu)_{ex}$ = 1.710 eV (Circularly Polarized) (Sample 1)

zero for transitions involving electron states that lie below both Fermi energies and switch, in a range of approximately 4 kT, to a constant value above the Fermi energies.

Obvious departures from this simple model are observed in the polarization spectra (especially at low temperatures) and a more refined model will be required to account for the processes that relax the energy and the spin of the optically excited carriers.

In the experiments the simplest polarization spectrum to understand qualitatively is observed at 76K. Only minor departures from monotonic behavior occur. The polarization does not go to zero at energies lower than the threshold for band to acceptor transitions. This is understandable, however, since transitions of a different nature occur in this energy region and can be expected to have different polarization dependence. A sharp rise in polarization occurs at the threshold for germanium-acceptor to conduction band transitions and continues to rise for energies up to 4 kT above the threshold for Zn-acceptor transitions. This behavior would be consistent with the simple model if the quasi-Fermi levels for electrons were close to the bottom of the conduction band at 76K. However, this is not likely to be the case and, therefore, one must conclude that the electrons in the conduction band have not quite achieved thermal equilibrium before they recombine with holes.

A peak in polarization occurs at 1.51 eV. This energy coincides with the band gap at 76K and therefore the threshold for interband transitions. At this energy interband transitions would involve electrons at the bottom of the conduction band and the polarization should decrease once again, to be consistent with the behavior of band to accepter transitions.

At higher energies the polarization rises monotonically to a value of 29% at 1.60 eV. Since this energy is many kT above E_g the corresponding luminescence involves "hot" carriers. The circular polarization of 29% can not be explained on the basis of spin alignment alone, and obviously contains a contribution due to orbital angular momentum alignment of the recombining holes.

The polarization structure near the threshold for band to acceptor transitions sharpens up at lower temperatures and a prominent peak occurs at 1.50 eV at somewhat higher energies than the two prominent peaks in the luminescent spectrum.

A possible explanation as to the source of the peak would be that it is associated with the lowest energy in the conduction band that can be reached by an electron that is excited by a circularly polarized 1.701 eV photon and relaxes, at least initially, solely with a cascade of optical phonons. This process is known to leave the spin alignment relatively unaffected. The electron can then recombine immediately displaying a high degree of spin alignment (and therefore a high degree of circular polarization of the luminescence). Otherwise, the electron can diffuse by other relaxation processes to other nearby states and in the process lose alignment. Correspondingly, the polarization of the luminescence would decrease.

We can check the feasibility of this explanation with a simple calculation. The total excitation energy and the peak luminescence energy are given by:

$$h\upsilon_x = E_g + \left(1 + \frac{m_e}{m_h}\right)\left(n\hbar\omega_{LO} + \delta\right)$$

$$h\upsilon_{lu} = E_g + \delta - E_A \qquad (3.1.1)$$

where δ is an energy less than the optical phonon energy $\hbar\omega_{LO}$ (0.036 eV for GaAs). A simple calculation shows that these relations can be satisfied in the experimental situation for n=6 phonons, δ = 0.010 eV and m_e/m_h = 0.1. These values are reasonable and the calculation supports the hypothesis. However, experiments varying the excitation energy are planned to establish whether this hypothesis is correct or whether there is some alternative explanation.

There are two additional features in the polarization spectra that deserve comment:

- In the polarization spectra for 4.2K and some of the higher temperatures the polarization is significantly different near the threshold for band to Zn transitions from that near the threshold for band to germanium transitions. This contradicts the simple model and seems to indicate that the holes retain some degree of alignment which differs depending upon the species of acceptor involved.

- Circularly polarized luminescence has been observed at 1.46 eV and lower energies. The associated optical transitions involve electrons bound in various complexes and this observation indicates that the carriers that relax into these bound states retain some of their alignment.

In Fig. 3.2.2 we show the variation of the polarization with energy for the chromium doped sample whose photoluminescence data is shown in Fig. 3.1.2. The striking features in this data is a broad peak in polarization at 1.45 eV and a sharp peak at about 1.53 eV (above the energy gap) which broadens at higher temperatures. The data at 4.5°K were not extended to sufficiently high energies to discern whether the peak is also present at this temperature. Neither of these peaks can be associated with distinctive features in the photoluminescence spectrum. The peak at lower energies would appear to be associated with a deep trap that quickly traps aligned carriers which retain their alignment over long periods of time than the free carriers.

The peak at higher energies would appear to be associated with some sharp levels overlapping the conduction (valence) band. However, these explanations must be regarded as extremely speculative. Much more experimental and theoretical work will be need to establish models to explain their existance.

The ultra pure insulating specimen offers the opportunity for very detailed polarization studies since the features in the photoluminescence spectrum are so varied and sharp. However, much time was expended in characterizing its photoluminescence spectrum toward the end of the contract period so that only a brief survey of the polarization properties were possible.

For this survey the circular polarization was measured at four discrete points as indicated in Figure 3.2.3. These points were selected to reflect various types of optical transitions. The measurements were made at 10°K with circular polarization excitation at 1.6003 eV. A table of the results are shown in Table 3.1.1.

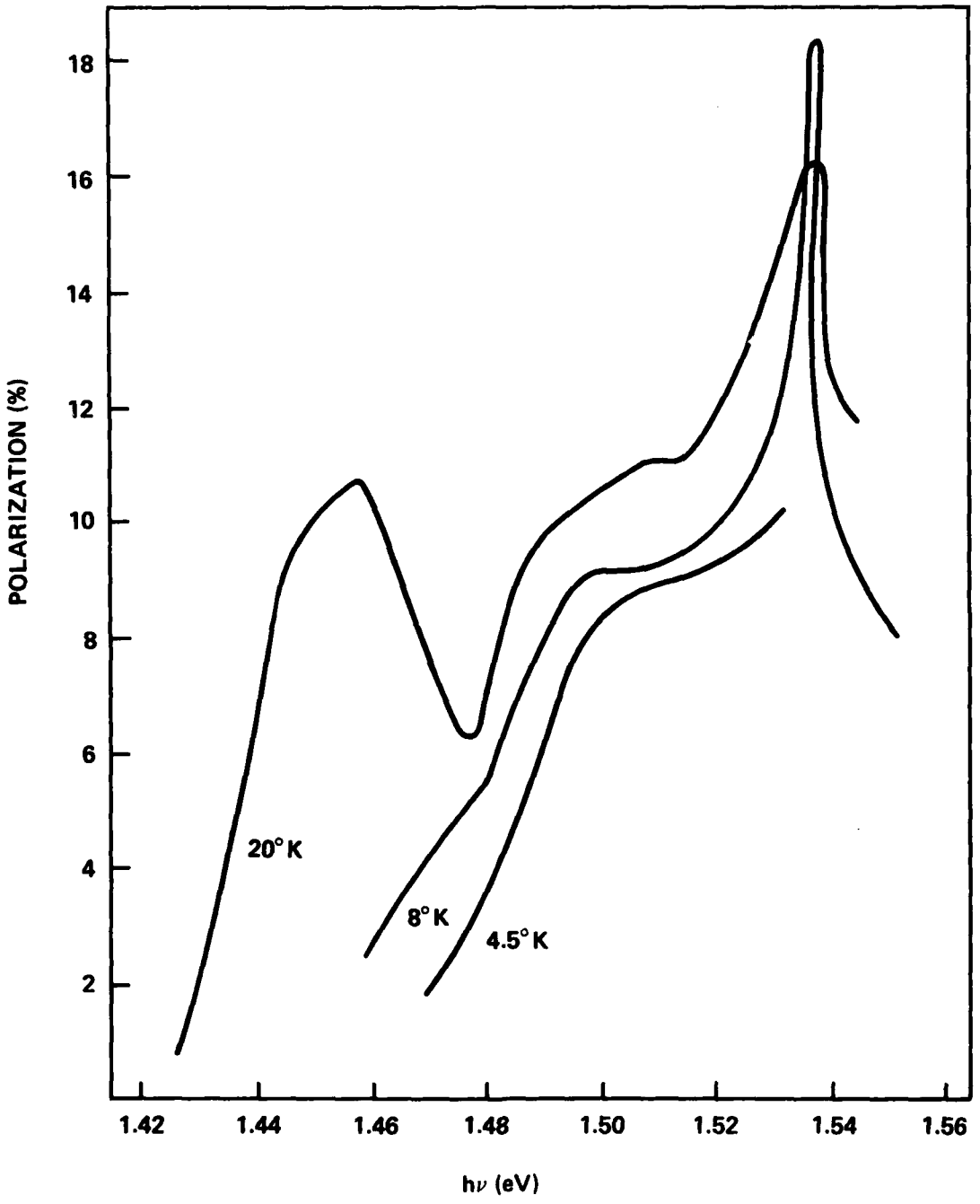

Figure 3.2.2. Circular Polarization Spectra for Sample 3

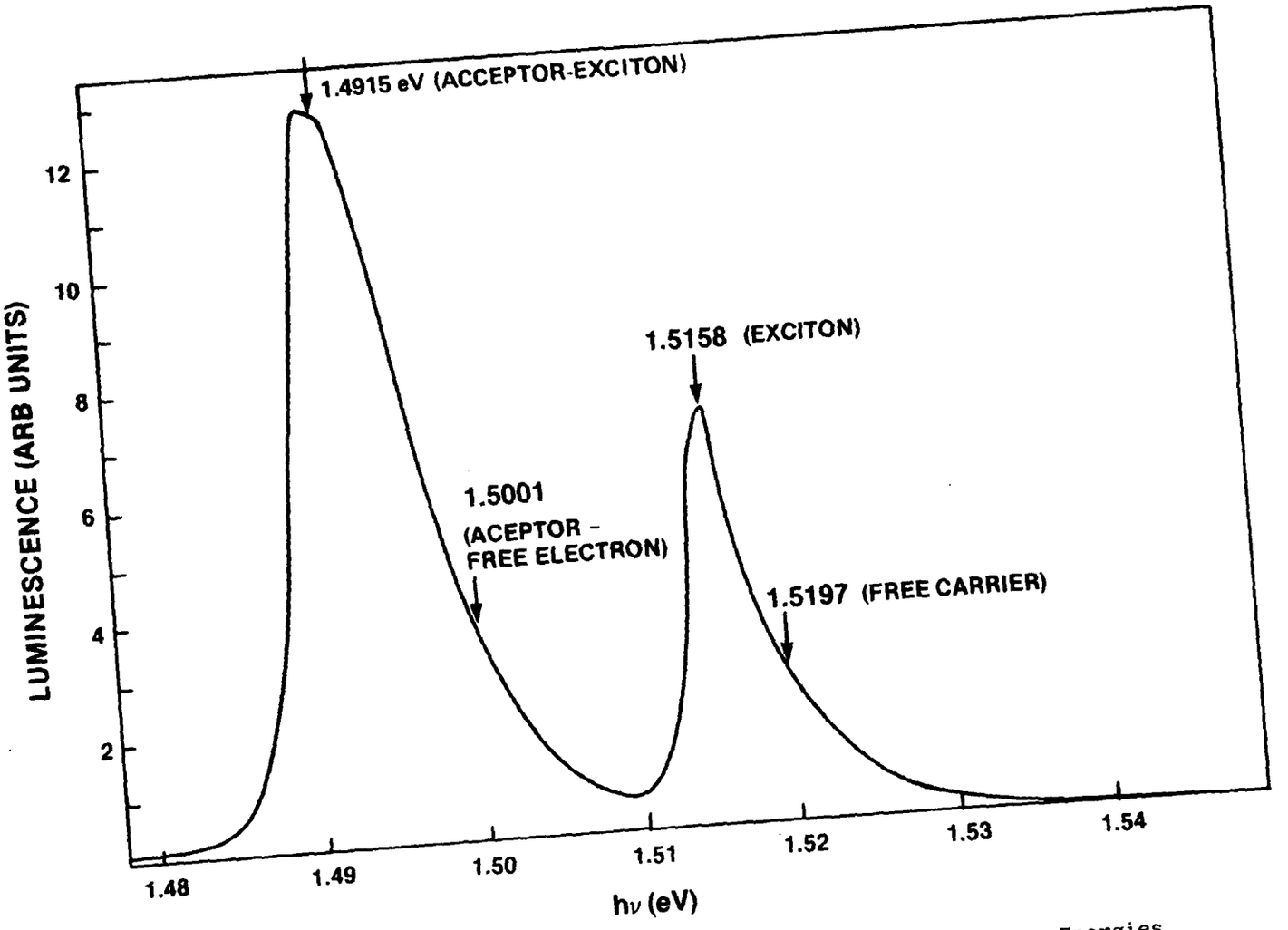

Figure 3.2.3. Photoluminesce of Ultra Pure GaAs Showing Photon Energies Used in Table 3.1.1

Table 3.1.1

hυ	Type of Recombination Transition	Circular Polarization of luminescence
1.5197	near bottom of energy gap	3%
1.5148	exciton	38%
1.5001	acceptor - free electron	2%
1.4915	donor-acceptor recombination	<1%

These results would seem to indicate that the excitons are formed early in the relaxation process and the component carriers retain a large amount of their original orientation. However, these data serve principally to motivate more extensive experiments.

Additional preliminary work has been performed on p-type samples of InP which show a variety of transitions involving free carriers, excitons and impurities. As in the case of GaAs structure is seen in the polarization of the photoluminescence, however, as in the case of GaAs extensive measurements on a variety of samples and experimental conditions will be necessary to understand the experimental results.

4.0 THEORY

There are various experiments one can do to detect optical orientations. Examples of such experiments are: (1) spin polarization of electron photo emission, (2) spin dependent recombination, (3) spin dependent transport, (4) EPR and (5) NMR. However, we came to focus our work on understanding polarized photoluminescence. This experiment is illustrated in Figure 4.0.1. We have already described experimental results of such experiments in Section 3. One shines polarized light on a luminescent sample. For simplicity of illustration we use linearly polarized light, although most of our experiments have been performed with circularly polarized light. The resulting luminescence in some direction is then examined for the degree of polarization. The luminiscence may be polarized if the excited electron "remembers" how it was excited. It can remember if electrons of a preferred spin are excited or if electrons of a preferred electron wave vector are excited as illustrated schematically in Fig. 4.0.1. In the case of holes, carriers can have nonzero orbital angular momentum and these can be ordered. Whether any of these effects occur can be determined by calculating the optical matrix elements as we do for GaAs type materials in Section 4.2. From the optical matrix elements one can calculate the degree of initial optical orientation (or spin polarization in the case of spin alignment). The proper treatment of the subsequent relaxation and emission processes is complicated, and various methods of dealing with this problem will be discussed in more detail in the sections which follow.

Usually the electron will undergo a sequence of scatterings and energy relaxations before it recombines with a hole as illustrated in Fig. 4.0.2. If the electron is excited high into the conduction band of a polar material, it will relax quickly to within 1 LO phonon energy of the bottom of the band and thermalize within 4 kT_e where T_e is the electron temperature which may be higher than the lattice temperature.[3.3] Further complications can occur if the electron relaxes further to form an exciton or impurity complex.

The energy relaxation and thermalization takes place through scattering interactions with phonons, impurities and other carriers. At any scattering event the spin, orbital angular momentum and electron wave vector will, in general, be changed and with sustained scattering these quantities become randomized, destroying the initial orientations.

When a carrier is in a given band state there is a roughly energy independent probability that radiative recombination might occur and the polarization of the luminescence will depend upon the degree of randomization that has taken place. As the electron dribbles down in the conduction band, the luminescence will shift to smaller photon energies and by studying the polarization of the photoluminescence as a function of photon energy one could hope to gain insight into the relaxation processes. Further information can be obtained by varying the excitation photon energy. Experimentally this is relatively straightforward and we have obtained such data in this project. Theoretical interpretation is much more difficult. In our initial work we obtain conclusions applicable to specific circumstances only. These conclusions are used to test the assumptions made. The current status is that the experimental results raise more questions than they answer, indicating that a more detailed theory than we outline here is necessary.

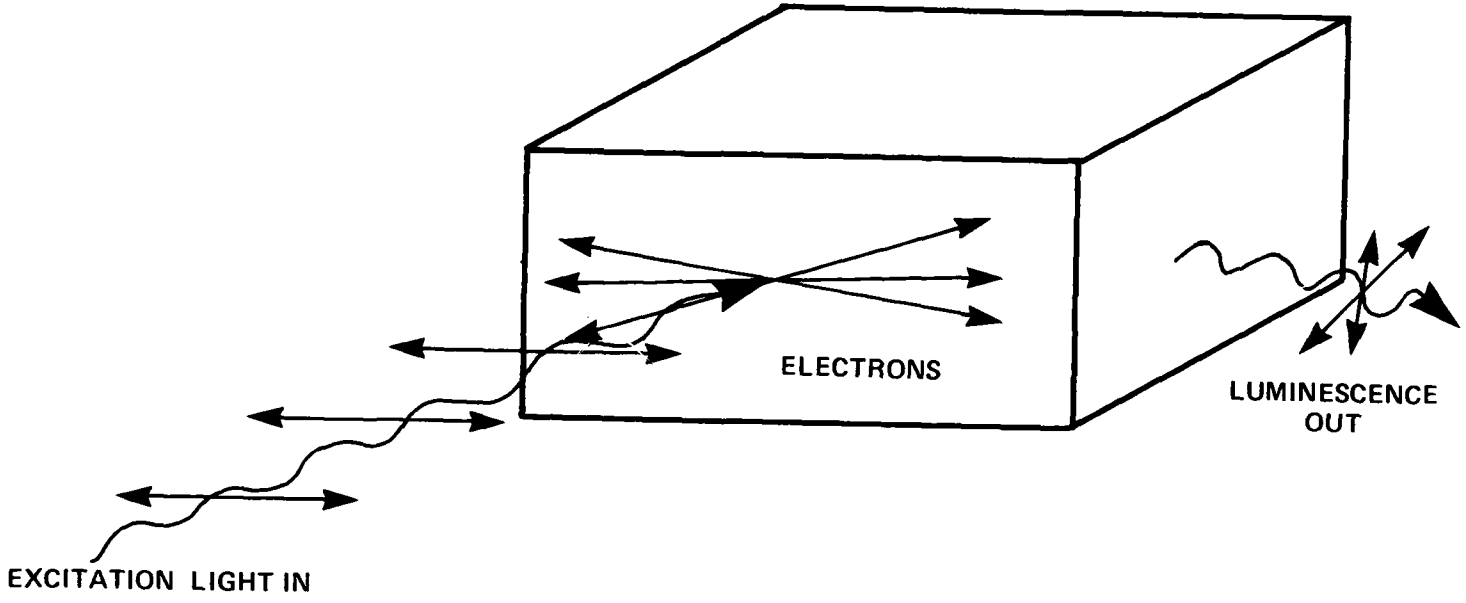

Figure 4.0.1. Optical Orientation in Solids

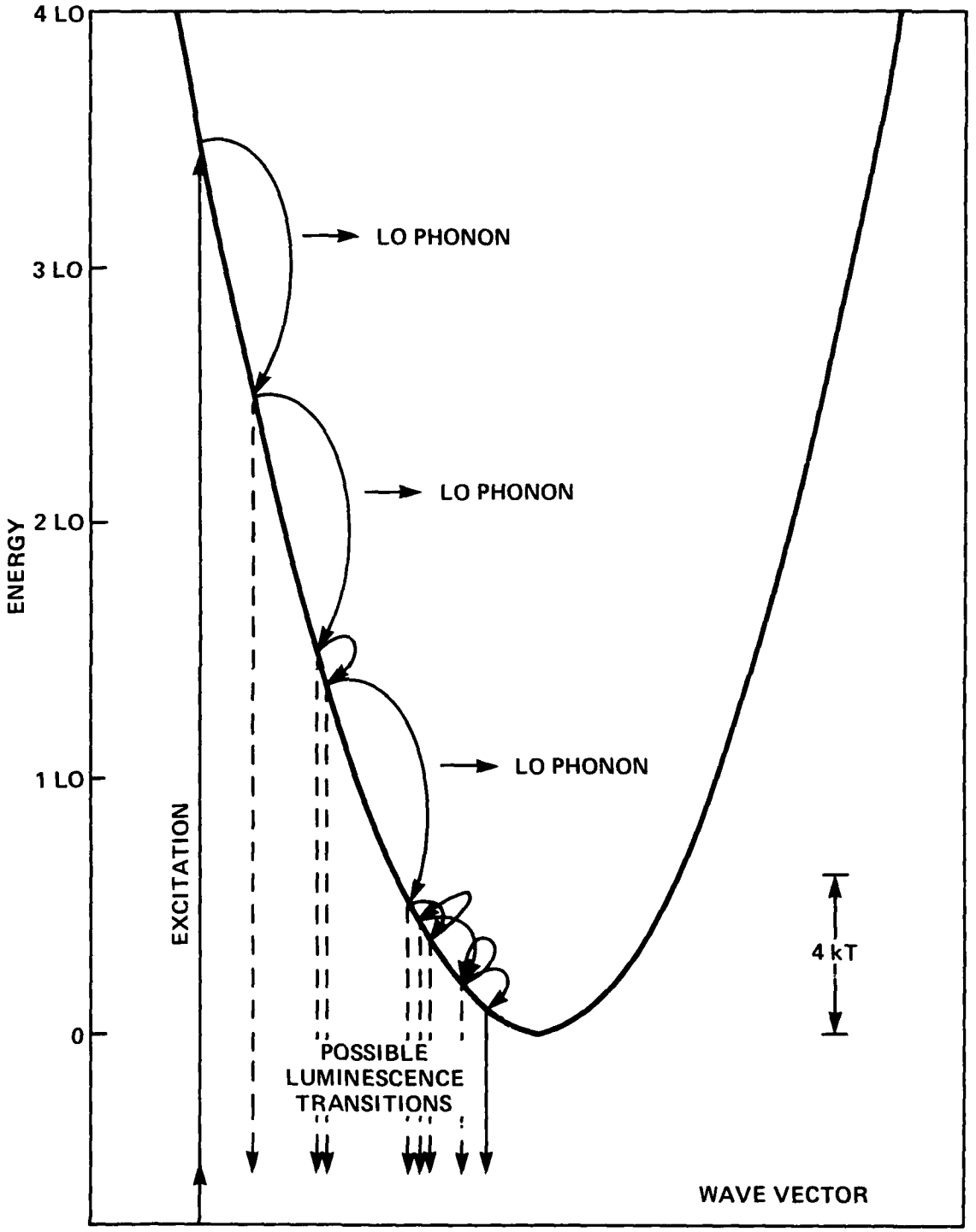

Figure 4.0.2. Schematic Diagram Illustrating Relaxation of Photoexcited Electron

4.1 Interactions of Optical Orientations with Light

In the presence of intrinsic light (i.e. $h\nu \gtrsim E_g$) transitions occur in a semiconductor

$$|v, \vec{k}', j', m'> \rightarrow | c, \vec{k}, j, m> \tag{4.1.1}$$

where v and c, denotes valence band and conduction band respectively j is the quantum number associated with the total angular momentum and m is associated with the magnetic quantum number along some axis of spacial quartization. Both j and m may contain spin and orbital angular momentum. In fact for the S-like conduction band j and m can be replaced by $s = 1/2$ and $m_s = \pm 1/2$. The photon can be represented by the vector potential

$$\vec{A} = A_o \hat{a} \exp(i(\omega t - \vec{q}, \cdot \vec{r})) \tag{4.1.2}$$

where $\hat{a}$ is a unit vector that gives the polarization. For linearly polarized light travelling along the Z-axis we will have the two states of linear polarization.

$$\begin{aligned} \hat{a}_1 &= \hat{i} \\ \hat{a}_2 &= \hat{j} \end{aligned} \tag{4.1.3}$$

and for circular polarization

$$\begin{aligned} \hat{a}_\alpha &= \hat{i} \cos \omega t + \hat{j} \sin \omega t \\ \hat{a}_\beta &= \hat{i} \cos \omega t - \hat{j} \sin \omega t \end{aligned} \tag{4.1.4}$$

Consider, for simplicity, one initially filled valence band and one initially empty conduction band. The rate at which electrons $\vec{k}$, s, m_s are created are given by:

$$w_{c, \vec{k}, s, m_s}^{(h\nu)} = \frac{2\pi A_o^2}{\hbar} \sum_{\vec{k}'} \sum_{j'} \sum_{m'} |<c, \vec{k}, s, m_s | \hat{a} \cdot \vec{p} | v, \vec{k}', j', m'>|^2 \times \delta(E_c - E_v - h\nu) \tag{4.1.5}$$

whereas holes are created as:

$$w_{v, \vec{k}', j', m'}^{(h\nu)} = \frac{2\pi A_o^2}{\hbar} \sum_{\vec{k}} \sum_{s} \sum_{m_s} |< c, \vec{k}, s, m_s | \hat{a} \cdot \vec{p} | v, \vec{k}', j', m'>|^2 \times \delta(E_c - E_v - h\ )$$

Summing these transition probabilities over all states gives an absorption rate

$$w(h\nu) = \sum_{\vec{k}} \sum_{s} \sum_{m_s} w_{c,\vec{k},s,m_s} = \sum_{\vec{k}'} \sum_{j'} \sum_{m'} w_{v,k',j',m'} \tag{4.1.7}$$

In general, for a given polarization the excited electrons will not be isotropic but will contain preferred directions of wave vector, angular momentum or spin. Consider first orientation of crystal momentum, $\hbar k$. The net crystal momentum in any direction will be zero. However, in general:

$$\langle \hbar^2 k_x^2 \rangle = \langle \hbar^2 k_y^2 \rangle \neq \langle \hbar^2 k_z^2 \rangle \tag{4.1.8}$$

Therefore, a bulge may occur in the wave vector distribution along some direction. We characterize this bulge by defining a crystal momentum polarization, $\hbar\vec{k}P_{xz}$. This polarization can be defined as

$$P_{\hbar\vec{k}\,xz} = \frac{\langle|\hbar k_x|\rangle - \langle|\hbar k_z|\rangle}{\langle|\hbar k_x|\rangle + \langle|\hbar k_z|\rangle} \tag{4.1.9}$$

If the light is circularly polarized, there is a tendency to transfer angular moment from the light to the electron system so that the net angular momentum along the propagation vector of the light (taken as the z-direction) may not be zero. Each electron will have a component of angular momentum, $m\hbar$, along some axis of spacial quantization. In the case of electrons (holes) this axis may lie along the electron wave vector. If a significant magnetization is set up, the wave functions will be modified and there will be a common axis of spacial quantization along the magnetization direction. In any case, the expectation value of the total angular momentum along the z direction $\langle M_z \rangle$, can be used to define an angular momentum polarization

$$M_z P = \frac{\langle M_z \rangle}{\langle|M_z|\rangle} \tag{4.1.9a}$$

A special case of angular momentum orientation is spin alignment in the presence of a magnetization in which case we can write:

$$P_s = \frac{n\uparrow - n\downarrow}{n\uparrow + n\downarrow} \tag{4.1.10}$$

The initial orientations (i.e. the polarization created by a hypothetical optical pulse short enough that relaxations have no time to take place) are related simply to the optical transition rates. Consider the orientation of crystal momentum of electrons produced by light travelling along the y axis

$$P_{xz}^{\hbar\vec{k}} = \frac{\sum\sum\sum_{\vec{k}sm_s} W_{c,\vec{k},s,m_s} |\vec{k}\cdot\hat{i}| - \sum\sum\sum_{\vec{k}sm_s} W_{c,\vec{k},s,m_s} |\vec{k}\cdot\hat{k}|}{\sum\sum\sum_{\vec{k}sm_s} W_{c,\vec{k},s,m_s} |\vec{k}\cdot\hat{i}| + \sum\sum\sum_{\vec{k}sm_s} W_{c,\vec{k},s,m_s} \vec{k}\cdot\hat{k}} \qquad (4.1.11)$$

A similar expression holds for hole orientation.

Likewise for the spin polarization of electrons in the presence of a magnetization:

$$P_s = \frac{\sum_{\vec{k}} \sum_s \sum_{m_s} W_{\vec{k},s,m_s} m_s}{1/2 \sum\sum\sum_{\vec{k}sm_s} W_{\vec{k},s,m_s}} \qquad (4.1.12)$$

In a similar manner one can calculate the alignment of orbital angular momentum.

The intensity of spontaneous emission at photon energy $h\upsilon$ for a given polarization $I(\hat{a},h\upsilon)$ is related to the probability of occupation of given conduction band states $\vec{k},j,m$ by electrons and by the probability of occupation of given valence band states $\vec{k}',j',m'$ by holes. These probabilities are respectively $n_{\vec{k},i,m}$ and $n_{\vec{k}',j',m'}$.

The intensity $I(\hat{a},h\upsilon)$ is then given by

$$I(\hat{a},h\upsilon) \sim \sum_{k',j',m'} \sum_{k,j,m} n_{k',j',m'}\, n_{k,j,m}\, |\langle c,\vec{k},j,m \,|\, \hat{a}\cdot\vec{p} \,|\, v,k',j',m'\rangle|^2 \times \delta(E_c - E_v' - h\upsilon) \qquad (4.1.13)$$

Therefore the polarization of the spontaneous luminescence is given by

$$P_{linear}(h\upsilon) = \frac{I(\hat{a}_1, h\upsilon) - I(\hat{a}_2, h\upsilon)}{I(\hat{a}_1, h\upsilon) + I(\hat{a}_2, h\upsilon)} \qquad (4.1.14)$$

or

$$P_{circular}(h\upsilon) = \frac{I(\hat{a}_2, h\upsilon) - I(\hat{a}_\beta, h\upsilon)}{I(\hat{a}_2, h\upsilon) + I(\hat{a}_\beta, h\upsilon)}$$

We will apply these concepts to calculations of optical orientations in GaAs, in the next section.

4.2 Role of Optical Selection Rules in Optical Orientation Processes

In a later section we shall discuss the problem of absorption and emission using a light scattering formalism. Although we regard this as the correct method of dealing with the problem on a fundamental level, the evaluation of the formula is extremely complicated, taking into account electron-phonon and other scattering mechanisms. Therefore, in this section we will present a somewhat simplified account which basically treats the absorption and emission as separate processes. A detailed treatment using this approach was presented at the NATO Summer School on Magneto-Optics in 1979.[4.1] We present a shortened version of this work here along with some additional updating.

Most previous analyses of spin orientations were based upon the properties of the wave functions at $\vec{k}=0$, which is basically an atomic model.[4.2] We have begun a program to extend such analysis to higher energy transitions using the techniques developed for studying states near band extreme developed by Dresselhaus[4.3], Kane[4.4], and Zeiger[4.5]. The calculations show that spin alignment is only a special case of more general optical orientations involving alignments of electronic wave vectors and orbital angular moments as well as spin. Further, optical alignment effects occur in linear as well as circular polarization. Spin alignment is the more commonly observed phenomena simply because it has the longest relaxation time. However, as has been shown by Russian workers, refs. 1.4,1.5, effects on the luminescence due to the more general alignments can be observed in weak luminescence due to short lived "hot" electrons. Weak luminescence involving direct transitions in indirect gap materials may also show such effects. We anticipate that stimulated photon emission, where the recombination time is shortened, might also be a situation where the more short lived alignment phenomena might be observed. The experimental fact that has been known for a long time is that injection lasers prefer to lase TE rather than TM. This could be explained by alignment effects on the stimulated emission involving the injection current.

One might find it surprising that one could obtain optical orientations in a highly symmetric crystal like GaAs which possesses cubic symmetry. However, if one considers the combined system of, say, a collimated light beam traveling along an axis of a cubic crystal one has a lower symmetry for the total system which provides for departures from isotropic behavior. Also, if one considers an individual electron with wave vector, $\vec{k}$, directed along a cubic axis, similarly one has a system of symmetry lower than cubic. To determine how an electron of a given wave vector, $\vec{k}$, interacts with a photon of wave vector $\vec{q}$ and polarization vector $\hat{a}$ one must examine the behavior of the optical matrix elements governing the optical transitions of electrons of different wave vectors.

We will discuss the role of relaxations and electron-phonon interactions in the dynamics of optical orientations in later sections. In this section, we emphasize the role of the optical selection rules and for simplicity, we ignore these phenomena and consider, somewhat hypothetically, what might be called resonant photoluminescence.

To examine optical effects that contribute to orientations involves obtaining good wave functions from which one can obtain the dipole moments. In calculating wave functions we consider only interactions between the conduction band and the three valence bands. In this approximation, the energy bands are spherically symmetric and do not reflect perturbations associated with electron-wave vectors along directions other than the symmetry direction Δ, i.e. (100). This eliminates effects which should result in quenching of angular momentum. This is, of course, the Kane band model for III-V compounds.[4.4] We repeat this calculation, however, in a slightly different way to illustrate the interactions that give rise to the optical orientations.

In the approach originated by Dresselhaus[4.3], the wave functions near $\vec{k} = 0$ are taken as linear combinations of those at the center of the zone neglecting spin. The group theory properties of these have been determined by Dresselhaus.[4.6] The cell periodic part of the Bloch functions, $u_{b,\vec{k}} \exp(\vec{k}\cdot\vec{r})$, must satisfy the Schrodinger equation:

$$\left[\frac{\vec{p}^2}{2m} + V + \frac{\hbar}{m}\ \vec{k}\cdot\vec{p} + \frac{\hbar}{4m^2c^2}\ (\nabla V \times \vec{P})\ \cdot\sigma\right] u_{b,\vec{k}} = \left[E - \frac{\hbar^2k^2}{2m}\right] u_{b,\vec{k}} \qquad (4.2.1)$$

In the absence of spin the wave functions must satisfy the first two terms at the center of the zone. No optical orientation occurs from these terms alone.

The third term mixes wave functions of different symmetry at Γ and along the symmetry axis Δ (100), results in spatial quantization of p-functions in the direction of the electron-wave vector. In our spherically symmetric model this holds also in any other direction, therefore we associate our wave functions with a magnetic quantum number $m_{\vec{k}}$. This term leads to orientation of crystal momentum (wave vectors) and angular momentum. The fourth term is the spin-orbit coupling which mixes states of different spin and gives rise to spin alignment.

Optical orientation occurs because the orientation of the dipole moments that govern the optical transitions depend upon the axis of spatial quantization. If the latter is initially random, then absorption of polarized light results in preferred orientations in the excited state. The first step in examining the optical orientation is to deduce the nature of these transition dipole moments from the wave functions. The interaction between these dipoles and the polarization of the incident light then gives the orientation.

We will first develop the concepts of optical orientation using the $\vec{k}\cdot\vec{p}$ interaction. Then we show how spin-orbit interaction gives rise to spin alignment and apply the results to the Kane band model. Finally, we will describe some experiments which illustrate the derived results.

PROPERTIES OF THE BASIS FUNCTIONS

The basis functions must be solutions of the first two terms in the Hamiltonian. The conduction band wave functions we designate as $|S>$. These belong to the symmetry type Γ_1 and have the transformation properties in the tetrahedral group of atomic S-functions. The valence band wave functions we designate $|X>$, $|Y>$, $|Z>$. These belong to the symmetry type Γ_4 and transform like atomic p-functions.

These have the momentum matrix elements:

$$\frac{\hbar}{m}\langle S|\vec{p}|X\rangle = \hat{i}P$$

$$\frac{\hbar}{m}\langle S|\vec{p}|Y\rangle = \hat{j}P$$

$$\frac{\hbar}{m}\langle S|\vec{p}|Z\rangle = \hat{k}P$$

$$\frac{\hbar}{m}\langle X|\vec{p}|Y\rangle = \langle Y|\vec{p}|Z\rangle = \langle Z|\vec{p}|X\rangle = 0$$

$$\langle X|\vec{p}|X\rangle = \langle Y|\vec{p}|Y\rangle = \langle Z|\vec{p}|Z\rangle = \langle S|\vec{p}|S\rangle = 0 \qquad (4.2.2)$$

When $\vec{k}$ is not zero it is convenient to transform these basis function to a new set. Consider the electron-wave rector, $\vec{k}$, given in polar coordinates

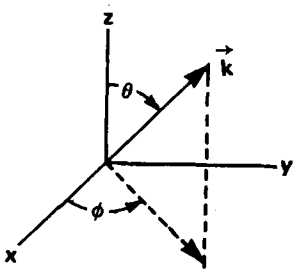

Figure 4.2.1. Electron Wave Vector in Polar Co-ordinates

by

$$\vec{k} = k\ [\hat{i}(\sin\theta\cos\phi) + \hat{j}\ (\sin\theta\sin\phi) + \hat{k}(\cos\theta)]$$

In this case a convenient set of basis functions for the valance band are given by:

$$|Z'\rangle = (\sin\theta\cos\phi)\,|X\rangle + (\sin\theta\sin\phi)|Y\rangle + (\cos\theta)|Z\rangle \qquad (4.2.3)$$

and

$$\frac{1}{\sqrt{2}}|X' \pm i\ y'\rangle$$

where

$$|X'\rangle = (\sin\phi)|X\rangle + (-\cos\phi)|Y\rangle$$

$$|Y'\rangle = (-\cos\theta\cos\phi)|X\rangle + (-\cos\theta\sin\phi)|Y\rangle + (\sin\theta)|Z\rangle$$

These have the nice property that the momentum matrix elements with the conduction band S-functions are either parallel or perpendicular to the wave vector and that the axis of spatial quantization lies along the wave vector.

The corresponding momentum matrix elements are:

$$\frac{\hbar}{m}\langle S|\vec{p}|X'\rangle = P\,\hat{r}_1$$

$$\frac{\hbar}{m}\langle S|\vec{p}|Y'\rangle = P\,\hat{r}_2 \qquad (4.2.4)$$

$$\frac{\hbar}{m}\langle S|\vec{p}|Z'\rangle = P\,\hat{r}_3$$

where

$\hat{r}_1$, $\hat{r}_2$, $\hat{r}_3$ are orthonormal unit vectors given by:

$$\hat{r}_1 = \hat{i}(\sin\phi) + \hat{j}(-\cos\phi)$$

$$\hat{r}_2 = \hat{i}(-\cos\theta\cos\phi) + \hat{j}(-\cos\theta\sin\phi) + \hat{k}(\sin\theta) \qquad (4.2.5)$$

$$\hat{r}_3 = \hat{i}(\sin\theta\cos\phi) + \hat{j}(\sin\theta\sin\phi) + \hat{k}(\cos\theta)$$

Note that $\vec{k} = k\,\hat{r}_3$.

ALIGNMENT OF MOMENTUM AND ANGULAR MOMENTUM INVOLVING THE $\vec{k}\cdot\vec{p}$ TERM

We treat the $\vec{k}\cdot\vec{p}$ interaction using Wigner-Brillion perturbation theory[4.5] Details are given in ref. 4.1.

We obtain the energies:[4.7]

$$E_c = \frac{E_g}{2} + \frac{E_g}{2}\sqrt{1 + 4\frac{P^2k^2}{E_g^2}} + \frac{\hbar^2k^2}{2m}$$

$$E_{v,\pm1} = \frac{\hbar^2k^2}{2m} \qquad (4.2.6)$$

$$E_{v,o} = \frac{E_g}{2} - \frac{E_g}{2}\sqrt{1 + 4\frac{P^2k^2}{E_g^2}} + \frac{\hbar^2k^2}{2m}$$

and the wave functions:

$$|c, \vec{k}, m_k = 0\rangle = a_c|S + b_c|Z'\rangle$$

$$|v, \vec{k}, m_, = \pm1\rangle = \frac{1}{\sqrt{2}}|X' \pm i\,y'\rangle \qquad (4.2.7)$$

$$|v, \vec{k}, m_, = 0\rangle = a_v|S\rangle + b_v|Z'\rangle$$

where

$$a_c = \frac{E_c}{\sqrt{E_c^2 + k^2P^2}}\;;\; b_c = \frac{kP}{\sqrt{E_c^2 + k^2P^2}}$$

$$a_v = \frac{kP}{\sqrt{(E_v - E_g)^2 + k^2p^2}} \; ; \; b_v = \frac{E_v - E_g}{\sqrt{(E_v - E_g)^2 + k^2p^2}} \qquad (4.2.8)$$

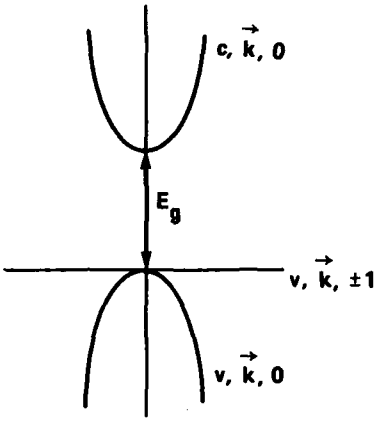

Figure 4.2.2. Energy Bands Resulting from $\vec{k} \cdot \vec{p}$ Interaction

The momentum matrix elements that govern the optical transitions are given by:

$$\begin{aligned} \langle c, \vec{k}, o|\vec{p}|v, \vec{k}, \pm 1\rangle &= P\frac{a_c}{\sqrt{2}}(\hat{r}_1 \pm i\,\hat{r}_2) \\ \langle c, k, o|\vec{p}|v, \vec{k}, o\rangle &= P(a_c b_v + a_v b_c)\,\hat{r}_3 \end{aligned} \qquad (4.2.9)$$

In the presence of light characterized by the vector potential $A_o \hat{a} \exp[i(\omega t - \vec{q}\cdot\vec{r})]$ the probability of exciting an electron of wave vector $\vec{k}^o$ from the valence band $m_k = \pm 1$ is given by[4.1]:

$$f_{\vec{k},\pm 1} = A_o^2 P^2 \frac{a_c^2}{2} [\hat{a} \cdot (\hat{r}_1 \pm i\,\hat{r}_2)]^2 \qquad (4.2.10)$$

and the probability for excitation from the valence band $m_k = 0$ is:

$$f_{\vec{k},0} = A_o^2 P^2 (a_c b_v + a_v b_c)^2 \; (\hat{a} \cdot \hat{r}_3)^2$$

if the light is traveling in the x, y plane and has polarization vector $\hat{a} = \vec{k}$ then:

$$f_{\vec{k},\pm 1} = A_o^2 P^2 \frac{a_c^2}{2} \sin^2\theta$$

$$f_{\vec{k},o} = A_o^2 P^2 (a_c b_v + a_v b_c)^2 \cos^2\theta \qquad (4.2.11)$$

These two equations demonstrate the optical orientation of crystal momentum. See Figure 4.2.3. Under linear polarized monochromatic illumination, electrons created at one energy in the conduction band have their wave vectors preferentially oriented perpendicular to the polarization vector, and electrons created at a somewhat lower energy have their wave vectors preferentially oriented parallel to the polarization vector. In the m = ±1 valence band, holes have their wave vectors preferentially oriented perpendicular to the polarization vector of the light and in the m = 0 valence band holes have their wave vectors oriented preferentially parallel to the polarization vector.

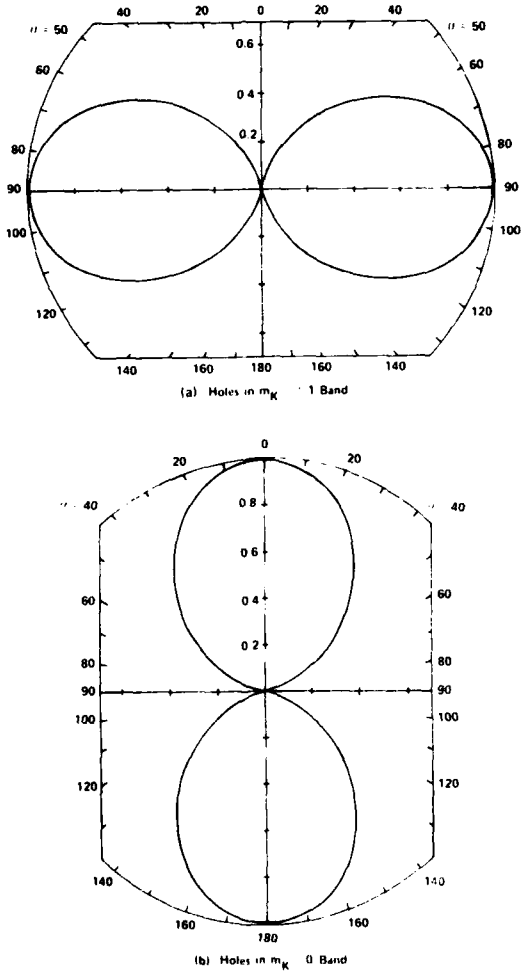

Figure 4.2.3. Polar Plots Illustrating Optical Orientation of Electron Wave Vectors

We can characterize this crystal momentum polarization quantitatively using the definition Eq. (4.1.9):

$$\hbar k \, P_{xz} = 1/5 \text{ for heavy hole transitions}$$

$$\hbar k \, P_{xz} = \sim 1/3 \text{ for light hole transitions}$$

There will be *no* net angular momentum orientation as long as the light is linearly polarized. On the other hand, suppose we have circularly polarized light traveling along the z-axis with the polarization:

$$\hat{a} = \frac{1}{\sqrt{2}} (\hat{1} + i\hat{j}) \tag{4.2.12}$$

then the distribution of m = ±1 valence band holes will be given by:

$$f_{\vec{k},\pm 1} \approx \frac{A_o^2 \, p^2 \, a_c^2}{4} (1 + \cos^2\theta \pm 2 \cos\theta) \tag{4.2.13}$$

The probability of exciting an electron of wave vector $\vec{k}$ is given by:

$$f_{\vec{k}} = f_{\vec{k},+1} + f_{\vec{k},-1} = \frac{A_o^2 \, p^2 \, a_c^2}{2} (1 + \cos^2\theta) \tag{4.2.14}$$

The net angular momentum along the wave vector $\vec{k}$ will be given by:

$$\hbar(f_{\vec{k},+1} - f_{\vec{k},-1}) = A_o^2 \, p^2 \, a_c^2 \cos\theta$$

These will add up to give the macroscopic net angular momentum given by:

$$\int_k^{k'+\Delta k} \int_0^{\pi} \hbar \int_{-1}^{1} (f_{k,+1} - f_{k,-1}) \cos\theta \, d(\cos\theta) \, d\phi k^2 dk) \tag{4.2.15}$$

This is proportional to:

$$2 \int_{-1}^{1} \cos^2\theta \, d(\cos\theta) = \frac{4}{3} \tag{4.2.16}$$

whereas the net excitations are proportional to:

$$\int_o^{\pi} (f_{k+1} + f_{k-1}) \, d(\cos\theta) \, d\phi k^2 dk = \frac{8}{3} \tag{4.2.17}$$

Therefore the angular momentum polarization given by (4.1.9a) is:

$$M_z^P = 1/2$$

The average angular momentum of excited holes is given by:

$$\hbar \frac{\frac{4}{3}}{\frac{8}{3}} = \frac{\hbar}{2} \tag{4.2.18}$$

The alignment of angular momentum corresponds to a macroscopic magnetization M given by:

$$M = \frac{1}{2} n_h g \mu_B \tag{4.2.19}$$

where n_h is the concentration of excited holes, g is the spectroscopic splitting factor and μ_B is the Bohr magneton.

The most direct experiment for demonstrating the optical alignment is to examine the polarization of the luminescence excited by polarized light. In the absence of relaxations, the same dipole moments that give rise to the excitations also govern the luminescent transitions.

Consider an electron-hole pair both with the $\vec{k}$-vector shown in Figure 4.2.4. We have already considered the probability of creating such an electron-hole pair with, say, the absorption of light with wave vector $\vec{q}_{in}$ along the x-axis and polarization vector $\hat{a}_{in}$ along the z-axis. The probability from Eq. 4.2.10 is proportional to:

$$(\hat{a}_{in} \cdot \hat{r}_i)^2 \tag{4.2.20}$$

where $\hat{r}_i$ is a unit vector along the dipole moment. Likewise, if there are no relaxations, the probability of emission of a photon with propagation vector $\vec{q}_{out}$ and polarization $\hat{a}_{out}$ with the radiative relaxation of this state is proportional to:

$$(\hat{a}_{out} \cdot \hat{r}_i)^2 \tag{4.2.21}$$

The total intensity at this polarization radiated by all excited electron hole pair states is proportional to the integral:

$$\int_0^{2\pi} \int_0^{\pi} (\hat{a}_{in} \cdot \hat{r}_i)^2 (\hat{a}_{out} \cdot \hat{r}_i)^2 \, d(\cos\theta) d\phi \tag{4.2.22}$$

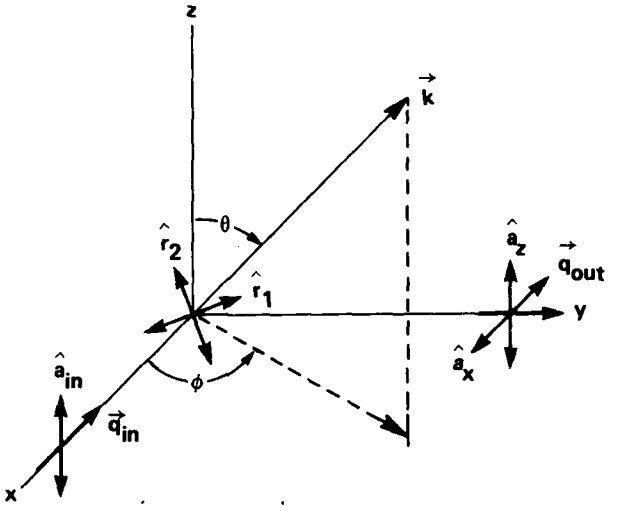

Figure 4.2.4. Diagram Showing the Role of an Electron of Wave Vector $\vec{k}$ in a Typical Photoluminescent Experiment

Therefore the linear polarization of the emitted light along y excited by light incident along the x-axis polarized along z is given by:

$$Pol = \frac{I_{zz} - I_{zx}}{I_{zz} + I_{zx}} \qquad (4.2.23)$$

where:

$$I_{zz} = \int_0^{2\pi}\int_0^{\pi} (\hat{k} \cdot \hat{r}_i)^2 (\hat{k}\cdot\hat{r}_i)^2 \, d(\cos\theta)d\phi$$

$$I_{zx} = \int_0^{2\pi}\int_0^{\pi} (\hat{k} \cdot \hat{r}_i)^2 (\hat{i}\cdot\hat{r}_i)^2 \, d(\cos\ \ )d\phi$$

For transitions involving the m = o valence band, $\hat{r}_i = \hat{r}_3$ and Eq. (27) gives Pol = 1/2. For transitions involving the $m_k = \pm 1$ valence bands we obtain Pol = 1/7.

We can do a similar analysis for circularly polarized light incident along the z-axis. Examination of the circular polarization of the light emitted along the same axis gives a circular polarization of 5/7 for transitions involving the $m_k = \pm 1$ valence band.

Therefore, the $\vec{k}\cdot\vec{p}$ interactions provide for an optical orientation of electron momentum when a III-V semiconductor is illuminated with either linear or circularly polarized light. For transitions involving the heavy mass bands ($m_k = \pm 1$), the electron wave vectors are oriented principally normal to the polarization vector. For transitions involving the light mass band ($m_k = 0$), transitions are principally parallel to the polarization

vector of the exciting light. If no relaxation processes occur, light viewed in a plane normal to the polarization vector is linearly polarized 1/7 for $m_k = \pm 1$ transitions and 1/2 for $m_k = 0$ transitions.

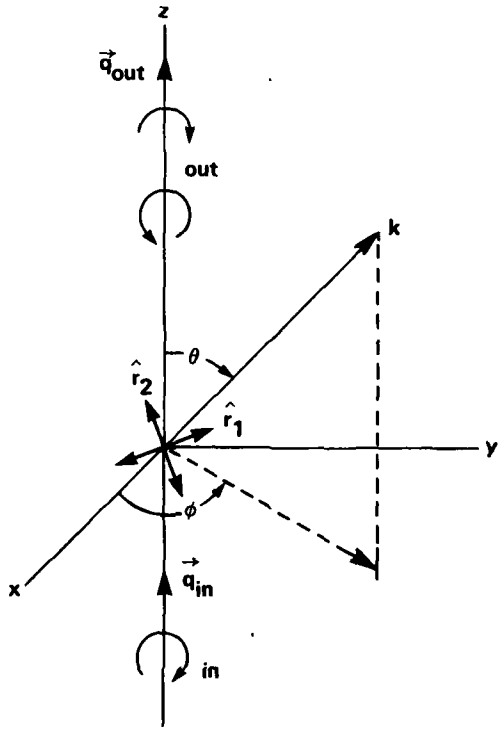

Figure 4.2.5. Photoluminescence Experiment Using Circularly Polarized Light

Illumination with circularly polarized light produces a 50% orientation of angular moment along the propagation vector of the exciting light for heavy hole transitions. If no relaxations occur the emitted light has a 5/7 circular polarization.

INTERACTIONS INVOLVING SPIN-ORBIT INTERACTION

To this point we have ignored effects due to spin. We have been able to do this since, in the absence of spin-orbit interaction, all states are degenerate with respect to spin and the momentum operator does not operate on the spin coordinates. Obviously, no orientation of spins occurs in this approximation. We now want to isolate effects due to spin-orbit interaction and will consider the problem for $\vec{k} = 0$. The spin-orbit interaction in this approximation affects only the valence band states.

The wave functions appropriate to the problem are obtained most easily using matrix diagonalization techniques. The treatment is identical to the splitting of a P state in the hydrogen atom.

The valence band energies obtained are:

$$E_{v,\ \frac{1}{2},\ \pm\frac{1}{2}} = 0 \qquad E_{v,\ \frac{1}{2},\ \pm\frac{1}{2}} = -\Delta \tag{4.2.24}$$

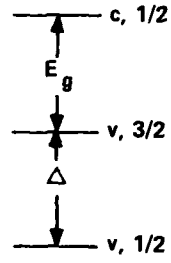

Figure 4.2.6. Energy Levels Resulting from Spin-Orbit Interaction

For wave functions we have:

$$|v, +\tfrac{3}{2}\rangle = |\frac{1}{\sqrt{2}}(X + iY)\uparrow\rangle$$

$$|v, -\tfrac{3}{2}\rangle = |\frac{1}{\sqrt{2}}(x - iY)\downarrow\rangle$$

$$|v, +\tfrac{1}{2}\rangle = \frac{1}{\sqrt{3}}|\frac{1}{\sqrt{2}}(x + iY)\downarrow\rangle + \sqrt{\frac{2}{3}}|Z\uparrow\rangle$$

$$|v, -\tfrac{1}{2}\rangle = \frac{1}{\sqrt{3}}|\frac{1}{\sqrt{2}}(x - iY)\uparrow\rangle + \sqrt{\frac{2}{3}}|Z\downarrow\rangle$$

$$|\Delta, +\tfrac{1}{2}\rangle = \sqrt{\frac{2}{3}}|\frac{1}{\sqrt{2}}(x + iY)\downarrow\rangle - \frac{1}{\sqrt{3}}|Z\uparrow\rangle$$

$$|\Delta, -\tfrac{1}{2}\rangle = \sqrt{\frac{2}{3}}|\frac{1}{\sqrt{2}}(x - iY)\uparrow\rangle - \frac{1}{\sqrt{3}}|Z\uparrow\rangle$$

For the corresponding dipole moments we have:

$$\langle c, \pm\tfrac{1}{2}|\vec{p}|v, \pm\tfrac{3}{2}\rangle = P\frac{1}{\sqrt{2}}(\hat{i} \pm i\hat{j})$$

$$\langle c, \pm\tfrac{1}{2}|\vec{p}|v, \mp\tfrac{3}{2}\rangle = 0$$

$$\langle c, \pm\tfrac{1}{2}|\vec{p}|v, \pm\tfrac{1}{2}\rangle = P\sqrt{\frac{2}{3}}\hat{k}$$

$$\langle c, \pm\tfrac{1}{2}|\vec{p}|v, \mp\tfrac{1}{2}\rangle = P\frac{1}{\sqrt{6}}(\hat{i} \mp i\hat{j})$$

$$\langle c, \pm \tfrac{1}{2} | \vec{p} | \Delta, \pm \tfrac{1}{2} \rangle = -P \frac{1}{\sqrt{3}} \hat{k}$$

$$\langle c, \pm \tfrac{1}{2} | \vec{p} | \Delta, \mp \tfrac{1}{2} \rangle = P \frac{1}{\sqrt{3}} (\hat{i} \mp i \hat{j}) \qquad (4.2.26)$$

Orientation of angular momentum occurs in both the conduction band and in the valence band similar to the situation with the $\vec{k}\cdot\vec{p}$ interaction. The new feature is the alignment of electron spins.

Consider excitation with a monochromatic beam of polarization vector:

$$\hat{a} = \frac{1}{\sqrt{2}} (\hat{i} + i \hat{j}).$$

By summing over all processes involving the four degenerate states that result in the excitation of an electron with spin up we obtain:

$$f_\uparrow = P^2 A_o^2 \left[\tfrac{1}{3}\right]$$

$$f_\downarrow = P^2 A_o^2 \, [1] \qquad (4.2.27)$$

This gives a maximum spin polarization of:

$$Pol_{spin} = \frac{f_\uparrow - f_\downarrow}{f_\uparrow + f_\downarrow} = -\frac{1}{2} \qquad (4.2.28)$$

If this spin alignment persists the polarization of the luminescence is given by:

$$Pol_{lum} = \frac{f_\uparrow f_\uparrow + f_\downarrow f_\downarrow - f_\uparrow f_\downarrow - f_\downarrow f_\uparrow}{f_\uparrow f_\uparrow + f_\downarrow f_\downarrow + f_\uparrow f_\downarrow + f_\downarrow f_\uparrow} = \frac{1}{4} \qquad (4.2.29)$$

This corresponds to a maximum circular polarization of 25% somewhat smaller than the 5/7 circular polarization corresponding to the alignment of orbital angular momentum.

THE KANE BAND MODEL

The dispersion relations for the energy bands and the wave function coefficients defined below resulting from Kane's calculations are shown in Figure 4.2.7. In this approximation in which interactions with more remote bands are neglected, the heavy holde valence band and the light hole valence band at large wave vectors appear flat. Interactions with more remote bands remove this anonaly. For nondegenerate material, the Fermi level lies in the energy gap between band E_c and band E_{v1}. The fundamental absorption corresponds to transitions involving bands E_c and E_{v1} or E_{v2}. At higher photon energies transitions involving E_{v3} can occur. Neglecting certain higher order corrections, we have found that the dispersion relations for the bands can be given by:

$$E_c = \frac{E_g}{2} + \frac{\hbar^2 k^2}{2m} + \frac{E_g}{2} \left[1 + 4 \frac{\hbar^2 k^2 \, f_1(E_c)}{2m_c \, E_g} \right]^{1/2} \qquad (4.2.30)$$

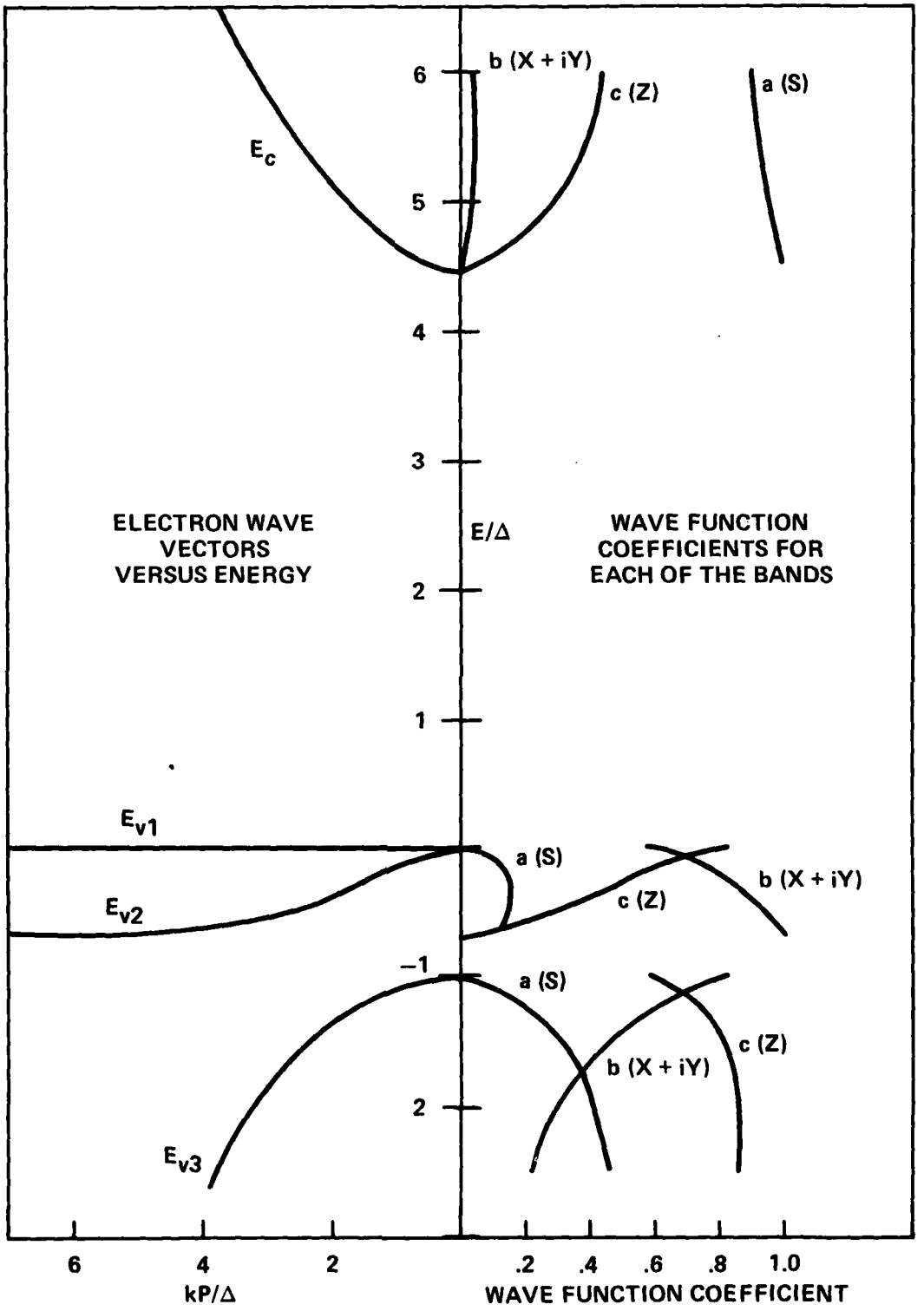

Figure 4.2.7. Variation of the Energies and Wave Function Coefficients for the Kane Calculation for GaAs

$$E_{v1} = \frac{\hbar^2 k^2}{2m} - \frac{\hbar^2 k^2}{2m_v}\left(1 - \gamma' \frac{k_x^2 k_y^2 + k_y^2 k_z^2 + k_z^2 k_x^2}{\frac{1}{3} k^4}\right)$$

$$E_{v2} = \frac{E_g}{2} + \frac{\hbar^2 k^2}{2m} - \frac{E_g}{2}\left[1 + 4 \frac{\hbar^2 k^2}{2m_c} \frac{2(E_g + \Delta)}{3E_g + 2\Delta} \frac{f_2(E_{v2})}{E_g}\right]^{1/2}$$

$$E_{v3} = -\frac{\Delta}{2} + \frac{\hbar^2 k^2}{2m} - \frac{\Delta}{2}\left[1 + 4 \frac{\hbar^2 k^2}{2m_c} \frac{E_g}{3E_g + 2\Delta} \frac{f_3(E_{v3})}{\Delta}\right]^{1/2}$$

The effective mass m_v and the warping term in E_{vi} result from interactions with bands more remote than the ones we have been considering. The warping is, of course, a departure from spherical symmetry and in this work we will neglect its effect on the optical orientation.

The functions f_1, f_2 and f_3 are slowly varying functions of energy that are equal to unity at $k = 0$.

$$\frac{1}{m_c} = 2 \frac{P^2}{\hbar^2} \frac{E_g + \frac{2}{3}\Delta}{E_g (E_g + \Delta)} \tag{4.2.31}$$

$$f_1 = \frac{(E_g + \Delta)(E_c + \frac{2}{3}\Delta)}{(E_g + \frac{2}{3}\Delta)(E_c + \Delta)}$$

$$f_2 = \frac{3}{2} \frac{E_{v2} + \frac{2}{3}\Delta}{E_{v2} + \Delta}$$

$$f_3 = \frac{3(\Delta + E_g)(E_{v3} + \frac{2}{3}\Delta)}{\Delta (E_{v3} - E_g)} \tag{4.2.32}$$

It should be noted that these are monotonic functions of energy with the limits

$$1 \leq f_1 \leq \frac{E_g + \Delta}{E_g + \frac{2}{3}\Delta} \leq \frac{3}{2}$$

$$1 \leq f_1 \geq 0$$

$$1 \leq f_3 \leq 3 + 3 \frac{E_g}{\Delta} \tag{4.2.33}$$

The band wave functions can be given as linear combinations of the wave functions S, X, Y, and Z. For k in the direction of z corresponding to one of the crystal symmetry axes, the wave functions for band E_{v1} depending upon spin are given by:

$$|v, \vec{k}, \pm \tfrac{3}{2}\rangle = \begin{Bmatrix} (X + iY)\frac{\uparrow}{\sqrt{2}} \\ \\ (X - iY)\frac{\downarrow}{\sqrt{2}} \end{Bmatrix} \tag{4.2.34}$$

and for the bands E_c, E_{v2}, and E_{v3} the wave functions are given by:

$$|b, \vec{k}, \pm \tfrac{1}{2}\rangle = \begin{Bmatrix} a_i(k)\,[iS\downarrow] + b_i(k)\left[(X - iY)\frac{\uparrow}{\sqrt{2}}\right] + c_i(k)[Z\downarrow] \\ \\ a_i(k)\,[iS\uparrow] + b_i(k)\left[-(X - iY)\frac{\downarrow}{\sqrt{2}}\right] + c_i(k)[Z\uparrow] \end{Bmatrix} \tag{4.2.35}$$

If $\vec{k}$ is not along the z-axis one can transform the basis functions according to:

$$\begin{bmatrix} \uparrow \\ \downarrow \end{bmatrix} = \begin{bmatrix} e^{-i\phi/2}\cos\theta/2 & e^{i\phi/2}\sin\theta/2 \\ -e^{-i\phi/2}\sin\theta/2 & e^{i\phi/2}\cos\theta/2 \end{bmatrix} \begin{bmatrix} \uparrow \\ \downarrow \end{bmatrix}$$

$$\begin{bmatrix} X' \\ Y' \\ Z' \end{bmatrix} = \begin{bmatrix} \cos\theta\cos\phi & \cos\theta\sin\phi & -\sin\theta \\ -\sin\phi & \cos\phi & 0 \\ \sin\theta\cos\phi & \sin\theta\sin\phi & \cos\theta \end{bmatrix} \begin{bmatrix} X \\ Y \\ Z \end{bmatrix} \tag{4.2.36}$$

In general, the coefficients are given by:

$$a_c = \frac{1}{N_c},\ b_c = \frac{1}{N_c}\frac{\sqrt{2}\Delta}{3(E_g + \epsilon_c) + 2\Delta}\frac{\epsilon_c}{kP},\ c_c = \frac{1}{N_c}\frac{\epsilon_c}{kP} \qquad (4.2.37)$$

$$a_{v2} = \frac{1}{N_{v2}}kP,\ b_{v2} = \frac{1}{N_{v2}}\frac{\sqrt{2}}{3}\Delta\frac{\epsilon_{v2} - E_g}{\epsilon_{v2} + 2\Delta/3},\ c_{v2} = \frac{1}{N_{v2}}(\epsilon_{v2} - E_g);$$

$$a_{v3} = \frac{1}{N_{v3}}kP,\ b_{v3} = \frac{1}{N_{v3}}\frac{\sqrt{2}}{3}\Delta\frac{(\epsilon_{v3} - \Delta - E_g)}{(\epsilon_{v3} - \Delta/3)},\ c_{v3} = \frac{1}{N_{v3}}(\epsilon_3 - \Delta - E_g);$$

where:

$$\epsilon(k) \equiv E(k) - E(0) - \frac{\hbar^2k^2}{2m}$$

The quantity $N_i^2 = N_i^2(k)$ is a normalizing factor such that $a_i^2 + b_i2 + c_i^2 = 1$. The band parameters Δ, m_c, and γ' are related to certain matrix elements. For example, consider heavy hole transitions to the conduction band, the appropriate dipole moments are given by:

$$\langle c, \vec{k}, \pm\tfrac{1}{2}|\vec{p}|v, \vec{k}, \tfrac{3}{2} \pm \tfrac{3}{2}\rangle = P\frac{a_c}{\sqrt{2}}(\hat{r}_1 \pm i\,\hat{r}_2) \qquad (4.2.38)$$

$$\langle c, \vec{k} \pm \tfrac{1}{2}|\vec{p}|v, \vec{k}, \tfrac{3}{2} \mp \tfrac{3}{2}\rangle = 0$$

In linear polarized light ($\hat{a} = \hat{k}$) orientation of the excited electron wave vectors occurs as with the k·p interaction being distributed as $\sin^2\theta$ In photoluminescence the light emitted in the x-y plane should be polarized 1/7.

In excitation with circularly polarized light, orientation of electron spins occurs as with angular momenta in the valence band. This orientation, by analogy with the analysis of the $\vec{k}\cdot\vec{p}$ interaction, corresponds to an average angular momentum per excitation of $\hbar/2$, and a spin orientation of 50%.

Orientation effects due to transitions involving the light hole and the split off valence bands will be more complicated but can be obtained in a straightforward way from the wave functions. In general, the heavy hole transitions will dominate the absorption and emission processes because of the larger density of states involved. The alignment effects for the light hole bands will, in general, be less, since each transition has dipole components along each of $\hat{r}_1$, $\hat{r}_2$ and $\hat{r}_3$.

CONCLUSIONS

Calculations of optical orientation effects in semiconductors employing essentially the techniques of the Kane band model for the states near the energy gap have shown that the $\vec{k}\cdot\vec{p}$ interaction results in spatial quantization along the wave vectors of the excited electrons and holes. This provides a connection between the orientation of the dipole moments that govern the associated optical transitions and the direction of the electron wave vector. Excitation with polarized light results in preferred orientations of electron wave vectors and angular momenta. Calculated values of 14% and 71%, respectively, for the linear and circular polarization of recombination radiation, compare reasonably well with observed values of 15% and 50%. However, there are a variety of complications that may affect the calculated values.

Intrinsic absorption and recombination involve exciton states. This interaction has been shown experimentally and theoretically to modify the fundamental absorption edge of semiconductors,[4.8] in both the discrete state and the continuum. Similar complications can be expected in the optical orientation.

In the Kane band model, angular momentum is a good quantum number since the model essentially possesses spherical symmetry rather than the lower cubic symmetry. When higher order corrections are taken into account, effects should occur due to quenching of angular momentum.

Finally, nowhere in our model do we take explicit account of interactions with the field due to the macroscopic magnetization created. This would tend to have the effect of producing spatial quantization along the axis of the magnetization. Techniques similar to those used by Pidgeon, Brown and Groves[4.9] for magneto-optical experiments might be appropriate.

4.3 Dynamics of Electron Spin Polarization

Suppose the optical selection rules, as determined by the matrix elements discussed in the last section, are such as to produce more electrons of one spin than the other. If we focus our attention on the electrons of a given energy, ϵ, we can restrict our definition of spin polarization to that energy by the definition

$$P(\epsilon) = \frac{n\uparrow(\epsilon) - n\downarrow(\epsilon)}{n\uparrow(\epsilon) + n\downarrow(\epsilon)} \tag{4.3.1}$$

where n is the concentration of electrons of energy, ϵ, and spin $\uparrow$ or $\downarrow$. We would like to consider the energy dependence of such a spin polarization and how it behaves with time and excitation conditions.

Consider an initially empty conduction band in which one creates a spin polarization by optically exciting electrons from the valence band at different rates $g\uparrow(\epsilon)$ and $g\downarrow(\epsilon)$, as determined by the optical selection rules. If one wanted to solve the problem in all generality one would have to solve an infinite set of coupled equations of the form:

$$\frac{dn\uparrow(\epsilon)}{dt} = g\uparrow(\epsilon) - \frac{n\uparrow(\epsilon)}{\tau_{RC}\uparrow(\epsilon)} + \sum_{\epsilon'}\Big[R\uparrow\uparrow((n\uparrow(\epsilon) \leftrightarrows n\uparrow(\epsilon')) + R\uparrow\downarrow((n\uparrow(\epsilon) \rightleftarrows n\downarrow(\epsilon'))\Big] \tag{4.3.2}$$

$$\frac{dn\downarrow(\epsilon)}{dt} = g\downarrow(\epsilon) - \frac{n\downarrow(\epsilon)}{RC\downarrow(\epsilon)} + \sum_{\epsilon'}\Big[R\downarrow\downarrow(n\downarrow(\epsilon) \leftrightarrows n\downarrow(\epsilon')) + R\uparrow\downarrow((n\downarrow(\epsilon) \rightleftarrows n\uparrow(\epsilon'))\Big]$$

where $1/\tau_{RC}\uparrow(\epsilon)$ and $1/\tau_{RC}\downarrow(\epsilon)$ are the respective recombination rates, $R\uparrow\uparrow$ and $R\downarrow\downarrow$ are the respective scattering rates without spin flip and $R\uparrow\downarrow$ and $R\downarrow\uparrow$ are the scattering rates with spin flip.

Equations (4.3.2) are obviously too formidable for any kind of general solutions. By making certain simpifying assumptions, however, one can gain some insight into the problem.

Consider the quasi-thermalized carriers at the bottom of tne conduction band (see Fig. 4.0.2). By assuming some form of quasi-equilibrium we can avoid the rigors of Eq. (4.3.2) and apply statistical thermodynamics. We assume that electrons of a given spin are in termal equilibrium with each other, but interact weakly with electrons of the opposite spin. The effect of the optical excitation, alignment and relaxations results in setting up an electron temperature, T_e, and a quasi-Fermi level for each spin, $\mu\uparrow$ and $\mu\downarrow$. The concentration of electrons of a given spin at an energy, ϵ, is then given by:

$$n_{\uparrow}(\epsilon) = \frac{\rho(\epsilon)}{1+e^{(\epsilon-\mu_{\uparrow})/kT}} \tag{4.3.3}$$

where $\rho(\epsilon)$ is the density of states at energy, ϵ. Here, in some complicated fashion $\mu\uparrow$, $\mu\downarrow$, T_e are determined by the g's and τ's in Eq. 4.3.2. If one neglects the effect of the magnetization on the density of states one obtains in steady state:

$$P(\epsilon) = \frac{e^{(\mu_o-\mu_\downarrow)/kT} - e^{(\mu_o-\mu_\uparrow)/kT}}{2e^{(\mu_o-\epsilon)/kT} + e^{(\mu_o-\mu_\downarrow)/kT} + e^{(\mu_o-\mu_\uparrow)/kT}} \tag{4.3.4}$$

where we have substituted (4.3.3) into (4.3.1), and set:

$$\mu_o = (\mu_\uparrow + \mu_\downarrow)/2 \tag{4.3.5}$$

The only energy dependence of the polarization occurs in the first term of the denominator of Eq. (4.3.4). A strong energy dependence will occur only for a degenerate carrier distribution and then only over a range of about ±4kT of μ_o. For a Boltzmann distribution the energy dependence will be negligible and the spin polarization will be given by:

$$P_{spin} \approx \frac{1-e^{-(\mu_\uparrow-\mu_\downarrow)/kT}}{1+e^{-(\mu_\uparrow-\mu_\downarrow)/kT}} \tag{4.3.6}$$

This energy independent spin polarization would indicate that the photoluminescence is, likewise, energy independent. If to the contrary, one observes that the photoluminescence associate with the conduction band electrons varys with energy then one of the following must be true:

1. The polarization dependence of the optical selection rules are varying with energy.
2. The polarization of the corresponding holes vary with energy.
3. The electron distribution is degenerate.
4. The electrons are not in quasi thermal equilibrium.
5. The assumption of two mildly interacting spin systems is not realistic.
6. Orientations other than spin are affecting the luminescence polarization.

In the above treatment we lost all connection with generation rates and relaxation times, these being implicit in the quasi-Fermi levels and electron temperature. We can re-establish some connection by returning to (4.3.2) and summing over energy giving:

$$\frac{d}{dt}\sum_\epsilon n\uparrow(\epsilon) = \sum_\epsilon g\uparrow(\epsilon) - \sum_\epsilon \frac{n\uparrow(\epsilon)}{\tau_{RC}{}^{\uparrow}(\epsilon)} + \sum_\epsilon \sum_{\epsilon'} \Big(R_{\uparrow\uparrow}(n\uparrow(\epsilon') \rightleftarrows n\uparrow(\epsilon')) + R\uparrow\downarrow(n\uparrow(\epsilon) \rightleftarrows n\downarrow(\epsilon')) \Big)$$

$$\frac{d}{dt}\sum_\epsilon n\downarrow(\epsilon) = \sum_\epsilon g\downarrow(\epsilon) - \sum_\epsilon \frac{n\downarrow(\epsilon)}{\tau_{RC}{}^{\downarrow}(\epsilon)} + \sum_\epsilon \sum_{\epsilon'} \Big(R\downarrow\downarrow(n\downarrow(\epsilon) \rightleftarrows n\downarrow(\epsilon')) + R\downarrow\uparrow(n\downarrow(\epsilon) \rightleftarrows n\uparrow(\epsilon')) \Big) \tag{4.3.7}$$

Setting:

$$N\uparrow = \sum_{\epsilon} n\uparrow(\epsilon) \; ; \quad N\downarrow = \sum_{\epsilon} n\downarrow(\epsilon)$$

$$\sum\sum_{\epsilon\epsilon'} R\uparrow\uparrow(n\uparrow(\epsilon) \leftrightarrows n\uparrow(\epsilon)) = \sum\sum_{\epsilon\epsilon'} R\downarrow\downarrow(n\uparrow(\epsilon) \leftrightarrows n\uparrow(\epsilon)) = 0 \qquad (4.3.8)$$

$$-\frac{N\uparrow - N\downarrow}{2\tau_{sf}} = \sum\sum_{\epsilon\epsilon'} R\uparrow\downarrow(n\uparrow(\epsilon) \leftrightarrows n\downarrow(\epsilon'))$$

We then get the pair of coupled equations:

$$\frac{dN\uparrow}{dt} = G\uparrow - \frac{N\uparrow}{\tau_{RC\uparrow}} - \frac{N\uparrow - N\downarrow}{2\tau_{sf}} \qquad (4.3.9)$$

$$\frac{dN\downarrow}{dt} = G\downarrow - \frac{N\downarrow}{\tau_{RC\downarrow}} + \frac{N\uparrow - N\downarrow}{2\tau_{sf}}$$

For times short relative to the relaxation times, these have the solutions:

$$N\uparrow + N\downarrow = (G\uparrow + G\downarrow)t$$

and

$$P = \frac{G\uparrow - G\downarrow}{G\uparrow + G\downarrow} \qquad (4.3.10)$$

Whereas the steady state solutions (i.e, τ much greater than the relaxation times) are given by:

$$N_{\uparrow} + N_{\downarrow} = \frac{(G_{\uparrow} + G_{\downarrow})\ \tau_{RC} + (G_{\uparrow} - G_{\downarrow})\ \frac{\tau_{RC}\,\tau_{sf}}{B}\ (\tau_{RC\uparrow} - \tau_{RC\downarrow})}{1 - \frac{\tau_{sf}}{B}\ \frac{(\tau_{RC\uparrow} - \tau_{RC\downarrow})^2}{\tau_{RC\uparrow} + \tau_{RC\downarrow}}}$$

$$P = \frac{\frac{G\uparrow - G\downarrow}{G\uparrow + G\downarrow} + \frac{1}{\tau_{RC}}\ \frac{\tau_{RC\uparrow} - \tau_{RC\downarrow}}{\tau_{RC\uparrow} + \tau_{RC\downarrow}}}{1 + \frac{\tau_{RC}}{\tau_{sf}} + \frac{1}{2}\ \frac{G\uparrow - G\downarrow}{G\uparrow + G\downarrow}\ \frac{\tau_{RC\uparrow} - \tau_{RC\downarrow}}{\tau_{RC\uparrow} + \tau_{RC\downarrow}}} \qquad (4.3.11)$$

where

$$\frac{1}{\tau_{RC}} = \frac{1}{2}\ \frac{\tau_{RC\uparrow} + \tau_{RC\downarrow}}{\tau_{RC\uparrow}\ \tau_{RC\downarrow}} \; ; \quad B = 2\ \tau_{RC\uparrow}\,\tau_{RC\downarrow} + \tau_{RC\uparrow}\ \tau_{sf} + \tau_{RC\downarrow}\,\tau_{sf}$$

Inspection of Eqs. (4.3.10) and (4.3.11) show that relaxations can either enchance or diminish the initial spin polarization. Enhancement can occur if recombination times for the two spins are different. Such a situation exists if the recombination occurs via paramagnetic recombination, and the recombination centers become aligned. Singlet recombination is faster than triplet

recombination and, therefore, the lifetime for carriers of the majority spin increases over that for carriers of the minority spin. Under these conditions both the polarization and the steady state excited electron concentration increases, as can be ascertained by examining Eq. (4.3.11).

In the more common situation where recombination is independent of spin (i.e. $\tau_{RC\uparrow}=\tau_{RC\downarrow}$), the steady state solutions are given by:

$$(N\uparrow+N\downarrow) = (G\uparrow+G\downarrow)\,\tau_{RC} \tag{4.3.12}$$

$$P = \frac{\frac{G\uparrow-G\downarrow}{G\uparrow+G\downarrow}}{1+\frac{\tau_{RC}}{\tau_{sf}}}$$

so that a high spin polarization is favored by a long spin relaxation time and by a short recombination time.

Next we consider the time dependence for the case where G↑ and G↓ are constant in time and N↑=N↓=0 at t=o. We then obtain:

$$(N\uparrow+N\downarrow) = (G\uparrow+G\downarrow)\,\tau_{RC}\,(1-e^{-\frac{t}{\tau_{RC}}})$$

$$P = \frac{\frac{G\uparrow-G\downarrow}{G\uparrow+G\downarrow}}{1+\frac{\tau_{RC}}{\tau_{sf}}}\;\frac{1-\exp\left[-t\left(\frac{1}{\tau_{RC}}+\frac{1}{\tau_{sf}}\right)\right]}{1-\exp\left[-\frac{t}{\tau_{RC}}\right]} \tag{4.3.13}$$

If at $t=t_o$, G↑ and G↓ abruptly go to zero, the excited electron concentration and the polarization decay as:

$$(N\uparrow+N\downarrow) = ((N\uparrow(t_o) + N\downarrow(t_o))e^{-(t-t_o)/\tau_{RC}} \tag{4.3.14}$$

$$P = P(t_o)e^{-(t-t_o)/\tau_{sf}}$$

From these equations one can see that the most direct measurement of the spin relaxation time and the recombination time is to observe the rate of decay following a narrow pulse excitation, as has been done by Seymour and Alfano for GaAs.[4.10]

The above treatment cannot be expected to apply very well to electrons having energies in a range where excitation or recombination varies strongly with energy. If electrons are excited by a monochromatic source to an energy, ϵ_x, then departures from equilibrium can be expected near the energy ϵ_x. If some rapid nonradiative recombination occurs due to some trapping level overlapping the conduction band at some energy, ϵ_t, then departures from equilibrium can be expected at the energy ϵ_t. A particular

case is where electrons are excited to an energy greater than the energy of an LO phonon $\hbar\omega_{LO}$. The most likely relaxation is by emission of an LO-phonon. Such relaxation occurs much faster than recombination times so that one can expect a steady state concentration given by

$$n\uparrow(\epsilon)+n\downarrow(\epsilon)=\left[g\uparrow(\epsilon) +g\downarrow(\epsilon)\right] \tau_{LO} \tag{4.3.15}$$

where τ_{LO} is the relaxation time associated with the emission of an optical phonon. In the absence of unusually high spin relaxation by other processes, the spin polarization of the excited electrons should approximate the initial polarization given by:

$$P(\epsilon) \simeq \frac{g\uparrow(\epsilon)-g\downarrow(\epsilon)}{g\uparrow(\epsilon)+g\downarrow(\epsilon)} \tag{4.3.16}$$

However, each emission of an optical phonon can contribute to randomization of the electron spin along with other scattering processes and one can expect an electron spin polarization that decreases monotonically with decrease in energy below the excitation energy ϵ_x approaching the constant polarization of the thermalized electrons.

From the above analysis of the energy dependence of the spin polarization, we would expect the polarization to increase monotonically with energy starting from essentially zero for very degenerate electrons much below the Fermi level, asymptotically approaching a constant value for thermalized electrons more than about 2kT above the Fermi Level, and rising again for "hot" electrons more than one LO phonon energy above the bottom of the conduction band approaching the initial polarization of the optically excited electrons. The above analysis has neglected additional effects that may become significant in specific cases. Yet to be considered are effects like the modification of the density of states and the wave functions due to the magnetization associated with the spin polarization, nuclear alignment, etc. In addition one should consider electron-hole interactions resulting in transfer of hole spin and orbital angular moments to the electron spin system.

4.4 Light Scattering Approach To The Photoluminescence Problem

In Section 4.2 we have treated the absorption and emission problems as essentially separate. In this section we discuss a second method which we believe to be more rigorous, but which will be difficult to evaluate numerical, since it requires treating electron-phonon and other relaxation mechanisms in the combined absorption and re-emission processes.

We remark that, with detailed analysis, it may turn out that the treatments of Sections 4.2 and 4.4 lead to substantially the same predictions for polarized photo luminescence. This remains to be demonstrated, however.

The theoretical analysis of the observed photon polarization is extremely interesting since it touches on a matter which has been the subject of great deal of controversy in the literature.[4.12-4.17] The central question concerns whether there is any real distinction between Resonant-Raman Scattering (RRS), and the process of Absorption followed by Emission (AE),

sometimes referred to as Hot Luminescence (HL). We shall discuss this problem in some detail below. However, here we point out that the spin-polarization measurements should be an extremely sensitive probe of any theory. In particular, most previous discussions of the problem concern themselves with properties such as intensities and lineshapes, with polarizations being averaged or summed over. A theory which is capable of explaining the observed polarization should settle the controversy in a convincing fashion.

Concerning the controversy itself, we agree with those who argue that there can be no real distinction between RRS and AE. Our argument goes as follows. Let $|\vec{k}_i\omega_i\hat{\epsilon}_i>|i>$ denote an initial state consisting of a photon with wave vector, frequency, and polarization given by $\vec{k}_i,\omega_i,\hat{\epsilon}_i$ respectively, with $|i>$ denoting a general atomic state. This state can be a many-body state, including all possible interactions, electron-electron, electron-phonon, electron-impurity, etc. Similarly let $|o>|I>$ denote a real intermediate state consisting of no photon ($|o>$ = vacuum state), with $|I>$ an intermediate atomic state. By real we mean that the physical process is initial → intermediate → final with total energy rigorously conserved in each step. Also let $|\vec{k}_f\omega_f\hat{\epsilon}_f>|f>$ denote the final state, with one photon present in the radiation field.

Clearly the above states are involved in what one intuitively might think of either as RRS or as AE. However, quantum electro-dynamics provides an unambiguous answer for the probability $|\vec{k}_i\omega_i\hat{\epsilon}_i>|i> \rightarrow |k_f\omega_f\hat{\epsilon}_f>|f>$. The transistion probability per unit time is given by:

$$\omega_{i\rightarrow f} = \frac{(2\pi)^3}{\Omega^2}\cdot\frac{\hbar}{\omega_i\omega_f}\cdot\delta(\epsilon_f-\epsilon_i+\hbar\omega_f-\hbar\omega_i)$$

$$*\left|\sum_I <f|\hat{\epsilon}_f.\vec{P}(-\vec{k}_f)|I><I|\hat{\epsilon}_i.\vec{P}(\vec{k}_i)|i>.\pi\delta(\epsilon_I-\epsilon_i-\hbar\omega_i)\right|^2 \qquad (4.4.1)$$

We note that the product of the two delta functions can be rewritten:

$$\delta(\epsilon_f-\epsilon_i+\hbar\omega_f-\hbar\omega_i)\ \delta(\epsilon_I-\epsilon_i-\hbar\omega_i)=\delta(\epsilon_f-\epsilon_i+\hbar\omega_f-\hbar\omega_i)\ \delta(\epsilon_I-\epsilon_f-\hbar\omega_f),$$

and corresponds to energy conservation as shown in Fig. 4.4.1

In Eq. (4.4.1), conservation of momentum is contained in the various matrix elements, Ω is the system volume, and

$$\vec{P}(\vec{k}_i) = \sum_j \frac{e_j}{m_j}\vec{p}_j e^{i\vec{k}_i.\vec{r}_j}, \qquad (4.4.2a)$$

$$\vec{P}(-\vec{k}_f) = \sum_j \frac{e_j}{m_j}\vec{p}_j e^{-i\vec{k}_f.\vec{r}_j}, \qquad (4.4.2b)$$

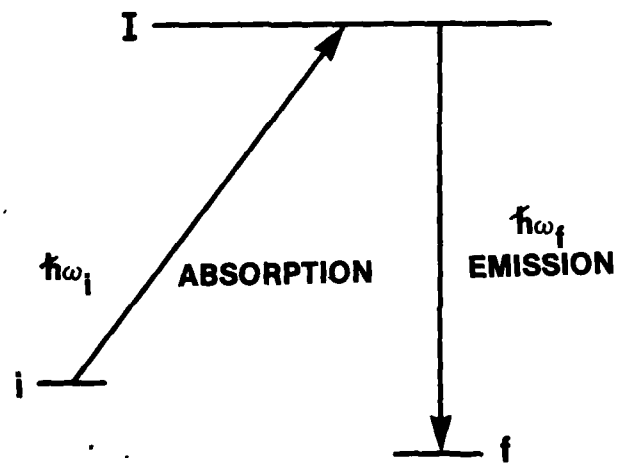

Figure 4.4.1. Definition of Absorption and Emission Processes Involving Initial State i, Intermediate State I and Final State f.

where the sums over j are over all charged particles in the system with charge e_j, mass m_j, and with $\vec{p}_j$, $\vec{r}_j$ the single-particle momentum and positio operators. We note that

$$\hat{\epsilon}_i \cdot \vec{P}(\vec{k}_i) = \sum_j \frac{e_j}{m_j} \hat{\epsilon}_i \cdot \vec{p}_j e^{i\vec{k}_i \cdot \vec{r}_j} \tag{4.4.3}$$

and we also note that $(\hat{\epsilon}_i \cdot \vec{p}_j)$ and $(e^{i\vec{k}_i \cdot \vec{r}_j})$ commute, because $\hat{\epsilon}_i$ is perpendicular to $\vec{k}_i$ (from transversality of the photon).

Now if we are interested in the correlation between the initial and final photon states, we must, in general, average over all initial atomic states $|i\rangle$ and sum over all final atomic states. This average is

$$\bar{w} = \sum_{if} \rho(\epsilon_i) w_{if} \tag{4.4.4}$$

where $\rho(\epsilon_i)$ is the equilibrium density matrix of initial states.

This gives

$$\bar{w} = \frac{(2\pi)^3}{\Omega^2} \frac{\hbar}{\omega_i \omega_f} \sum_{if} \rho(\epsilon_i) \delta(\epsilon_f - \epsilon_i + \hbar\omega_f - \hbar\omega_i) ,$$

$$* \left| \sum_I \langle f | \hat{\epsilon}_f \cdot \vec{P}(-\vec{k}_f) | I \rangle \langle I | \hat{\epsilon}_i \cdot \vec{P}(\vec{k}_i) | i \rangle \cdot \pi \delta(\epsilon_I - \epsilon_i - \hbar\omega_i) \right|^2 \tag{4.4.5}$$

We now assert that this general formula must cover both intuitive notions of RRS and AE, and yield the transition probability per unit time $\bar{w}(\hat{\epsilon}_i \to \hat{\epsilon}_f)$ for the polarizations of the photons.

Intuitively one talks about RRS if the time spent in the intermediate state $|I\rangle$ is short, and about AE if this time is relatively long. Mathematically these details are buried in the matrix elements for emission and absorption, and in the delta functions for conservation of energy.

However one might argue that mathematically there should also be a difference between RRS and AE. Let us rewrite Eq. (4.4.5) as

$$\bar{w} = \frac{(2\pi)^3}{\Omega^2} \frac{\hbar}{\omega_i \cdot \omega_f} \sum_{if} \rho(\epsilon_i) \delta(\epsilon_f - \epsilon_i + \hbar\omega_f - \hbar\omega_i)$$

$$\sum_I \langle f | \hat{\epsilon}_f \cdot \vec{P}(-\vec{k}_f) | I \rangle \langle I | \hat{\epsilon}_i \cdot \vec{P}(\vec{k}_i) | i \rangle \cdot \pi \delta(\epsilon_I - \epsilon_i - \hbar\omega_i) \tag{4.4.6}$$

$$* \sum_{I'} (\langle f | \hat{\epsilon}_f \cdot \vec{P}(-\vec{k}_f) | I' \rangle \langle I' | \hat{\epsilon}_i \cdot \vec{P}(\vec{k}_i) | i \rangle)^* \cdot \pi \delta(\epsilon_{I'} - \epsilon_f - \hbar\omega_f) .$$

Now if AE is "what is really going on", one expects that this should somehow reduce to an expression involving the separate probabilities for emission and absorption, i.e., to an expression involving

$$|\langle f|\ \hat{\epsilon}_f.\vec{P}(-\vec{k}_f)\ |\ I\rangle|^2$$

and

$$|\langle I|\ \hat{\epsilon}_i.\vec{P}(\vec{k}_i)\ |\ i\rangle|^2$$

Several authors[4.16] have made attempts to justify the existence of such factors. However, most treatments consider atoms or molecules with the simplified assumptions of three levels of interest $|i>$, $|f>$, and $|I>$, whose only degeneracy is the usual $(2J + 1)$ degeneracy associated with the magnetic quantum numbers m. The problem of justifying such factors for a spin-orbit mixed semiconductor such as GaAs seems a good deal more complicated. Moreover, in our treatment here, $|i>$, $|f>$, and $|I>$ are really many-body states containing electron-phonon, electron-impurity, and electron-electron coupling.

Let us try some very crude arguments to see what is involved. Following the treatment of the atomic case, we assume that the main effects of electron-electron, electron-phonon, electron-impurity scattering is to broaden the delta functions in Eq. (4.4.6) into Lorentzian functions. Thus, very crudely,

$$\bar{w} = \frac{(2\pi)^3}{\Omega^2}\,\frac{\hbar}{\omega_i\omega_f}\sum_{if}\rho(\epsilon_i)\,\frac{1}{\pi}\,\frac{\Gamma_{if}}{(\epsilon_f-\epsilon_i+\hbar\omega_f-\hbar\omega_i)^2+\Gamma_{if}^2}$$

$$*\sum_I \langle f|\hat{\epsilon}_f.\vec{P}(-\vec{k}_f)\ |\ I\rangle\langle I|\epsilon_i.\vec{P}(\vec{k}_i)|\ i\rangle$$

$$\cdot\ \frac{\Gamma_{iI}}{(\epsilon_I-\epsilon_i-\hbar\omega_i)^2+\Gamma_{iI}^2}$$

$$*\ \sum_I \langle f|\hat{\epsilon}_f.\vec{P}(-\vec{k}_f)\ |\ I'\rangle{}^*\langle I'|\hat{\epsilon}_i.\vec{P}(\vec{k}_i)|i\rangle{}^*$$

$$\cdot\ \frac{\Gamma_{fI'}}{(\epsilon_{I'}-\epsilon_f-\hbar\omega_f)^2+\Gamma_{fI'}^2} \qquad (4.4.7)$$

where the states $|i>$, $|f>$, $|I>$ and $|I'>$ now refer to single-electron states, and where $\rho(\epsilon_i)$ is now the single-particle (thermal equilibrium) density matrix

$$\rho(\epsilon_i) = f(\epsilon_i) = \frac{1}{e^{\beta(\epsilon_i-\mu)}+1}$$

Now let us assume that $|i>$ is a valence band state, $|f>$ is some (perhaps different) valence band state, and that only a single conduction band corresponding to $|I>$ is important.

The wave functions can be denoted by $|i\rangle=|v_i\vec{k}_i\sigma_i\rangle$, where v_i is the band index, $\vec{k}_i$ is the reduced zone wave vector, and σ_i denotes the spin state (which is generally mixed). Then our formula becomes

$$\bar{w} = \frac{(2\pi)^3}{\Omega^2}\frac{\hbar}{\omega_i\omega_f}\sum_{if} f(\epsilon_i)\cdot\frac{1}{\pi}\frac{\Gamma_{if}}{(\epsilon_f-\epsilon_i+\hbar\omega_f-\hbar\omega_i)^2+\Gamma_{if}^2}$$

$$\cdot\sum_{\vec{k}_c\sigma_c}\langle v_f\vec{K}_f\sigma_f|\hat{\epsilon}_f\cdot\vec{P}(-\vec{k}_f)|c\vec{k}_c\sigma_c\rangle$$

$$\cdot\langle c\vec{k}_c\sigma_c|\hat{\epsilon}_i\cdot\vec{P}(\vec{k}_i)|v_i\vec{K}_i\sigma_i\rangle\frac{\Gamma_{iI}}{(\epsilon_I-\epsilon_i-\hbar\omega_i)^2+\Gamma_{iI}^2}$$

$$\cdot\sum_{\vec{k}_c'\sigma_c'}\langle v_f\vec{K}_f\sigma_f|\hat{\epsilon}_f\cdot\vec{P}(-\vec{k}_f)|c\vec{k}_c'\sigma_c'\rangle^*$$

$$\cdot\langle c\vec{k}_c'\sigma_c'|\hat{\epsilon}_i\cdot\vec{P}(\vec{k}_i)|v_i\vec{K}_i\sigma_i\rangle^*$$

$$\cdot\frac{\Gamma_{fI}'}{(\epsilon_I'-\epsilon_f-\hbar\omega_f)^2+\Gamma_{fI}'^2} \qquad (4.4.9)$$

Now we consider the matrix element

$$\langle c\vec{k}_c\sigma_c|\hat{\epsilon}_i\cdot\vec{P}(\vec{k}_i)|v_i\vec{K}_i\sigma_i\rangle$$

$$=\frac{e}{m}\langle c\vec{k}_c\sigma_c|\hat{\epsilon}_i\cdot\vec{p}e^{i\vec{k}_i\cdot\vec{r}}|v_i\vec{K}_i\sigma_i\rangle$$

$$\simeq\frac{e}{m}\delta_{\vec{k}_c,\ \vec{K}_i+\vec{k}_i}\cdot\langle c\vec{K}_i\sigma_c|\hat{\epsilon}_i\cdot\vec{p}|v_i\vec{K}_i\sigma_i\rangle \qquad (4.4.10)$$

Likewise then

$$\langle c\vec{k}_c'\sigma_c'|\hat{\epsilon}_i\cdot\vec{P}(\vec{k}_i)|v_i\vec{K}_i\sigma_i\rangle^*$$

$$\simeq\frac{e}{m}\delta_{\vec{k}_c',\ \vec{K}_i+\vec{k}_i}$$

$$\cdot\langle c\vec{K}_i\sigma_c'|\hat{\epsilon}_i\cdot\vec{p}|v_i\vec{K}_i\sigma_i\rangle^* \qquad (4.4.11)$$

Clearly then the product

$$\delta\vec{k}_c,\vec{K}_i+\vec{k}_i \quad \delta\vec{k}_c' ,\vec{K}_i+\vec{k}_i$$

requires

$$\vec{k}_c' = \vec{k}_c = \vec{K}_i+\vec{k}_i.$$

Thus the sums over $\vec{k}_c'$ and $\vec{k}_c$ can be eliminated in Eq. (4.4.8). If we take the energies and Γ's to be approximately independent of spin, we obtain

$$\begin{aligned}
\bar{w} = \frac{(2\pi)^3}{\Omega^2} \frac{\hbar}{\omega_i\omega_f} \sum_{if} & f(\epsilon_i)\,\delta\vec{K}_f+\vec{k}_f,\ \vec{K}_i+\vec{k}_i \\
& * \frac{1}{\pi} \frac{\Gamma_{if}}{(\epsilon_f-\epsilon_i+\hbar\omega_f-\hbar\omega_i)^2+\Gamma_{if}^2} \\
& * \frac{\Gamma_{ic}}{(\epsilon_c,\vec{K}_i+\vec{k}_i-\epsilon_i-\hbar\omega_i)^2+\Gamma_{ic}^2} \\
& * \frac{\Gamma_{ic}}{(\epsilon_c,\vec{K}_f+\vec{k}_f-\epsilon_f-\hbar\omega_f)^2+\Gamma_{fc}^2} \qquad (4.4.12) \\
& * \frac{e^4}{m^4} \sum_{\sigma_c\sigma_c'} <v_f\vec{K}_f\sigma_f|\hat{\epsilon}_f\cdot\vec{p}|c\vec{K}_f\sigma_c> \\
& .<v_f\vec{K}_f\sigma_f|\hat{\epsilon}_f\cdot\vec{p}|c\vec{K}_f\sigma_c'>^* \\
& .<c\vec{K}_i\sigma_c|\hat{\epsilon}_i\cdot\vec{p}|v_i\vec{K}_i\sigma_i> \\
& .<c\vec{K}_i\sigma_c'|\hat{\epsilon}_i\cdot\vec{p}|v_i\vec{K}_i\sigma_i>^*
\end{aligned}$$

The Kronecher delta in the first line of the above equation expresses conservation of <u>total</u> momentum, involving the initial photon and electron momenta $(\vec{k}_i,\vec{K}_i)$, and the final photon and electron momenta $(\vec{k}_f,\vec{K}_f)$.

Now if the spin states were pure, because $\vec{P}$ is a spin-independent operator, we would obtain (from the matrix elements) the selection role $\delta\sigma_i,\sigma_f$ $\delta\sigma_c,\sigma_i$ $\delta\sigma_c,\sigma_i$, and this would give

$$\bar{w} = \frac{(2\pi)^3}{\Omega^2}\frac{\hbar}{\omega_i\omega_f}\sum_{if} f(\epsilon_i)\,\delta\vec{K}_f+\vec{k}_f,\ \vec{K}_i+\vec{k}_i$$

$$*\,\delta\sigma_f,\ \sigma_i\ \frac{1}{\pi}\ \frac{\Gamma_{if}}{(\epsilon_f-\epsilon_i+\hbar\omega_f-\hbar\omega_i)^2+\Gamma_{if}^2}$$

$$*\frac{\Gamma_{ic}}{(\epsilon_{c,\vec{K}_i+\vec{k}_i}-\epsilon_i-\hbar\omega_i)^2+\Gamma_{ic}^2}\ |<c\vec{K}_i\sigma_i|\hat{\epsilon}_i.\vec{p}|v_i\vec{K}_i\sigma_i>|^2 \qquad (4.4.13)$$

$$*\frac{\Gamma_{fc}}{(\epsilon_{c,\vec{K}_f+\vec{k}_f}-\epsilon_f-\hbar\omega_f)^2+\Gamma_{fc}^2}\ |<v_f\vec{K}_f\sigma_i|\hat{\epsilon}_f.\vec{p}|c\vec{K}_f\sigma_i>|^2$$

where for simplicity $\epsilon_i=\epsilon v_i\vec{K}_i$, $\epsilon_f=\epsilon v_f\vec{K}_f$.

The above expression is now seen to involve the magnitude squared of the absorption and emission probabilities, multiplied by a Lorentzian lineshape for each process. Note, however, that the above "derivation" required a rather severe approximation for the case of GaAs, namely, the neglect of spin-orbit mixing of the electronic wavefunctions. It is clear that the neglect of spin-orbit coupling is probably completely justified for describing the intensity of the photoluminescence. However, the polarization of the photoluminescence may be quite sensitive to such approximations.

Strictly speaking such a treatment would rule out the spin-density fluctuation (non-resonant) Raman scattered measured by Moorodian,[4.17] and explained theoretically by Hamilton and McWhorter.[4.18] We should caution, however, that the two processes are somewhat different. In particular, in Mooradian's non-resonant measurements for GaAs, both charge and spin density fluctuations are involved. Then at carrier concentrations in excess of 10^{17} cm^{-3} (for n-type GaAs) the charge density fluctuations become heavily screened, leaving the spin-density fluctuations as the dominant scattering mechanism. Now as Wolff[4.19] has pointed out, the charge density fluctuations are essentially longitudinal waves which arise from the charge density operator

$$\rho = \sum_j e_j e^{i\vec{r}_j\cdot(\vec{k}_i-\vec{k}_f)} \qquad (4.4.14)$$

rather than the $\vec{P}.\vec{A}$ interaction considered in the resonance case. The light scattering associated with charge density fluctuations is essentially a direct process (no significant contribution from intermediate states), with the electrons in the conduction band undergoing quasielastic scattering. Thus we again emphasize the difference between the resonant and non-resonant cases.

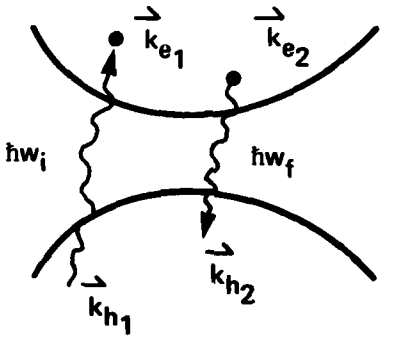

(a) BASIC ELECTRONIC STATES INVOLVED

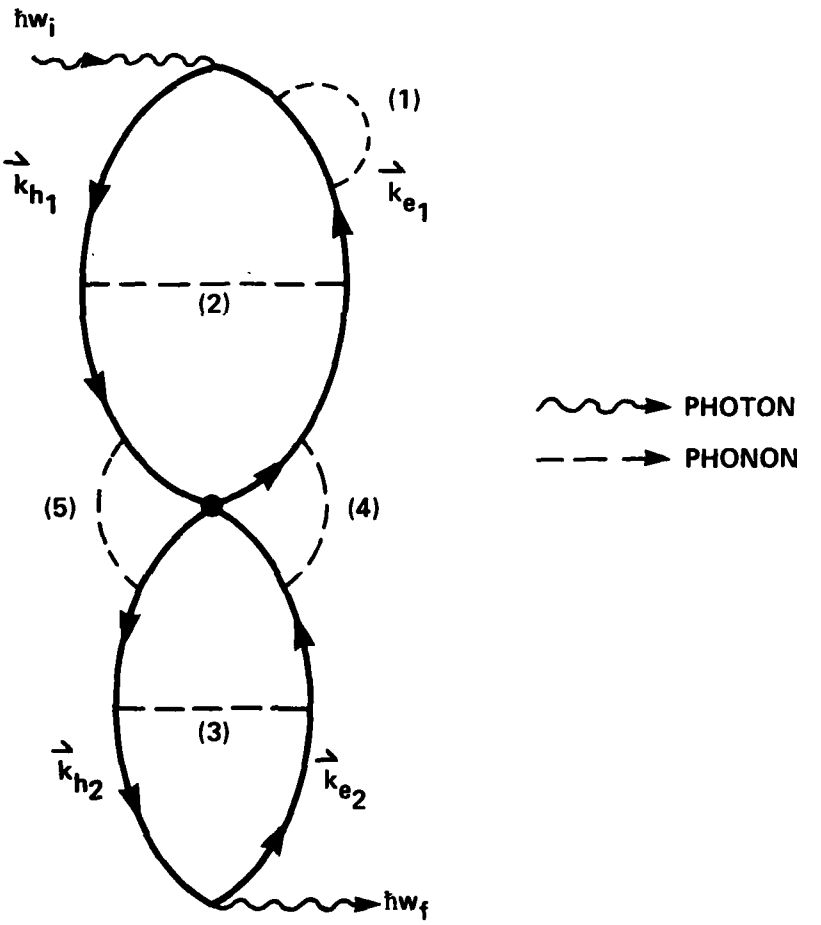

(b) FEYNMAN DIAGRAM OF TYPICAL ELECTRON-PHONON INTERACTIONS

Figure 4.4.2. Dynamical Interactions in Light Scattering

We also remark that the simple Lorentzian damping approximation considered here must be regarded as extremely crude. It seems unlikely that such an approximation can correctly account for multi-LO-phonon energy cascade in the conduction band, or that it correctly treats slower spin-relaxation processes (see the next section) such as the Elliott-Yafet mechanism. It may be possible, when collisions are correctly treated, that a formula similar to Eq. (4.4.13) can be justified. However, we feel that this is precisely the problem which remains to be solved. Certainly if Eq. (4.4.13) has any validity, an effort should be made to evaluate it using accurate Kan model wave functions for the conduction and valence bands.

In order to appreciate some of the complexity of treating the light scattering formula rigorously, e.g., including electron-phonon and other scattering mechanisms, we present in Fig. 4.4.2, some dynamical interactions which can take place. In Fig. (a) we show the four basic electronic states involved. In Fig. (b) we show a Feynman diagram of some typical electron-phonon interactions. In Fig. (b), a wiggly line denotes a photon, solid lines up(down) represent electrons (holes), and dashed lines represent phonons. Process (1) is a simple self-energy correction which converts a bare particle into a dressed "quasiparticle", i.e., a broadened and shifted state. Processes (2), (3) are vertex corrections in the absorption and emission processes respectively. Processes (4), and (5) are more complicated vertex corrections corresponding to electron and hole relaxation in the excited intermediate state.

Going beyond the approximations a careful analysis of various spin-relaxation processes and their dependence on conduction electron energy is needed. In a detailed study of photocreated electrons in P-type GaAs, Fishman and Lampel[4.20] have analyzed their results in terms of four spin-relaxation processes:

1. D'yakonov and Perel relaxation mechanism, arising from spin splitting of the conduction band.

2. Lattice modulated spin-orbit coupling (Elliott & Yafet mechanism).

3. Hyperfine interaction with the nuclei (Overhauser mechanism).

4. Exchange interaction between electrons and holes (Bir, Aronov, Pikus (BAP) mechanism).

Under certain circumstances, Fishman and Lampel conclude that the BAP process may be dominant. They also point out that motional narrowing effects can be important.

Finally, the problem of photon polarization in the presence of free or bound exiton complexes should provide a great deal of additional information concerning spin-relaxation in semiconductors.

4.5 Brief Discussion of Spin Relaxation Processes

It is usually assumed, for relatively pure semi-conductors (at not too low temperatures), the dominant mechanism for electron spin relaxation is spin-orbit coupling, modulated via the lattice vibrations.* Since spin-dependent interactions are weak compared to the interactions which lead to momentum and energy randomizing collisions, one expects the spin (τ_s) and

*More recently the role of electron-hole exchange has been considered for GaAS. See G. Fishman and G. Lampel[4.20].

momentum (τ_p) relaxation times to satisfy the condition $\tau_s >> \tau_p$, with typical estimates being $\tau_s \approx 10^{-8} - 10^{-9}$ sec., $\tau_p \approx 10^{-12} - 10^{-13}$ sec.

A rather general theory of electron spin relaxation in metals and semiconductors, has been developed by Overhauser[4.21], Elliott[4.22], and Yafet[4.23]. The theory is sufficiently general that it is capable of treating a wide-range of interaction mechanisms, in addition to the spin-lattice mechanism discussed above.

The starting point of the theory is the assumption that quasi-thermal equilibrium is established by momentum and energy randomizing collisions, which are much more rapid than spin-relaxation processes. Under this condition, the up and down spin populations can be described by quasi-fermi functions.

$$f_{\uparrow}(\vec{k},t) = \frac{1}{e^{\beta(\epsilon_{\vec{k}} - \mu_{\uparrow}(t))} + 1} \tag{4.5.1}$$

$$f_{\downarrow}(\vec{k},t) = \frac{1}{e^{\beta(\epsilon_{\vec{k}} - \mu_{\downarrow}(t))} + 1} \tag{4.5.2}$$

where $\mu_{\uparrow,\downarrow}(t)$ are chemical potentials which can be written as small deviations from the true equilibrium chemical potential according to

$$\mu_{\uparrow}(t) = \mu_o + \delta\mu_{\uparrow}(t) \tag{4.5.3}$$

$$\mu_{\downarrow}(t) = \mu_o + \delta\mu_{\downarrow}(t) \tag{4.5.4}$$

When the $\delta\mu$,s are small, the condition that total spin is conserved leads to the condition

$$\delta\mu_{\uparrow}(t) = -\delta\mu_{\downarrow}(t) \tag{4.5.5}$$

so that

$$\mu_{\uparrow}(t) + \mu_{\downarrow}(t) = 2\mu_o \tag{4.5.6}$$

Now the spin relaxation time τ_s can be defined phenomenologically by the equation

$$\frac{dD}{dt} = (D_o - D(t)) \frac{1}{\tau_s} \tag{4.5.7}$$

where

$$D = N_{\downarrow}(t) - N_{\uparrow}(t) \tag{4.5.8a}$$

$$D = \sum_{\vec{k}} [(f_{\downarrow}(\vec{k},t) - f_{\uparrow}(\vec{k},t)] \tag{4.5.8b}$$

is the difference of spin populations, and where D_o is the equilibrium difference. In the absence of an external field we assume $D_o = 0$, hence

$$D(t) = D(o)\, e^{-t/\tau_s} \tag{4.5.9}$$

describes the relaxation of a spin deviation with value D(o) at t = o.

One can next express the left hand side of(Eq. (4.57) in terms of transition probabilities, W, according to

$$\frac{dD}{dt} = 2 \sum_{\vec{k},\vec{k}'} \left\{ f_{\uparrow}(\vec{k},t)\ [1 - f_{\downarrow}(\vec{k}',t)]\, W_{\vec{k}_{\uparrow},k'_{\downarrow}} - f_{\downarrow}(\vec{k},t)\ [1 - f_{\uparrow}(\vec{k}',t)]\ W_{\vec{k}_{\downarrow},k'_{\uparrow}} \right\} \tag{4.5.10}$$

If we now insert Eq. (4.5.8b) into the right hand side of Eq. (4.5.7), expand the f's on both sides to first order in the $\delta\mu$'s, and make use of relation (4.5.5), we obtain the following general relation for the relaxation time in terms of the transition probabilities and equilibrium f's

$$\frac{1}{\tau_s} = 2 < \sum_{\vec{k}'} [1 - f(\vec{k}',\mu_o)]\ W_{\vec{k}\uparrow;k'_{\downarrow}} + f(\vec{k}',\mu_o)\ W_{\vec{k}'_{\uparrow};\vec{k}_{\downarrow}} > \tag{4.5.11}$$

where

$$< o_{\vec{k}} > \equiv \frac{\sum_{\vec{k}} f(\vec{k},\mu_o)[1 - f(\vec{k},\mu_o)]\ o_{\vec{k}}}{\sum_{\vec{k}'} f(\vec{k}',\mu_o)\ [1 - f(\vec{k}',\mu_o)]} \tag{4.5.12}$$

In general, the transition probabilities in Eq. (4.5.11) can be obtained via Fermi's "Golden Rule." For the case where the dominant interaction is spin-orbit coupling through lattice vibrations, the result can be written:

$$W_{\vec{k}_{\uparrow};\vec{k}'_{\downarrow}} = \frac{2\pi}{\hbar} \sum_{\vec{q},\lambda} \left[\frac{\hbar}{2N\omega_{\vec{q},\lambda}}\right] \left| <\vec{k}'_{\downarrow} | W_{\vec{q},\lambda} | \vec{k}_{\uparrow}> \right|^2 \left\{ n(\vec{q},\lambda)\ \delta(\epsilon_{\vec{k}_{\uparrow}} - \epsilon_{k'_{\downarrow}} + \hbar\omega_{\vec{q},\lambda}) + [n(\vec{q},\lambda) + 1]\ \delta(\epsilon_{\vec{k}_{\uparrow}} - \epsilon_{\vec{k}'_{\downarrow}} - \hbar\omega_{\vec{q},\lambda}) \right\} \tag{4.5.13}$$

where the n's are phonon population factors, $\vec{q}$ and λ are the phonon wavevector and polarization indices, and $<\vec{k}'_{\downarrow} \mid W_{\vec{q},\lambda} \mid \vec{k}_{\downarrow}>$ is the off-diagonal (in spin) electron-phonon matrix element. Equations (4.5.12) and (4.5.13) can be further reduced depending on temperature and the degree of complication of the phonon spectrum.

The case of GaAs seems particularly complicated for detailed evaluation, due to lack of inversion symmetry, which causes the acoustic phonon modes to be piezoelectrically active.(4.23) At present, therefore, we have not attempted a full evaluation of Eqs. (4.5.12, 4.5.13).

5.0 CONCLUSIONS

Sophisticated instrumentation has been developed to observe simultaneously photoluminescence and subtle effects in the circular polarization of photoluminescence of semiconductors over a wide range of excitation and luminescence photon energies and many orders of magnitude in luminescence intensity. Straightforward extensions of this setup would also provide for analyzing linear polarization of the photoluminescence.

Applications of the full capability of this experimental setup to studying optical orientation effects and the dynamics of the relaxation of optically excited carriers in semiconductors have begun. In particular the ability to vary the excitation photon energies over wide ranges has not been exploited. Already we have observed structure in the variation of the circular polarization with energy that is not easily explained on the basis of current theory. The establishment of these effects will require extension measurements of a variety of samples over a range of experimental conditions. We have addressed many of the theoretical problems but also much remains to be done.

Experimentally the circular polarization has been found to vary with photon energy in ways that cannot always be correlated with structure in the photoluminescence intensity. In some cases sharp peaks in polarization occur at photon energies associated with transitions involving free carriers. These effects need documenting with more extensive data particularly involving a variety of excitation photon energies. Explanations involving LO photon emission and sharp impurity states must be considered as preliminary at this stage. This situation indicates that a detailed interpretation of radiative and nonradiative processes in III-V compounds is far from complete.

Particularly interesting as a focus of future work to study optical orientation and relaxation dynamics is the newly available ultrapure insulating GaAs. The material is technologically very important. The photoluminescence spectrum is rich in structure, and we have already seen strong circular polarizations of luminescence associated with exciton transition relative to luminescence associated with other transitions. An intriguing mystery concerning this material is why it is insulating, since it is quite unrealistic to believe that it is pure enough to be a truly intrinsic semiconductor. Studies of the relaxation of photo-excited carriers using polarized luminescence studies may help solve this mystery.

Theoretically we have advanced considerably in relating the optical orientations to the selection rules. Orientation of orbital angular momentum and electron wave vectors occur due to the k.p interaction. Since spin flip cannot occur under the action of an electric dipole matrix element the alignment of electron spins require the intercession of spin-orbit interaction. In the Kane band model these two alignment interactions occur simultaneously and all three optical orientations are possible near the zone center. However at light hole band energies approaching $-2/3\,\Delta$ spin orbit effects are minimized and spin becomes a good quantum number once again. (See Fig. 4.2.7.) Little spin alignment should occur for transitions involving these states. However detailed predictions of this effect require involved integrations over the zone and this work remains to be done. A question that arises is whether such effects may be, at least, partially responsible for the strong decrease in spin alignment for excitation energies near $E_g + \Delta$ as observed by others and in some of our

earlier work which does not appear in this report. Additional effects which remain to be taken into effect include the roles of exciton interactions, quenching of angular momentum and induced magnetization on the density of states.

A phenomenological rate equation approach to the dynamics of spin polarization which replaces matrix elements by energy and spin dependent generation rates has been developed. It approximates channels for optical or scattering processes by simple relaxation times τ_{RC}, $\tau_{spin\,flip}$, τ_{LO} etc. A general solution to the rate equations obtained is formidable and conclusions are possible only for very specific cases. Relaxations can either enhance or decrease the optically induced orientations depending upon the recombination mechanisms. It is found that the spin polarization is independent of the carrier energy for a quasi-thermalized nondegenerate carriers. This conclusion would not be valid if (1) the optical selection rules vary with energy, (2) the assumptions of two mildly interacting spin systems is not realistic or if (3) orientations other than spin (such as orbital angular momentum) interact with the spin system.

An underlying question relevant to the treatment of the photoluminescent process is the question of how valid is the approach of treating the absorption and emission problems as essentially separate. Although we have considered this approach in Section 4.2, we have also advanced a more sophisticated light scattering approach (Section 4.4) which treats the two processes as coupled.

The choice of using orientational effects as a tool for studying a variety of interactions in GaAs has proved to be extremely rewarding and is likely to play an increasing role in the future. We have developed a sensitive experimental approach to the problem and outlined the theoretical problems. A full experimental and theoretical description of orienting and disorienting processes is a severe task which remains to be accomplished.

Acknowledgments

The authors would like to acknowledge very stimulating discussions with S.J. Nettle, L. Andrews and W.J. Miniscalco. The technical assistance of William Dyes is greatly appreciated as well as the help on electronic circuits by William Freudenthal and John Egan.

6.0 REFERENCES

1.1 G. Lampel Int Conf on Semiconductors, Stuttgart (1974).

1.2 E.J. Johnson, L.A. Riseberg, A. Lempicki and H. Samelson, Appl. Phys. Letters 26 444-447 (1975).

1.3 See for example: D.H.B. Miller, S.D. Smith and A. Johnston, Appl. Phys. Letters 35 658 (1979) and references therein.

1.4 V.I. Zemskii, B.P. Zakharchenya and D.N. Mirlin, JETP Lett. 24, 82 (1976).

1.5 V.D. Dymnikov, M.I. Kyakonov and N.I. Perel, Sov. Phys. JETP 44, 1252 (1976).

2.1 P. Fisher, W.H. Haak, E.J. Johnson and A.K. Ramdas, Proceedings of the Eighth Symposium on the Art of Glassblowing (1963); The American Scientific Glassblowers Society p. 136.

3.1 See for example E.W. Williams and H. Barry Bebb, in "Semiconductors and Semimetals" (R.K. Willardson and A.C. Beer, Eds.), Vol. 8 p. 321, Academic Press, New York, 1972.

3.2 D.J. Ashen, P.J. Dean, D.T.J. Hurle, J.B. Mullin, A.M. White and P.D. Greene, J. Phys. Chem. Solids 36 1041 (1975).

3.3 R.C.C. Leite, Solid State Electronics 21 177 (1978).

3.4 E.W. Williams, Brit J. Appl Phys 18 253 (1967).

3.5 E.W. Williams, C.T. Elliott, Brit J. Appl Phys (Phys D) 2 117 (1969).

4.1 E.J. Johnson, Optical Orientations in Semiconductors, in Proceedings of the NATO Advanced Study Institute on Theoretical Aspects and New Developments in Magneto-Optics-Antwerpt (1979).

4.2 R.R. Parsons, Canadian J. Physics 49, 1850 (1971).

4.3 Thesis Electronic Energy Bands in Semiconductors with Cubic Crystal Structure by Gene Dresselhaus (University of California) 1951.

4.4 E.O. Kane, J. Phys. Chem. Solids 1, 249 (1956).

4.5 H.J. Zeiger and G.W. Pratt, Magnetic Interactions in Solids, Clarendon Press, Oxford (1973).

4.6 G. Dresselhaus, Phys. rev. 100, 580 (1955).

4.7 Frank Stern, Solid State Physics 15, (1963) p. 371.

4.8 E.J. Johnson, Semiconductors and Semimetals Vol. 3, edited by R.K. Willardson and A.C. Beer (Academic Press, New York) p. 154.

4.9 C.R. Pidgeon and R.N. Brown, Phys. Rev. 146, 575 (1966).

4.10 R.J. Seymour & R.R. Alfano, Appl. Phys. Lett. 37 (2) 231 (1980).

4.11 P.Y. Yu, Y.R. Shen, Y. Petroff and L.M. Falicov, Phys. Rev. Lett. 30, 283 (1973).

4.12 M.V. Klein, Phys. Rev. B8, 919 (1973).

4.13 Y.R. Shen, Phys. Rev. B9, 622 (1974)

4.14 D.G. Fouche and R.K. Chong, Phys. Rev. Lett. 29, 536 (1972).

4.15 R.L. St. Peters, S.D. Silverstein, M. Lapp, and C.M. Penny, Phys. Rev. Lett. 30, 191 (1973)

4.16 J.R. Solin and H. Merkelo, Phys. Rev. B12, 624 (1975)

4.17 A. Mooradian in Light Scattering Spectra of Solids, Edited by G.B. Wright, Springer-Verlag, 1969, Page 285.

4.18 See Ref. 4.17, page 309.

4.19 See Ref. 4.17, page 273.

4.20 G. Fishman and G. Lampel, Phys. Rev. B16, 820 (1977).

4.21 A.W. Overhauser, Phys. Rev. 89, 689 (1953).

4.22 R.J. Elliott, Phys. Rev. 96, 2661 (1954).

4.23 Y. Yafet, Solid State Physics (Edited by Seitz & Turnbull) Vol. 14 (1963).

7.0 PUBLICATIONS

- Optical Orientation in Semiconductors - to be published in the Proceedings of the NATO Advanced Study Institute on Theoretical Aspects and New Development in Magneto-Optics, Antwerp, Belgium (July, 1979).
- Anomalies observed in the circular polarization of the photoluminescence of GaAs (In preparation).
- Photoluminescence of unintentionally doped Insulating GaAs (in preparation).
- A sensitive experimental arrangement for measuring Polarization of Photoluminescence of Semiconductors (in preparation).
- Mechanisms that provide for optical orientation effects in III-V Semiconductors (in preparation).
- Conditions for efficient application of cavity dumping techniques for ion laser pumped dye lasers (in preparation).
- Theory of polarized photoluminescence in semiconductors (in preparation).
- Microprocessor Application to analysis and orchestration of optical orientation experiments in GaAs (in preparation).

APPENDIX

COMPUTER ANALYSIS AND ORCHESTRATION OF OPTICAL ORIENTATION EXPERIMENTS IN GaAs

Lauren Martens
P.I.: E.J. Johnson
8 August 1980

NSF INDUSTRIAL UNDERGRADUATE RESEARCH PARTICIPATION
GRANT TO UNIVERSITY OF NEVADA AT RENO

Microprocessors are rapidly becoming common in many areas of industry and in the laboratory. A unique application of the microprocessor, computer control of sophisticated laboratory equipment, was made during the IURP-80 summer project under the supervision of E.J. Johnson at the General Telephone and Electronics Laboratories. During the course of the ten-week project, a microcomputer was modified, installed in the laboratory, and given the capability to conduct a complete experiment. The following paragraphs briefly describe the nature of the experiment, the accomplishment of computer control, and the benefits which will be derived from the work completed during the project.

The experiments being performed by Dr. Johnson involve the spectroscopy of photoluminescence of semiconductors. The equipment required for this work is rather sophisticated and includes a tuneable dye laser to illuminate the sample material and a spectrometer and photon-counting electronics to analyze the photoluminescence. The introduction of a microcomputer into the laboratory setup was desired in order to provide more sophisticated methods of synchronizing laboratory equipment, orchestrating experiments, and collecting and reducing data.

The goal of the summer project was to implement the first step in this open-ended and continuing process: to interface the microcomputer with the spectrometer and photon counter, and to program it to conduct a simple experiment. The experiment required the computer to: drive the spectrometer to an initial wavelength, successively advance the spectrometer by some set interval, and to collect and print out a set of data at each interval (see flowchart in Figure 1).

The microcomputer used was the commercially-available AIM65 by Rockwell. By the end of the ten weeks, all of the needed computer expansion, interface wiring and programming had been provided, and the AIM65 was conducting the experiment as desired. A printout of an experiment performed by computer is shown in Figure 2. After the command to initiate an experiment, the AIM asks for the initial wavelength, the interval which the spectrometer is to be advanced by, and the number of points to be taken. Upon receipt of this information, the AIM drives the spectrometer to the initial wavelength and commands the photon counter to begin counting. When the count is completed, the AIM collects the data, performs the desired calculations on it, and prints out the results, as shown. The spectrometer is then advanced by the desired interval, and the cycle is repeated until the specified number of readings has been taken.

A plot of part of the emission spectrum of a mercury lamp, obtained by the computer-controlled experiment described above, is shown in Figure 3. The example illustrates one of the benefits of the method: the data which has been plotted was obtained directly from a printout such as the one in Figure 2. The significance of this is that the plot in Figure 3 is in reduced form, ready for analysis. Before the installation of the microcomputer, it was necessary to read the data from a chart recorder, and digitize it and reduce it by hand. The microcomputer, then, has made possible both an increase in accuracy (since there always existed uncertainty in the digitized chart recorder readings) and considerable savings in time.

Another major benefit of the computer system is due to the automatic control. Since the photoluminescence signal being observed is very weak, all experiments must be performed in the dark, and the counting times must be large (to build up the signal). To complete a data-taking scan, then, a technician would have to spend tedious hours in the dark. With the microcomputer controlling the experiment, the techniciam is freed from this time-consuming and unpleasant task.

This summarizes what has been accomplished during the summer project. In order to describe in more detail how all this has been accomplished, it will be necessary to go into more detail concerning the following aspects of the project: (1) the organization of the laboratory and operation of the equipment, (2) the internal architecture and operation of microcomputers, (3) the actual interfacing (both the hardware and operational elements), and (4) the software, or programming. The report concludes with some recommendations for the future expansion of the system.

I. THE LABORATORY

The interaction of polarized light with electronic spins is an extremely interesting physical phenomenon about which little is empirically known. Aside from offering knowledge of the quantum mechanics of solids, exploration of this phenomenon could lead to electronic devices which are much faster than those which now exist (by transmitting information by light and storing it by making use of this interaction between light and matter).

Theoretical calculations made by Dr. Johnson and others have predicted that Gallium Arsenide (GaAs), when illuminated with circularly polarized light, will emit partially polarized photoluminescence. In his laboratory, Dr. Johnson, has been observing this effect. The laboratory configuration being used is shown schematically in Figure 4. A tuneable dye laser illuminates the sample with radiation of the chosen wavelength. The polarizing optics determine the polarization of the incident light. The photoluminescence of the sample is focused onto the entrance slit of a dual-pass spectrometer; and the signal exiting the spectrometer is detected by photon counting electronics.

Observing these polarization effects requires great sophistication and care; since the photoluminescence of interest is expected to be at a wavelength close to that of the pump light, the desired signal may be small compared to scattered incident light. Among other measures taken to increase the signal-to-noise ratio, long data-taking times and dark lab conditions are required. It was hoped that the introduction of a microcomputer to handle the data-taking automatically would reduce both the time and effort expended in obtaining a good signal-to-noise ratio.

To obtain such control, the microcomputer needed to have the capability to communicate with the photon counter, the spectrometer controls, and the remote wavelength indicator of the spectrometer. In addition, it was desired to provide sample temperature information to the computer. Each of these instruments is equipped with digital control inputs which mimic the pushbutton controls on the front panel, and/or digital data outputs which provide the front panel display information in coded form. In particular, microcomputer control of the spectrometer is made possible by sending digital pulses to a stepping motor (which advances the spectrometer a given amount for each pulse it receives). All of these devices have Transistor-Transistor Logic (TTL), which is compatible with the AIM65.

To allow a more detailed discussion of these interfaces, we now turn to a brief discussion of microcomputer architecture.

II. THE HARDWARE

The outline of microcomputer architecture and operation which follows is general in nature, but makes particular reference to the AIM65. The AIM is a "microcomputer on a board". It communicates with the user by means of a complete keyboard, a one-line alphanumeric LED display, and a small thermal printer. It can store programs in an ordinary cassette tape recorder. The AIM was chosen because it provides these features at a low cost, allowing the introduction of computer control into the laboratory without a large initial investment.

The central element in the AIM65, as in any microcomputer, is the microprocessor chip itself, or central processing unit (CPU). This chip contains all the logic, arithmetic, and control functions of the computer. It also has complete control of all of the other chips in the microcomputer, turning then "on" when it wants to communicate with them, and "off" otherwise. All of the operations of the computer are performed by this central chip; the other components are subservient to it.

The memory is the second element of the microcomputer (see Figure 5). In memory are stored both the programmed instructions for the CPU, and the data to be acted upon. The third primary set of components of a microcomputer are interface chips. These provide buffering the CPU and the "real world" (more about these later).

The CPU communicates with the other chips on the board through sets of connections called "buses". In microcomputers there are three buses: the address, control, and data buses.

The address bus is usually sixteen lines (or bits. A bit is one binary digit: it can either be in the logic "1" state - high voltage - or logic "0" - low voltage. A set of bits in parallel is used to transmit binary data). The CPU uses it to perform two functions: first, it carries the code used to select the chip which the CPU wishes to "address"; and second, it carries the address of the desired location within that chip. The chip selection is usually performed by a "decoder", which inputs the (binary) code for the desired chip, and outputs a single signal which turns that chip "on" (the decoder has one output line to each of the chips it services). The selection of the correct register within each chip is accomplished within the chip.

The control bus is usually eight bits, and allows the CPU to exercise control functions. The most important of these are the Read/Write (tells the chip being addressed whether it is to send data to the CPU - read - or receive data from the CPU - write), and the clock (provides a means of synchronizing the operations of the CPU and the auxiliary chips).

Finally, the data bus is comprised of the lines which actually carry data to and from the CPU. It is usually eight bits; the restriction to eight is due to the limit on the number of pins which can be put on the CPU package.

Notice that only the data bus carries information to, as well as from, the CPU. The address and control buses only carry information and commands from the CPU to the auxiliary chips.

With the summary of microcomputer architecture in mind, we now outline the operation of one. At the heart of all digital computers is the clock. The clock is simply a square-wave signal of constant frequency which synchronizes all elements of the microcomputer. A simplified, though not entirely inaccurate, view is that the CPU carries out one operation per clock cycle. All microcomputer operations are sequenced, with the order of operations determined by the CPU. Some operations only involve the process for example, the addition of numbers which are already stored in the CPU. Other operations require an exchange of information between the CPU and another chip. By sequencing its operations, then, the CPU avoids the possibility of conflicting information on the data bus. Even though each chip is at all times connected to the data bus, at any particular time there is (at most) one chip which is enabled to send or receive data: hence the CPU always knows exactly with whom it is communicating.

The problem of interfacing the microcomputer with internal electronic equipment (peripherals) can now be discussed. Consider a hypothetical, self-contained microcomputer, consisting only of the CPU and memory. Under control of the clock, the CPU is performing operations: reaching and writing memory, making decisions, and doing calculations (assume a program has been pre-loaded into memory). Now suppose that it is desired to introduce data from some external source, such as a keyboard. Since it is desirable to allow the keyboard user to send information whenever he/she desires (and not only when the CPU asks for it), it is clear that the data from the keyboard cannot be brought directly into the CPU via the data bus. Therefore, a buffer of some kind must be provided to isolate the CPU from the outside world and allow the information to be transferred into the CPU only at the correct times (when the CPU asks for it). This is the function of the interface chips.

The interface chip, then, is an intermediary between the CPU and the peripheral. It allows the peripheral to send information to the microcomputer without regard for the operations of the CPU; and it allows the CPU to access this information when it enables the interface chip. In the case of output, the interface chip allows the CPU to make information available to the peripheral without tying up the CPU. The interface chip may also perform other functions, such as providing a timer of its own which can be used to generate time intervals.

Rockwell's Versatile Interface Adaptor (VIA), which is used with the AIM65, provides buffering and handshaking capabilities for two eight-bit-ports. These ports can be programmed to function as either inputs or outputs. Each VIA has two timers, which provide the following capabilities: operating a time interval, outputting a digital pulse of specified time width, and counting input pulses.

III. HARDWARE INTERFACING

Giving the AIM communication with laboratory equipment first required the wiring connections and buffering between the AIM and the peripherals. Immediately the problem arose of the large number of bits required for the complete interfacing: over one hundred bits were needed (the breakdown of these is given in Table 1).

Since the AIM65 as it comes out of the box has one VIA interfacing chip (capable of handling twenty bits) available for the user, expansion was needed. No suitable expansion boards were available commercially (the Rockwell systems have a serious deficiency of support modules), so it was necessary to design and construct our own. The expansion board which was constructed is shown in highly schematic form in Figure 6. It provides an additional five VIA chips and the address decoding necessary to enable these chips. Since the edge connector which was available on the photo-board only provided for 44 bits, the board incorporates plug-in connections (using standard dip sockets) to bring in an additional eighty bits.

The design and assembly of the expansion board consumed a large portion of the ten-week project. All of the hardware - connectors cables, chips, the photo-board - has to be planned for, located, and ordered. While waiting for the parts to arrive, the layout and design of the board, including all pin-pin designations, was completed. Finally using solder and wire-wrapping, the board was assembled.

In addition to the microcomputer expansion, there were interfacing considerations which led to the construction of a small circuit board. These complications involved the interface with the spectrometer control unit: both the remote readout unit and the microcomputer needed to have the capability to control the status of certain pins on the spectrometer. It was necessary to provide logic circuits to ensure that at all times it is clear

which unit is doing the controlling. The connector board (shown schematically in Figure 7) provides the necessary logic functions, as well as making a "Y" connection between the spectrometer control unit, remote readout, and microcomputer. It was designed to plug into the spectrometer control unit, so that the power for the chips is obtained directly from this unit. This allows the remote readout to function even when the microcomputer is turned off or unplugged.

The hardware assembly was completed in a series of steps as parts became available. Chronolcgically, the assemble process was: connections for photon counter data transer; expansion board (partial); connections for control of photon counter; expansion board (complete); connector board; remote readout and spectrometer control connections. As each step was completed, it was necessary to program the AIM to communicate successfully with the peripheral. This was the last phase of the project: the software.

IV. SOFTWARE INTERFACING AND DESIGN

The first programming task was to teach the AIM the language of the other instruments. The essence of this interface programming involved reading and writing certain memory locations in the VIA chips. All of the programming was done in the BASIC language, a very convenient optional feature of the AIM 65. The following paragraphs describe typical data reading and command operation.

Data reading operations, such as accepting the results of a counting operation from the photon counter, often involve handshaking signals. The sequency of a data dump from the photon counter is typical: when the photon counter has completed a counting operation and placed the data on the data lines, it sends a "data ready" signal to the microcomputer by raising a certain pin from "low" to "high". The microcomputer, which has been waiting for this signal, stores the data in memory and sends a "data received" signal back to the photon counter. This handshaking process is repeated four times, since the photon counter dumps four pieces of data after each count operation. The microcomputer must be correctly programmed to execute this series of events.

A variety of control counter functions can be performed by the microcomputer. Some of these are listed, with examples, in Table 2. A typical example of a central function is a command to the spectrometer to scan at a computer-selected speed. First the desired speed, a 4-bit binary code, is loaded into the VIA chip and sent to the spectrometer control unit. On a different pin, a low-pulse, the spectrometer commences scanning at the desired speed, and continues to do so until commanded to change speeds or stop. In another important control application, the microcomputer takes control of the spectrometer and sends pulses to the stepping motor directly. This allows the microcomputer to advance the spectrometer precisely to any desired position.

Once the microcomputer knew how to speak with the peripheral instruments, the next task was to use this ability to write subroutines designed to be called upon to accomplish specific tasks. The subroutines written included ones that performed these functions: read wavelength, and store the result; advance the spectrometer, under computer control, to a desired wavelength; slew the spectrometer to a desired wavelength using the slew command of the spectrometer control unit; and accept a complete data dump from the photon counter and store the numbers (converted to a useful form).

The next level of programming assembled these task-oriented subroutines into larger subroutines which interact with the user and perform functions and experiments useful in the everyday operation of the laboratory. The routines currently available can: read and print out the current wavelength; drive the spectrometer to a wavelength input by the user; and, most importantly, conduct the experiment described earlier.

All of these subroutines are overlaid by a master program which acts as a monitor, accepting user commands to execute the subroutines just described. Designed to be entered in the morning and exited at the end of the day, the monitor asks the user for the date and name of the sample being observed, and then enters a waiting mode. At this point, the user can operate any of the equipment manually, or enter a command to the computer. The monitor eliminates the need to run separate programs to perform different tasks and make the computer highly interactive with the user.

The design of the software - a monitor program accepting commands to enter function - performing subroutines, which in turn call lower level task-performing subroutines - will allow easy expansion of microcomputer capabilities. If the need arises for a new computer - controlled experiment, it can be simply written as a subroutine and added to the existing program. In this way the microcomputer will eventually become the command center of the laboratory, allowing the technician to perform almost any desired function or experiment at the touch of a key.

V. CONCLUSION

The first big step in the implementation of a microcomputer into the laboratory has been successfully completed. The microcomputer is both useful now and has the capacity for expansion in the future. The AIM65 system now provides automation of the tedious and time-consuming task of obtaining a spectra with a good signal-noise ratio. It provides digital data, which eliminates the need to digitize an analog recording by hand and gives more precise data. Finally, it performs corrections and manipulations of the data which were formerly done by hand.

In the future, the system will be expanded to handle more information valuable to the experiment and allow the introduction of more sophisticated lab techniques. Some of the immediate expansion possibilities are:

1. Software expansion - the library of subroutines can be enlarged. An immediate possibility is programming for the photon counter control interface, which has already been debugged. As it becomes necessary, subroutines can be written to perform a variety of experiments.

2. Hardware expansion - It will soon be necessary to increase the memory of the AIM65. The additional memory chips can be placed on the expansion board, or pre-assembled memory boards can be ordered.

Two additional pieces of equipment, the temperature sensor and a TTL logic-operated shutter, will be added to the system in the near future. The hardware for the temperature sensor is in place, but needs to be debugged. The TTL shutter will be placed in the optical path prior to the entrance to the spectrometer. Controlled by the microcomputer, it will allow the measurement of dark counts and improve the signal-noise ratio.

Another important expansion will be an interface of the AIM65 with the IBM370 main-frame computer located at the labs. This will allow quick access to the extremely good data analysis and plotting capabilities of the IBM.

The microcomputer system installed this summer promises to be useful both in the present form and as it is expanded. The possibilities are limited only by the imagination of the user.

ACKNOWLEDGEMENTS

The author gratefully acknowledges the expert advise of John Egan, the assistance and thought provoking conversation of Bill Dyes, and especially the direction and eduction provided by Earnie Johnson.

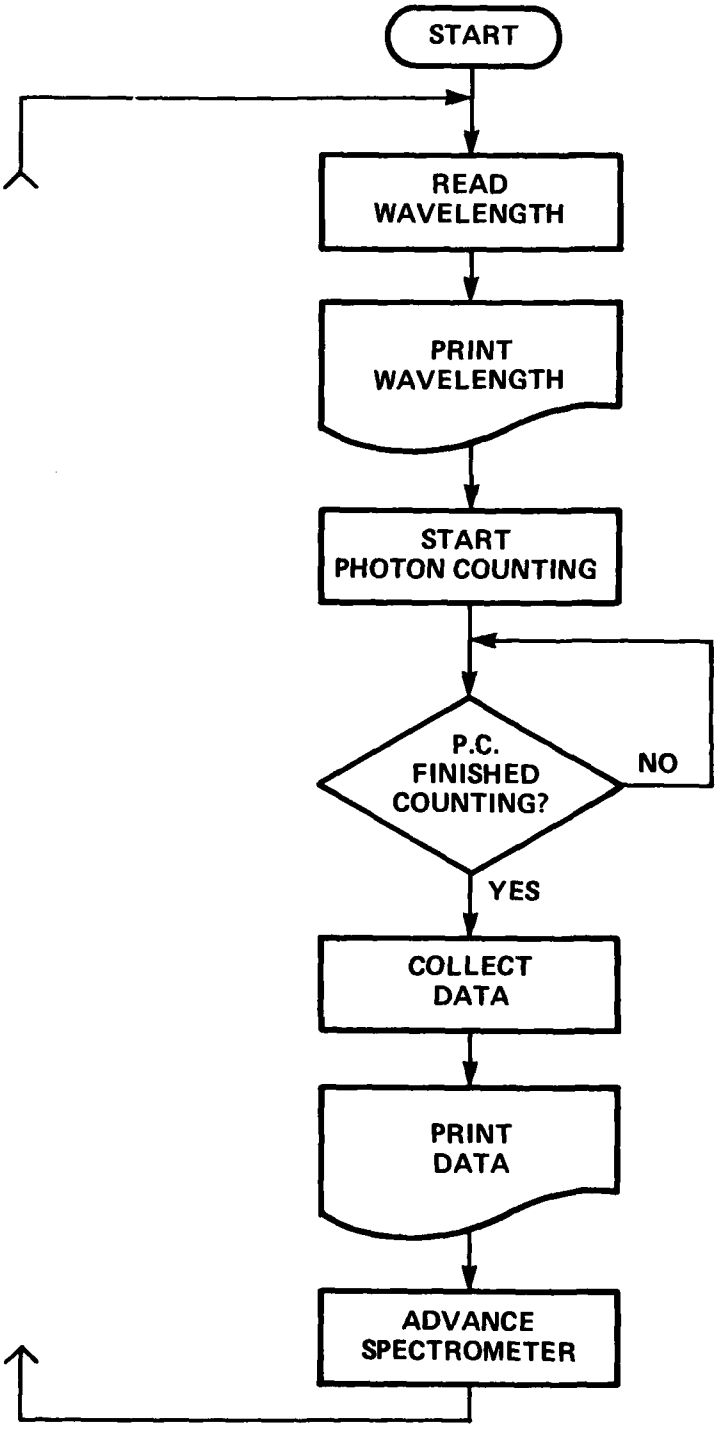

Figure 1. Computer-Controlled Experiment

```
COMMAND? 4
INITIAL WAVELENGTH
? 12780
INTERVAL? 1.0
# OF READINGS? 30
DATE:8-6-80
SAMPLE:MERC


====================

 --- WAVELENGTH ---
 12780

-- PHOTON ENERGY --
 .9703

     --- A ---
 43000

     --- B ---
 3470

    --- A+B ---
 46470

   --- RATIO ---
 1.18


====================

 --- WAVELENGTH ---
 12781

-- PHOTON ENERGY --
 .9702

     --- A ---
 44400

     --- B ---
 3470

    --- A+B ---
 47870

   --- RATIO ---
 1.17


====================

 --- WAVELENGTH ---
 12782

-- PHOTON ENERGY --
 .9701

     --- A ---
 46300

     --- B ---
 3470

    --- A+B ---
 49770

   --- RATIO ---
 1.16


====================

 --- WAVELENGTH ---
 12783

-- PHOTON ENERGY --
 .97

     --- A ---
 49600

     --- B ---
 3470

    --- A+B ---
 53070

   --- RATIO ---
 1.15


====================

 --- WAVELENGTH ---
 12784

-- PHOTON ENERGY --
  97
```

Figure 2. Computer Controlled Equipment: Sample of a Scan

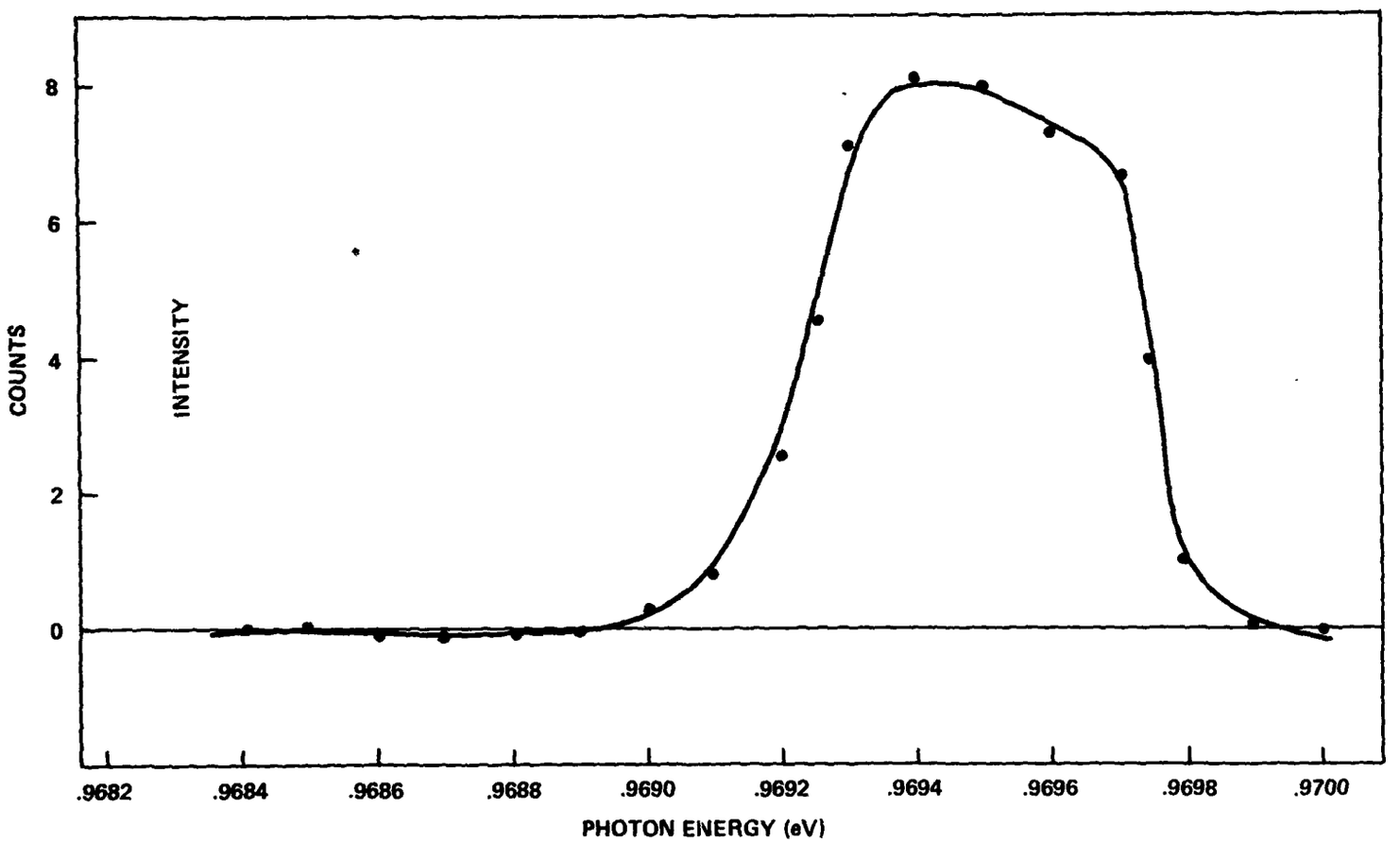

Figure 3. Computer-Controlled Scan Showing Mercury Lamp Emission Line

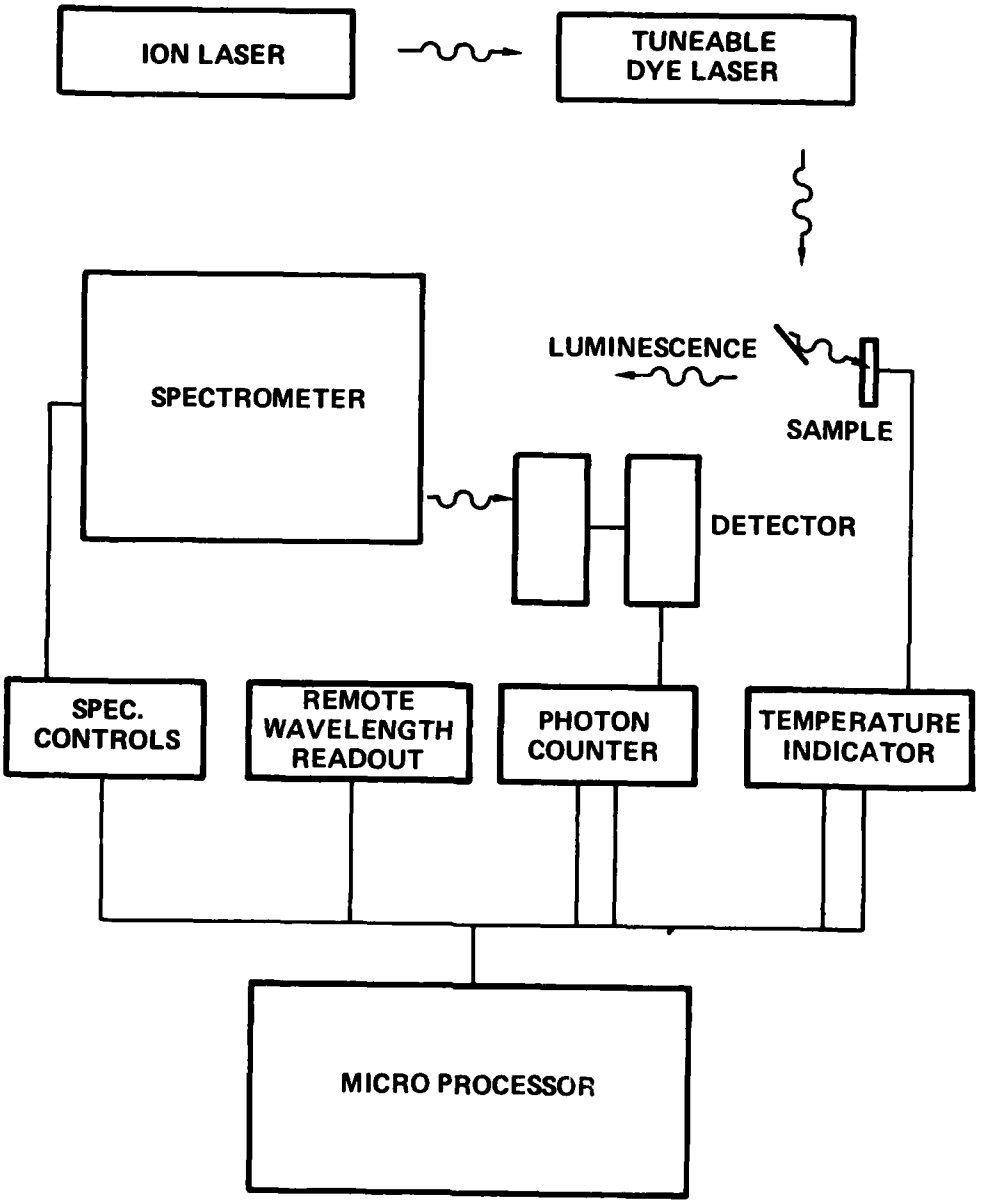

Figure 4. Schematic of the Laboratory

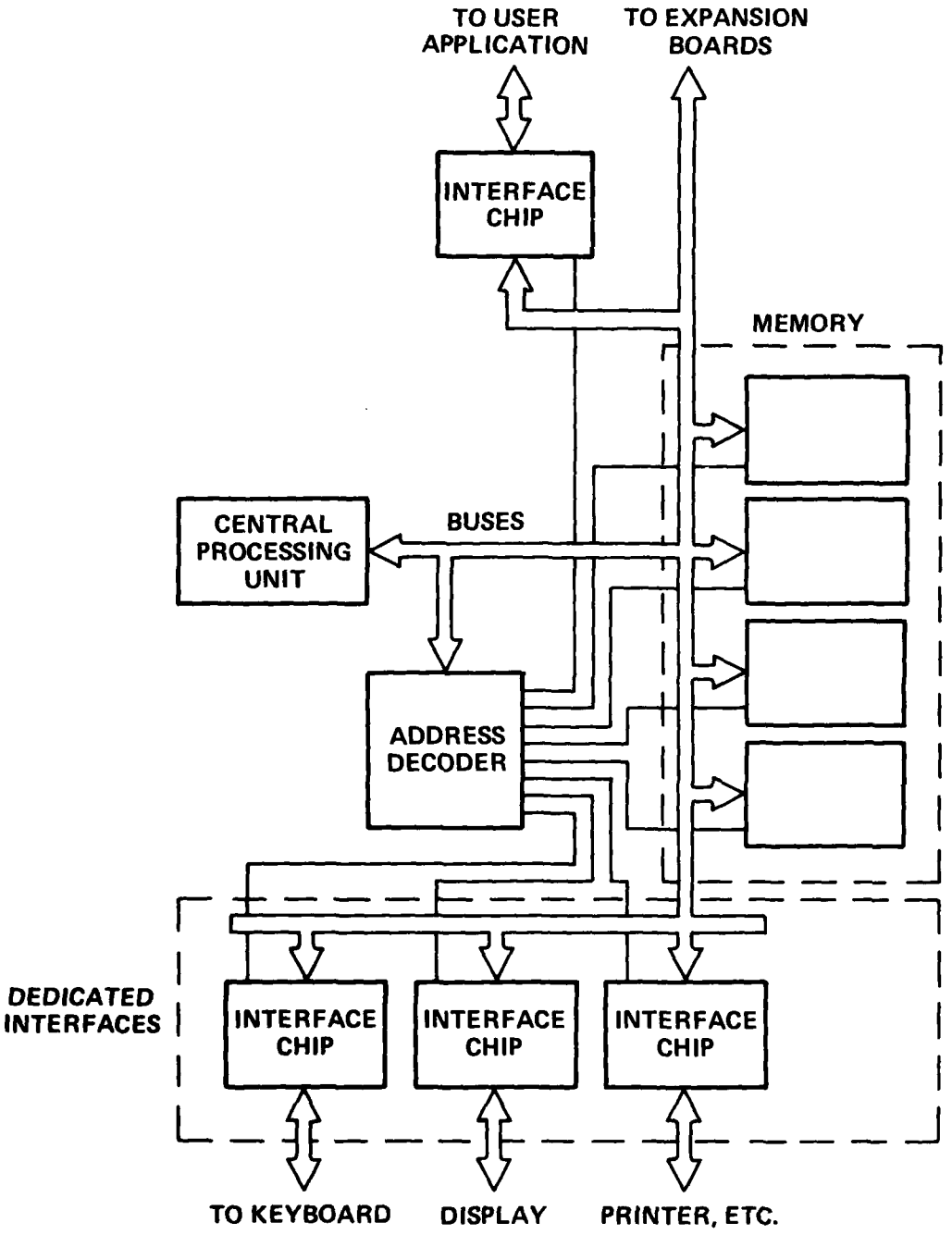

Figure 5. Simplified Microcomputer Architecture

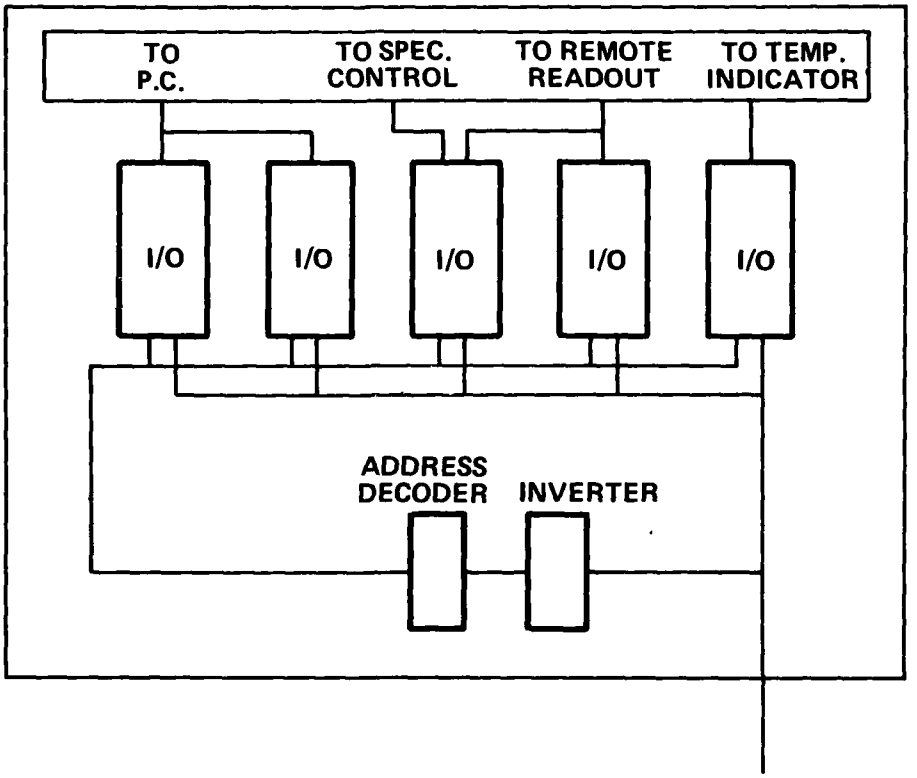

Figure 6. Expansion Board

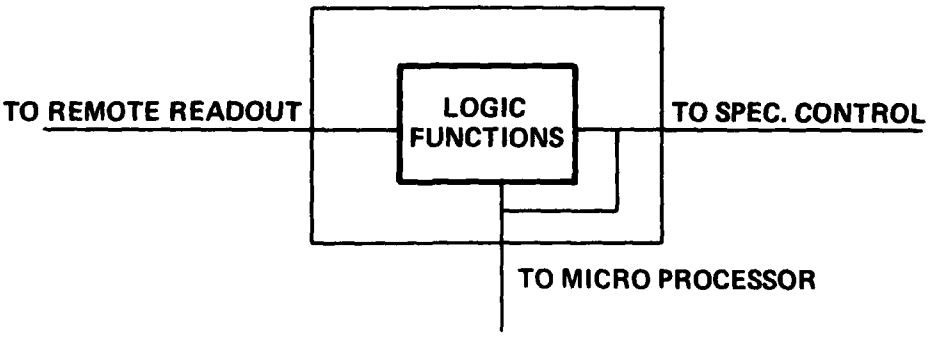

Figure 7. Connector Board

Table 1. Bits Required for Interfacing

Number of Bits	Instrument
48	Photon Counter
-18	Inputs (4 digits in Binary-Coded Decimal for the data; and two handshake bits)
-30	Control (including 4 digits in BCD to preset counting time; the remainder set the mode of operation)
40	Spectrometer
-24	Inputs (6 digits in BCD for the wavelength readout in Angstroms)
-16	Control (including setting scan speed, sendin pulses to stepping motor)
20	Temperature Indicator
-16	Inputs (4 digits in BCD for the temperature)
-4	Control

AD-A093 652 GTE LABS INC WALTHAM MA F/G 20/5
NONLINEAR INTERACTIONS BETWEEN LASER RADIATION AND SPIN-ALIGNED--ETC(U)
NOV 80 E J JOHNSON, R W DAVIES, A LEMPICKI F49620-78-C-0082
UNCLASSIFIED AFOSR-TR-80-1324 NL

2 OF 2
AD A 093652

END
DATE FILMED
2-81
DTIC

Table 2. Interfacing Details of Control Techniques

Control Function Which the Microprocessor Can Perform	Example
Pushbuttons -set on/off	1. Set photon counter mode (choose one of eight possible modes of operation) 2. Command Spectrometer to Slew
Send Data -usually in binary or BCD	1. Preset the time interval of a data count in the photon counter. 2. Set the spectrometer scan speed.
Send Pulses -the width of the pulse can be programmed and is determined by the requirements of the equipment being controlled.	1. Send pulses to the spectrometer stepping motor 2. Command the photon counter to start counting
Handshaking -VIA can be programmed to automatically send handshake signal upon receipt of data by the processor.	1. Collect photon counter's data. The P.C. dumps four pieces of data, sequentially. Between each piece it waits for a handshake signal.